ADVANCED GLIOBLASTOMA MODELS TO STUDY TUMOUR MICROENVIRONMENT AND TO SUPPORT NOVEL GLIOBLASTOMA THERAPEUTICS

Bernarda Majc

Doctoral Dissertation
Jožef Stefan International Postgraduate School
Ljubljana, Slovenia

Supervisor: Prof. Dr. Tamara Lah Turnšek, Jožef Stefan International Postgraduate School, National Institute of Biology, Ljubljana, Slovenia
Co-Supervisor: Dr. Metka Novak, National Institute of Biology, Ljubljana, Slovenia

Evaluation Board:
Prof. Dr. Kristina Gruden, Chair, Jožef Stefan International Postgraduate School, National Institute of Biology, Ljubljana, Slovenia
Prof. Dr. Janko Kos, Member, Jožef Stefan Institute, Ljubljana, Faculty of Pharmacy, Ljubljana, Slovenia
Asst. Prof. Marija Skoblar Vidmar MD, Member, Institute of Oncology, Ljubljana, Slovenia

MEDNARODNA PODIPLOMSKA ŠOLA JOŽEFA STEFANA
JOŽEF STEFAN INTERNATIONAL POSTGRADUATE SCHOOL

Bernarda Majc

ADVANCED GLIOBLASTOMA MODELS TO STUDY TUMOUR MICROENVIRONMENT AND TO SUPPORT NOVEL GLIOBLASTOMA THERAPEUTICS

Doctoral Dissertation

NAPREDNI MODELI GLIOBLASTOMA ZA PREUČEVANJE TUMORSKEGA MIKROOKOLJA IN ZA PODPORO NOVIM TERAPIJAM GLIOBLASTOMA

Doktorska disertacija

Supervisor: Prof. Dr. Tamara Lah Turnšek

Co-Supervisor: Dr. Metka Novak

Ljubljana, Slovenia, December 2022

To my love, family and friends.

Acknowledgments

This PhD has been a truly life-changing experience for me and would not have been possible without the support and guidance I have received from many people.

First of all, I would like to thank my supervisor Prof. Dr. Tamara Lah Turnšek for giving me the opportunity to work in her research group in the Department of Genetic Toxicology and Cancer Biology at the National Institute of Biology in Ljubljana. I am grateful for her immense knowledge, valuable advice, professional lectures, discussions, and support during my PhD training. I would also like to thank her for revising and proofreading this dissertation and all other manuscripts.

I am exceptionally grateful to my co-supervisor Dr. Metka Novak for her patience, motivation, and guidance during my dissertation. I would also like to thank her for all the encouraging and positive advice and discussions, as well as for all the manuscript revisions and corrections of this thesis.

I would like to thank Assoc. Prof. Dr. Bojana Žegura, the head of the Department of Genetic Toxicology and Cancer Biology, for giving me the opportunity to continue our research work at the department.

I am grateful to the members of the evaluation committee: Prof. Dr. Kristina Gruden, Prof. Dr. Janko Kos, and Asst. Prof. Marija Skoblar Vidmar MD, for reviewing this dissertation.

This dissertation would not be possible without our collaboration with medical doctors at the Faculty of Medicine and the University Clinical Centre in Ljubljana. I would like to thank pathologist Jernej Mlakar at the Institute of Pathology, Faculty of Medicine, for providing us with paraffin-embedded tumour sections. I also thank neurosurgeons Andrej Porčnik and Prof. Dr. Roman Bošnjak from the Department of Neurosurgery, University Clinical Centre Ljubljana, for providing tumour tissue samples and information about the patients. I would also like to thank oncologist Asst. Prof. Marija Skoblar Vidmar for providing us with oncological data.

I would like to thank Prof. Dr. Janko Kos and Assoc. Prof Anja Pišlar from The Faculty of Pharmacy for our collaboration on cathepsin X research.

I am also grateful to Marta Malavolta and Doc. Dr. Aleksander Sadikov from the Faculty of Computer and Information Science for data analysis.

I would like to extend my sincere thanks to Doc. Dr. Miloš Vittori for the scanning electron microscopy results and Prof. Dr. Cornelis Van Noorden for valuable discussions and advice.

I would like to thank my "Rakice" colleagues Barbara B., Anamarija H. and Mateja M., for their unselfish help and fruitful discussions, and other GENious, Martina Š., Alja Š., Matjaž N., Katja K., Tina E., Maša Z., Anže S., Jelka P., Karmen S., and Mojca D. in creating a pleasant and friendly atmosphere at NIB.

This doctoral dissertation was funded by the Slovenian Research Agency, Programme P1-0245 (»Ecotoxicology, toxicogenomics and carcinogenesis«, National Institute of Biology, Ljubljana (2019-2024), PI Assist. Prof. Bojana Žegura), ARRS Young Researcher grant (51984) dedicated to PhD training of Bernarda Majc (2018-2022), Project of

European Programme of Cross-Border Cooperation for Slovenia-Italy (Interreg) TRANS-GLIOMA and Contract Research Grant by MGC Pharmaceuticals Ltd "Diagnostic platform for precision cannabinoids treatment of cancer patients", PI Prof. Tamara Lah Turnšek, NIB (2019-2022).

I would like to thank my family, my mother, my father, my sister Meta and my nieces for their support and love, as well as my friends who have encouraged me on this journey and for all the beautiful and fun moments we have spent together.

And finally to Blaž, who has been by my side throughout this PhD, living every single minute of it, and without whom, I would not have had the courage to start this journey in the first place. For his endless love and support.

Abstract

Glioblastoma (GB) is the most common and aggressive primary tumour of the central nervous system. Despite maximal possible surgical resection of the tumours and aggressive treatment regimens with radiotherapy and chemotherapy, patient overall survival is less than 2 years, as patients eventually develop resistance to therapy, resulting in recurrent tumours. The main challenges of therapeutic failure are based on the infiltrative growth of the tumour into the brain parenchyma, the presence of a small population of therapy-resistant GB stem cells (GSCs), and extensive inter- and intra-tumour heterogeneity. Cancer models that efficiently represent the complexity of the tumour are therefore crucial in the era of precision medicine.

The establishment of a standardized tissue bank of high-quality biospecimens annotated with clinical information is central for reliable translational research. We contributed glioma samples to the Slovenian GlioBank, containing glioma tissue samples, cell models, and corresponding clinical data for use in cancer research. We used GB differentiated cells and GSCs as models to screen for the efficacy of the cannabinoids delta-9-tetrahydrocannabinol (THC), cannabidiol (CBD), and cannabigerol (CBG) on cell viability and invasion. CBG effectively impaired the relevant hallmarks of GB progression, with comparable cytotoxic effects to THC, but with the additional ability to inhibit GB cell invasion. Moreover, CBG could target therapy-resistant GSCs, which are the root of cancer development and extremely resistant to various other treatments. Thus, CBG could represent a new yet unexplored adjuvant treatment strategy for GB.

We established a novel 3D *in vitro* model of GB organoids (GBOs) prepared from patient-derived tumours that represents a more clinically relevant tumour model. The GBOs, unlike the previously used 3D GB cells and GSCs, capture the entire tumour microenvironment. The intra- and inter-tumour heterogeneity of *in vivo* tumours (including variable transcriptional profiles and cellular compositions) was thus preserved in GBOs. We demonstrated that GBOs from most of the patients were resistant to irradiation and chemotherapy with temozolomide, as no significant effects on GBO viability or invasion were observed. Further analyses revealed that certain target genes were differentially expressed in the treated GBOs, such as E3 ubiquitin-protein ligase (*MDM2*) and cyclin-dependent kinase inhibitor 1A (*CDKN1A*). Both genes are involved in the DNA damage response and cell cycle signalling pathways. Our results implicate on activation of p53-related pathways in the tumour microenvironment (TME) of GB tumours and shed light on possible mechanisms underlying the resistance of GB to therapy. GBOs can represent a novel, clinically-relevant culture system for evaluating specific responses of GB patients to therapy and have the potential to change drug and novel biomarker discoveries.

Discovering novel therapeutic targets is critical for developing efficient treatments. We explored the role of the novel potential biomarker cathepsin X in GB progression. Cathepsin X expression and activity were found to be upregulated in human GB tissues compared to low-grade gliomas and nontumour brain tissues. Cathepsin X was localised in GB cells and tumour-associated macrophages and microglia. Subsequently, potent, selective, irreversible (AMS36) and reversible (Z7) cathepsin X inhibitors were tested *in*

vitro. These inhibitors decreased the viability of patient-derived GB cells. Furthermore, there was a correlation between the high proteolytic activity of cathepsin X and C-terminal cleavage of neuron-specific enzyme γ-enolase, a target of cathepsin X. Cathepsin X and γ-enolase were colocalised in GB tissues, preferentially in GB-associated macrophages and microglia. Taken together, our results on patient-derived tissues and cells suggest that cathepsin X plays a role in GB progression and as such is a potential target for therapeutic approaches against GB.

Overall, this work contributes to the establishment of a platform for basic and translational research in the field of neuro-oncology and to a deeper understanding of the pathobiology and therapeutic resistance of GB.

.

Povzetek

Glioblastom (GB) je najpogostejši in najagresivnejši primarni tumor osrednjega živčnega sistema. Kljub maksimalni kirurški odstranitvi tumorjev in agresivnim režimom zdravljenja z radioterapijo in kemoterapijo je skupno preživetje bolnikov manj kot dve leti, saj bolniki sčasoma razvijejo odpornost na terapijo, kar povzroči ponovitev tumorja. Glavni izzivi terapevtskega neuspeha temeljijo na invazivni rasti tumorja v možganski parenhim, prisotnosti majhne populacije proti terapiji odpornih matičnih celic GB (GSC) in obsežni heterogenosti med in znotraj posameznega tumorja. Modeli raka, ki učinkovito predstavljajo kompleksnost tumorja, so zato ključni v dobi precizne medicine in medicine po meri posameznika.

Vzpostavitev standardizirane tkivne banke kakovostnih bioloških vzorcev, vključno s kliničnimi podatki, je osrednjega pomena za zanesljive translacijske raziskave. V sklopu slovenske GlioBanke zbiramo vzorce glioma, ki vključujejo vzorce tkiv, celične modele in ustrezne klinične podatke za uporabo pri raziskavah raka. V naših raziskavah smo na bolnikovih diferenciranih celicah GB in celicah GSC testirali učinkovitost kanabinoidov, delta-9-tetrahidrokanabinola (THC), kanabidiola (CBD) in kanabigerola (CBG) na sposobnost preživetja in invazijo celic GB. Ugotovili smo, da je CBG učinkovito vplival na znake napredovanja GB, s primerljivimi citotoksičnimi učinki kot THC, vključno s sposobnostjo zaviranja invazije celic GB. Poleg tega smo pokazali, da bi lahko s CBG ciljali na terapijo odporne celice GSC, ki so vzrok za razvoj raka in so izjemno odporne na različna druga zdravljenja. Tako bi lahko CBG predstavljal novo, še neraziskano strategijo adjuvantnega zdravljenja GB.

Vzpostavili smo nov 3D *in vitro* model organoidov GB (GBO), pripravljenih iz tumorjev bolnikov, ki predstavlja klinično pomemben model v raziskavah raka. GBO, za razliko od 3D GB celic in celic GSC, ohranjajo celotno tumorsko mikrookolje (TME). Pokazali smo, da je heterogenost, tako med tumorji in znotraj tumorja (vključno s spremenljivimi transkripcijskimi profili in celično sestavo), v modelu GBO ohranjena. Dokazali smo, da so bili GBO pri večini bolnikov odporni na obsevanje in kemoterapijo s temozolomidom, saj nismo opazili pomembnih učinkov na sposobnost preživetja ali invazijo GBO. Nadaljnje analize so pokazale, da so bili nekateri ciljni geni različno izraženi v GBO, izpostavljenih standardni terapiji, kot sta E3 ubikvitinska ligaza (*MDM2*) in od ciklina odvisni inhibitor kinaze 1A (*CDKN1A*). Oba gena sta vključena v odziv na poškodbe DNK in signalne poti celičnega cikla. Naši rezultati kažejo na aktivacijo poti, povezanih s p53, v tumorjih GB in osvetljujejo možne mehanizme, na katerih temelji odpornost GB na terapijo. GBO lahko predstavljajo nov, klinično pomemben sistem za ocenjevanje specifičnih odzivov bolnikov z GB na terapijo in lahko prispevajo k odkritju novih zdravil in bioloških označevalcev.

Odkrivanje novih terapevtskih tarč je ključnega pomena za razvoj učinkovitega zdravljenja. Raziskali smo vlogo novega potencialnega biološkega označevalca katepsina X pri napredovanju GB. Ugotovili smo, da sta izražanje in aktivnost katepsina X povečana v tkivih GB v primerjavi z gliomi nizke stopnje in netumorskimi možganskimi tkivi. Katepsin X se je izražal v celicah GB in tumorskih makrofagih in mikrogliji. Testirali smo učinkovitost selektivnih, ireverzibilnih (AMS36) in reverzibilnih (Z7) zaviralcev katepsina

X. Delovanje zaviralcev je zmanjšalo sposobnost preživetja bolnikovih celic GB. Poleg tega smo pokazali korelacijo med visoko proteolitično aktivnostjo katepsina X in C-terminalno cepitvijo nevronsko specifičnega encima γ-enolaze, tarče katepsina X. Katepsin X in γ-enolaza sta se izražala v tkivih GB, predvsem v makrofagih in mikrogliji. Naši rezultati na tkivih in bolnikovih celicah kažejo na vlogo katepsina X pri napredovanju GB, ki je kot tak potencialna tarča za terapevtske pristope proti GB.

Na splošno to delo prispeva k vzpostavitvi platforme za temeljne in translacijske raziskave na področju nevroonkologije ter k globljemu razumevanju patobiologije in terapevtske odpornosti GB.

Contents

List of Figures

List of Tables

Abbreviations

2D	... Two-dimensional
3D	... Three-dimensional
ACSBG1	... Acyl-CoA Synthetase Bubblegum Family Member 1
AIF1	... Allograft inflammatory factor 1
ATM	... Ataxia telangiectasia mutated
ATR	... Ataxia telangiectasia and Rad3 related
BAX	... Bcl-2-like protein 4
BCL2	... B-cell lymphoma 2
CBD	... Cannabidiol
CBG	... Cannabigerol
CCL2	... Monocyte chemoattractant protein-1 (MCP-1)
CCL5	... Chemokine (C-C motif) ligand 5
CD15 (FUT4)	... Fucosyltransferase 4
CD44	... CD44 molecule
CD68	... CD68 Molecule
CD9	... CD9 antigen
CDH1	... Cadherin 1
CDK4	... Cyclin Dependent Kinase 4
CDKN1A	... Cyclin Dependent Kinase Inhibitor 1A
CDKN2A	... Cyclin Dependent Kinase Inhibitor 2A
CHEK1	... Checkpoint Kinase 1
CHI3L1	... Chitinase-3-like protein 1; YKL-40
COL1A1	... Collagen Type I Alpha 1 Chain
COL1A2	... Collagen Type I Alpha 2 Chain
CTSZ	... Cathepsin X
CXCL12	... C-X-C motif chemokine 12 (SDF-1)
CXCR4	... C-X-C chemokine receptor type 4
DAB2	... DAB Adaptor Protein 2
ECM	... Extracellular matrix
EGF	... Epidermal growth factor
EGFR	... Epidermal growth factor receptor
EMT	... Epithelial-to-mesenchymal transition
ERBB3	... Erb-B2 Receptor Tyrosine Kinase 3
FCGR3A	... Fc Gamma Receptor IIIa
FGF	... Fibroblast growth factor
FOXP3	... Forkhead box P3

FUT4 ... Fucosyltransferase 4
GAPDH ... Glyceraldehyde 3-phosphate dehydrogenase
GB ... Glioblastoma
GBOs ... GB organoids
GFAP ... Glial Fibrillary Acidic Protein
GPR55 ... G Protein-Coupled Receptor 55
GSCs ... GB stem cells
hESC ... Human embryonic stem cell
HPRT1 ... Hypoxanthine Phosphoribosyltransferase 1
ID1 ... Inhibitor Of DNA Binding 1
IDH ... Isocitrate Dehydrogenase
IDO1 ... Indoleamine 2,3-Dioxygenase 1
IL6 ... Interleukin 6
IR ... Irradiation
KCNF1 ... Potassium Voltage-Gated Channel Modifier Subfamily F Member 1
MDM2 ... E3 ubiquitin-protein ligase
MGMT ... O^6-methylguanine-DNA methyltransferase
MMP ... Matrix metalloprotease
MTOR ... Serine/threonine-protein kinase mTOR
NANOG ... Nanog Homeobox
NCAM1 ... Neural Cell Adhesion Molecule 1
NF1 ... Neurofibromin 1
NF-KB ... Nuclear factor-kappa B
NOTCH1 ... Neurogenic locus notch homolog protein 1
OLIG2 ... Oligodendrocyte Transcription Factor 2
P2RX7 ... Purinergic Receptor P2X 7
PDGFRA ... Platelet-derived growth factor receptor alpha
PIK3CA ... Phosphatidylinositol-4,5-Bisphosphate 3-Kinase Catalytic Subunit Alpha
POU3F2 ... Octamer-Binding Transcription Factor 7
POU5F1B ... POU Class 5 Homeobox 1B; OCT4-PG1 (OCT4 pseudogene)
PROM1 ... Prominin-1; CD133 antigen
qRT-PCR ... Quantitative real-time polymerase chain reaction
S100A4 ... S100 Calcium Binding Protein A4
SALL1 ... Spalt Like Transcription Factor 1
SNAI1 ... Snail Family Transcriptional Repressor 1
SOX10 ... SRY-Box Transcription Factor 10
SOX2 ... SRY-Box Transcription Factor 2
STAT3 ... Signal Transducer And Activator Of Transcription 3
STMN4 ... Stathmin 4
TAM ... Tumour-associated macrophages
TCGA ... The Cancer Genome Atlas
TERT ... Telomerase reverse transcriptase
TGFBI ... Transforming growth factor beta 1

THBS1	...	Thrombospondin 1
THC	...	Δ9-tetrahydrocannabinol
TME	...	Tumour microenvironment
TMZ	...	Temozolomide
TRPV1	...	Transient Receptor Potential Cation Channel Subfamily V Member 1
TUBB3	...	Tubulin Beta 3 Class III
WHO	...	World Health Organization

Chapter 1

Introduction

As the most aggressive and common primary brain tumour in adults, glioblastoma (GB) responds poorly to standard therapy and has one of the shortest patient survival rates among all cancers. Successful treatment of GB remains one of the most difficult challenges in the treatment of brain tumours. This is partly due to the presence of a small population of therapy-resistant GB stem cells (GSCs) and partly due to inter-tumour and intra-tumour heterogeneity, represented by three GB subtypes and the presence of different stromal cells. New cancer therapies, including immunotherapy, account for up to 90% of failed clinical trials. Failure of preclinical studies in subsequent clinical trials can also be attributed to the lack of appropriate preclinical models that do not mimic the complexity of GB tumours and a lack of understanding of GB biology. Compared to cancer cell monocultures, GB organoids (GBOs) represent advanced *in vitro* models, in which a complex microenvironment is preserved, thereby representing a preclinical model that better mimics responses to *ex vivo* therapy. Organoids could thus reduce the number of animal models, increase the success of preclinical studies, and thus bridge the gap between cell models and clinical trials. GBO models derived from patient tumours also represent a step towards novel therapeutic discoveries for targeted treatment tailored to individuals. Importantly, there is also a lack of reliable biomarkers and drug targets associated with GB disease progression. Identifying new biomarkers would thus enable more effective strategies for treating GB patients and preventing disease relapse.

The overview of our research in GB is shown in Figure 1.

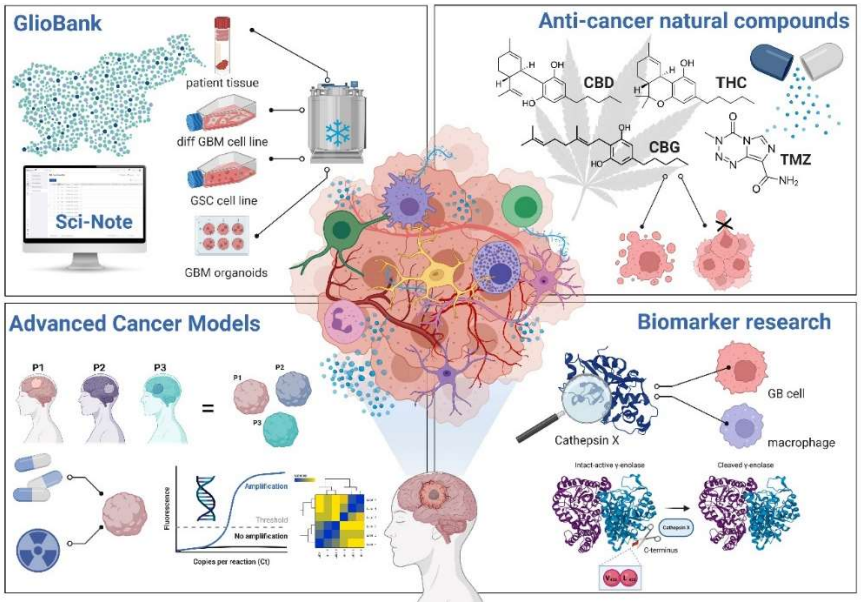

Figure 1: Overview of our research work on glioblastoma (GB). We have contributed to the establishment of the Slovenian biobank (GlioBank) containing glioma samples, GB cell models, and corresponding clinical data; tested cannabinoid extracts on GB cell models and showed their potential cytotoxic and anti-invasive properties in GB; established GB organoids (GBOs) that mimic the patient's TME to model and explore the therapeutic resistance of GB to standard therapy; revealed the role of cathepsin X in GB progression.

1.1 Glioblastoma (GB)

GB is the most common type of malignant primary brain tumour, with a 5-year relative overall survival rate of only 6.8%, which varies according to the sex and age of the patient at diagnosis (Wen et al., 2020). The incidence of GB in the United States is 3.22/100 000 persons (Wen et al., 2020), and the number of newly diagnosed patients with malignant gliomas in Slovenia was 148 cases in 2019 (*Rak v Sloveniji Cancer in Slovenia*, n.d.). According to the World Health Organization (WHO) 2021 classification of central nervous system tumours, GB is defined as diffuse astrocytic glioma without mutations in isocitrate dehydrogenase (IDH) and with features of microvascular proliferation and necrosis. It has unique molecular features, such as a telomerase reverse transcriptase (*TERT*) promoter mutation, epidermal growth factor receptor (*EGFR*) gene amplification, and a +7/–10 cytogenetic signature (Weller et al., 2020). Although the biology of these cancers has become better understood, there have been no appreciable advances in treatments or patient outcomes. With the standard-of-care therapy for newly diagnosed patients introduced in 2005 (Stupp et al., 2005), which includes maximal surgical resection followed by radiotherapy (60 Gy in 30 fractions) with concomitant daily treatment with the alkylating agent temozolomide (TMZ), the median overall survival is only 15−18 months. Radiation (IR) causes a series of DNA lesions leading to DNA strand breaks. If these are not repaired by the DNA damage response mechanism, cells undergo cell cycle arrest, which leads to apoptosis (Gousias, Theocharous, & Simon, 2022). TMZ passes the blood-brain barrier and methylates DNA at specific sites on guanine and adenine bases, forming O^6-methylguanine DNA adducts that cause double-strand breaks in the DNA, disrupting subsequent DNA replication, arresting the cell cycle in G2/M phase, and eventually activating the apoptosis pathway (Thomas, Recht, & Nagpal, 2013).

O^6-methylguanine-DNA methyltransferase *(MGMT)* promoter methylation has limited diagnostic relevance in GB patients, although enables the prediction of the benefit of alkylating agents. The median survival of GB patients with *MGMT* promoter methylation receiving TMZ is approximately 50% longer than that with unmethylated *MGMT* (Stupp et al., 2005). Besides TMZ, alkylating agents from the nitrosourea class, such as lomustine, are used to treat GB progression or recurrence (Weller et al., 2020). In addition to standard treatment options, monoclonal antibodies such as bevacizumab, which targets vascular endothelial growth factor (VEGF) in *MGMT* promoter-unmethylated recurrent GB, are frequently but unsuccessfully used to prevent angiogenesis. Following such treatment, increased GB cell invasion has been noted, usually caused by the creation of hypoxic zones within the tumour, leading to the ineffectiveness of bevacizumab (Wick et al., 2017).

Additional treatment options for combined therapeutic options are becoming an attractive strategy for the treatment of cancer (Deshaies, 2020). One of these are cannabinoids, such as Δ9-tetrahydrocannabinol (THC), cannabidiol (CBD), and cannabigerol (CBG), terpenophenolic compounds from the cannabis plant that exhibit anticancer activity and have low toxicity compared to chemotherapeutic agents (Afrin et al., 2020). Cannabinoids have already been tested in several clinical trials for GB, either alone or in combination with standard therapy. Natural or synthetic THC alone or in combination with TMZ in patients with recurrent GBs was used in clinical trials CT-NCT01812603 and CT-NCT01812616, CBD alone in CT-NCT02255292, and an equimolar THC:CBD combination drug (e.g. Sativex) in CT-NCT01812603. THC has been shown to induce cancer cell apoptosis and cytotoxicity by primarily binding to the cannabinoid receptors CB1 and CB2, both of which are abundant in GBs (Massi et al., 2006; Pertwee et al., 2010; Torres et al., 2011). Non-THC cannabinoids also affect the activation of G protein-coupled receptors (e.g. GPR55, GPR3, GPR6, and GPR12), vanilloid transient receptor potential channels (e.g. TRPV1/2 and TRPM8), and peroxisome proliferator-activated receptor alpha (De Petrocellis et al., 2013; De Petrocellis, Nabissi, Santoni, & Ligresti, 2017; Lah et al., 2022; Nabissi, Morelli, Santoni, & Santoni, 2013) CBD and THC in combination showed "synergistic" effects in GB by reducing viability and promoting apoptosis in GB cancer cells (Doherty & de Paula, 2021). CBG has been shown to inhibit cell proliferation in several cancer cell lines, including human breast (Ligresti et al., 2006; McAllister, Christian, Horowitz, Garcia, & Desprez, 2007), prostate, and colorectal carcinomas, gastric adenocarcinomas, C6 rat gliomas, rat basophilic leukaemia, and transformed thyroid cells, as reviewed by Ligresti et al. (Ligresti, De Petrocellis, & Di Marzo, 2016). However, no effect on GB has been demonstrated to date.

1.2 GB Heterogeneity

GBs are characterized by their extensive inter-tumour (between patients) and intra-tumour (within one patient) heterogeneity. Based on the bulk expression analyses of DNA copy number, gene expression, and methylation status, The Cancer Genome Atlas (TCGA) divided GBs into three main subtypes: proneural (PN), classical (CL), and mesenchymal (MES) (Behnan et al., 2016; Verhaak et al., 2010). Specific genomic alterations define each of the subtypes: *PDGFRA* (platelet-derived growth factor receptor alpha), *OLIG2*, *TCF3*, and *IDH* mutations define PN, *EGFR* (epidermal growth factor receptor) alterations define CL, and neurofibromin 1 deletions define MES (Verhaak et al., 2010). According to Behnan et al. (Behnan et al., 2016), subtypes can be determined based on the expression of specific genes. The PN subtype was determined by the expression levels of the genes *OLIG2, P2RX7, STMN4, SOX10, NOTCH*, and *ERBB3*. The CL subtype was defined by the expression levels of *NF-KB, ACSBG1, S100A4*, and *KCNF1*. The MES subtype was

defined by the expression levels of *DAB2, TGFB1, THBS1, COL1A2*, and *COL1A1*. Originally, GB subtypes showed different prognostic and therapeutic implications, with the MES subtype being the most aggressive and linked with the poorest prognosis (Ehman et al., 2017). Such subtyping could lead to more targeted treatments that focus on a specific pathway relevant to the specific subtype. In addition to the aforementioned subtypes, PN, MES, and CL (Behnan et al., 2016), Neftel et al. (Neftel et al., 2019) described four cellular states of GB, namely the astrocyte-like, oligodendrocyte precursor-like, neural progenitor-like, and mesenchymal-like states. Cellular states are characterized by the amplifications of *EGFR* for the astrocyte-like, *CDK4* for the neural progenitor cell-like, *PDGFRA* for the oligodendrocyte precursor cell-like, and mutations in *NF1* for the mesenchymal-like state. These genetic alterations define the identity of the cellular states. Nevertheless, GB cells exhibit inherent phenotypic plasticity and transition between states (Neftel et al., 2019) that is driven by environmental factors, such as interactions with immune cells and response to therapy (Hara et al., 2021; Schmitt et al., 2021).

1.3 Glioblastoma Stem Cells

The small population of GB cells with stem-like characteristics (GSCs) represents another layer of GB heterogeneity (Lathia, Mack, Mulkearns-hubert, Valentim, & Rich, 2015) and is considered to drive GB development. The main characteristics of cancer stem cells, including GSCs, are self-renewal and tumour-initiating properties. In addition, these cells are characterized by their quiescent phase, in which proliferation slows down and DNA synthesis is reduced (Recasens & Munoz, 2019). This allows the cells to become resistant to chemotherapy and radiotherapy, evading the immune system and promoting tumour recurrence (Lathia et al., 2015). GSC radio- and chemoresistance is also promoted by active DNA repair capacity and overexpression of ATP-binding cassette transporters that pump out a variety of xenobiotic and toxic compounds, including anticancer agents (Rama, Alvarez, Madeddu, & Aranega, 2014). Another highly relevant characteristic is the specific location of GSCs in so-called "niches" within primary tumours (Hira et al., 2019). The GSC niche is a complex microenvironment that consists of various so-called stromal cell types, such as endothelial, immune, and mesenchymal stem cells. Intercellular communication between tumours and stromal cells maintains GSCs in a quiescent state or stimulates proliferation and differentiation, protecting GSCs from therapy and immune surveillance (Borovski, De Sousa E Melo, Vermeulen, & Medema, 2011; Prager, Xie, Bao, & Rich, 2019).

GSCs are regulated by several transcriptional regulators, including SOX2, OLIG2, SALL1, NANOG, and POU3F2. These cells are also characterized by the expression of cell surface markers with varying degrees of selectivity, including prominin-1 (CD133), CD44, inhibitor of differentiation protein 1 (ID1), and Lewis x (CD15) (Lathia et al., 2015). In addition, the transmembrane protein CD9 has been proposed as a selective GSC marker that can distinguish between GSCs and normal neural stem cells (Podergajs et al., 2015). None of these markers are fully sensitive or specific to stem cell populations, as there are multiple states of GSCs (which also contribute to the cellular heterogeneity of GBs).

1.4 The Tumour Microenvironment

Malignant brain tumours are a complex ecosystem composed of various neoplastic and stromal components (Gimple, Yang, Halbert, Agnihotri, & Rich, 2022). In addition to tumour cells, GB tumour lesions contain a mixture of various brain-resident and infiltrating

cells, including immune cells, endothelial cells, astrocytes, and neurons, as well as extracellular matrix (ECM) (Khaddour, Johanns, & Ansstas, 2020).

The GB tumour microenvironment (TME) is defined as immunologically 'cold', signifying that it lacks effector lymphocytes and is infiltrated with large amounts of suppressive myeloid cells and regulatory T cells (Majc, Novak, Jerala, Jewett, & Breznik, 2021). Recent advances in molecular profiling revealed that among non-neoplastic cells in GB, the innate immune compartment represents 39% of the cell population (Ruiz-Moreno et al., 2022). Innate immune cells that are most represented in the GB TME are dendritic cells and tumour-associated macrophages (TAMs) (Ruiz-Moreno et al., 2022). TAMs generally represent a major component of myeloid cells in tumours and are subdivided into blood-derived macrophages, which account for 85% of total TAMs, and tumour-resident microglia, which account for the remaining 15%. Historically, macrophages have been divided into M1 (proinflammatory or tumour-suppressive) and M2 (anti-inflammatory or tumour-supportive) macrophages, depending on their polarisation status. However, upon closer examination of the population, it is very likely that it is composed of heterogeneous subpopulations of macrophages. The macrophage population can now be divided into protumour macrophages and antitumour macrophages (Ma, Chen, & Li, 2021). TAMs are thought to promote carcinogenesis and cancer progression by stimulating tumour-associated angiogenesis, promoting cell metastasis and resistance to chemotherapeutic agents, and suppressing antitumour immune responses (X. Li et al., 2019).

Immune cell populations include tumour-infiltrating lymphocytes, which account for 17% of the cell population in GB and are composed of CD4+/CD8+ T cells, NK cells, B/plasma, and mast cells (Ruiz-Moreno et al., 2022). These cell populations are dysfunctional, exhibiting exhaustion, anergy, or senescence, characteristics promoted by GB cells, TAMs, and regulatory T cells (Antunes et al., 2020; Woroniecka et al., 2018).

Vascular cells represent 1% of non-neoplastic cells (Ruiz-Moreno et al., 2022) and consist of endothelial cells, smooth muscle cells, and pericytes. Vascularization is a very important feature of GBs, as they supply GB cells with nutrients and oxygen. Blood vessels are also involved in evasion of the tumour immune system, changes in the ECM, and activation of stem cells, all of which contribute to tumour resistance to therapy and poor patient survival (Pacheco et al., 2022). Among non-neoplastic cells, neurons, which constitute 5% of the GB TME, have been shown to interact with GB cells and promote GB growth and aggressiveness (Venkatesh et al., 2019). All these key players in the TME provide GB with important proliferative signals that promote tumour progression.

1.5 GB Invasion

Diffuse infiltration of GB cells into the soft brain parenchyma tissue makes complete surgical resection impossible and is another hallmark of GB and a reason for the inevitable recurrence of GB after standard therapy. GB cells invade along pre-existing structures, such as blood vessels and nerve and astrocytic tracts, and through the ECM (Cuddapah, Robel, Watkins, & Sontheimer, 2014). There are different types of GB invasion: amoeboid and mesenchymal. The main difference between these migration modes is the attachment to the surrounding ECM mediated by integrins and the involvement of proteolytic degradation of the ECM in the mesenchymal migration mode (Talkenberger, Ada Cavalcanti-Adam, Voss-Böhme, & Deutsch, 2017).

The essential mechanism controlling invasion is the epithelial-to-mesenchymal transition (EMT), which occurs when cells lose polarity, cell-cell adhesion, and cell surface and cytoskeletal protein expression, giving them the ability to migrate (Majc et al., 2020) into the brain tissue in the case of GB. An important factor for GB cell invasion is the

composition of the brain's ECM, which mainly consists of hyaluronic acid, proteoglycans, and glycoproteins (Moretto, Stuart, Surana, Vargas, & Schiavo, 2022). The vascular components of the ECM contain collagen IV, laminin, fibronectin, and proteoglycans (Goldbrunner, Bernstein, & Tonn, 1999). This composition is under tight control under physiological conditions, whereas in cancer, it is dysregulated and contributes to invasion and metastasis. Invasion is associated with an increased ability to degrade the ECM through protease activity (Hatoum, Mohammed, & Zakieh, 2019).

The proteases involved in this process are cysteine cathepsins (Lah, Durán Alonso, & Van Noorden, 2006), urokinase-type plasminogen activators (Gondi et al., 2004), and matrix metalloproteases (MMPs) (Q. Li et al., 2016). MMPs are important proteases involved in ECM degradation. Their expression and activity correlate with poor prognosis of cancer patients (Deryugina et al., 2001). MMP2 and MMP9 have been shown to be overexpressed in GB tumours and correlate with GB progression (M. Wang, Wang, Liu, Yoshida, & Teramoto, 2003). Similarly, urokinase-type plasminogen activators contribute to cancer cell migration and invasion by directly degrading ECM or activating other MMPs (Blasi & Carmeliet, 2002). Overexpression of plasminogen activator inhibitor-1 (PAI-1) has been associated with poor prognosis and shortened survival in GB patients (Colin et al., 2009). The final protease group involved in cell invasion are cysteine cathepsins, which are described in detail in Section 1.6.

1.6 GB-Associated Proteases: Cathepsins

In the human genome, 884 genes encode proteases ("MEROPS - the Peptidase Database," n.d.), which are classified into five major classes based on their catalytic processes: serine, cysteine, threonine, and asparagine proteases and metalloproteases (Rawlings et al., 2018). The activity of proteases is tightly regulated under normal physiological conditions by gene expression, protein expression, posttranslational modifications, protein activation, inter-/intracellular trafficking, and the presence of selective endogenous protease inhibitors (Habič, Novak, Majc, Lah Turnšek, & Breznik, 2021). Dysregulated proteolytic activity can lead to pathological conditions, including cancer (Mason & Joyce, 2011; Vizovisek, Ristanovic, Menghini, Christiansen, & Schuerle, 2021). In the TME, proteases are involved in ECM degradation that enhances cancer cell invasion. In addition, proteases control other processes in cells, such as the activation of growth factors, cytokines, cell surface receptors, and adhesion molecules and the modulation of intracellular signalling pathways (Breznik, Motaln, & Turnšek, 2017; Kessenbrock, Plaks, & Werb, 2010; Vizovisek et al., 2021).

One of the most important protease groups are cathepsins, which belong to the C1A papain superfamily of cysteine peptidases that includes 11 members (cathepsins B, C, F, H, K, L, O, S, V, W, and X). Most of them have endopeptidase activity that cleaves peptide bonds within polypeptide chains. Others have carboxy-exopeptidase activity (cathepsins B and X) and amino-exopeptidase activity (cathepsins C and H) that cleaves their substrates at the C- and N-terminus, respectively (Kos, Vižin, Fonović, & Pišlar, 2015). Cathepsins are involved in intracellular protein catabolism (Turk et al., 2012) and are primarily expressed in endosomes and lysosomes. Under pathological conditions, cathepsins may be present in the nucleus or are released into the cytoplasm or extracellularly (Brix, Dunkhorst, Mayer, & Jordans, 2008). The expression of lysosomal cysteine cathepsins is often increased in malignant tumours and is usually associated with poor patient prognosis (Olson & Joyce, 2015). Cathepsins have been found to promote tumour development, invasion, and treatment resistance (Olson & Joyce, 2015; Rudzińska et al., 2019), but some of them also contribute to tumour suppression (Benavides et al., 2012; Dennemärker et al., 2009; Lah et al., 2006; López-Otín & Matrisian, 2007),. In the

TME, not only cancer cells, but also stromal cells, such as fibroblasts, neutrophils, mast cells, T cells, endothelial cells, and TAMs, express cathepsins, playing specific roles in cancer and antitumour immune responses (Olson & Joyce, 2015).

In our previous studies, we discovered high expression of cathepsin X (a cysteine carboxy-peptidase) in GB and its localisation in perivascular GSC niches; however, its function remained unknown (Breznik et al., 2018). Primarily, cathepsin X is expressed in immune cells, including macrophages, monocytes, and dendritic cells (Kos et al., 2015), suggesting its role in immune cell maturation, proliferation, migration, adhesion, and signal transduction (Dolenc et al., 2021; Kos et al., 2005). Moreover, it has also been found in brain glial cells, neurons, oligodendrocytes, and ependymal cells (Hafner et al., 2013; Kos et al., 2005, 2015; Pišlar & Kos, 2014; Stichel & Luebbert, 2007). Higher levels of cathepsin X have been associated with other cancers and is likely to be involved in tumour growth pathways leading to alterations in cellular processes such as cell proliferation and invasion. Cathepsin X is also implicated in neurodegeneration (Pišlar et al., 2020; Stichel & Luebbert, 2007) as it is involved in cleaving the C-terminal end of its target substrate γ-enolase (Nataša Obermajer, Doljak, Jamnik, Pečar Fonović, & Kos, 2009). γ-enolase or neuron-specific enolase is an enzyme of the glycolytic pathway found mainly in neurons and cells of the neuroendocrine system. Another catalytic site of γ-enolase, which is not involved in the glycolytic pathway, plays a role in neurotrophic activity that promotes neuronal growth, survival, and differentiation and is regulated by cathepsin X cleavage. In this doctoral dissertation, we have highlighted a possible role of cathepsin X, involved in modifying γ-enolase, in brain and GB pathophysiology.

1.7 GB *In Vitro* Models (From Patient-Derived Cell Lines to Organoids)

GBs are extremely diverse in terms of cellular composition, gene expression, and clinical features (Marusyk & Polyak, 2010). The development of clinically relevant models that accurately represent tumour complexity is necessary to fully comprehend GB characteristics, imitate their distinct therapeutic responses, and thus enable individualized therapy.

1.7.1 Established versus Patient-Derived Cell Lines

Cancer cell lines are valuable *in vitro* model systems commonly used in cancer research and drug discovery (Mirabelli, Coppola, & Salvatore, 2019). The first established human cancer cell line (HeLa) from the cervical cancer patient Henrietta Lacks dates back to 1951 (Lucey, Nelson-Rees, & Hutchins, 2009). To date, significant improvements have been made to the 2D cell culturing technique. There are many advantages to using established cell lines, for instance, they are easy to maintain, inexpensive, and represent a pure population of cells, which is important for obtaining reproducible results, when used with a well-established protocol (van Staveren et al., 2009). In contrast to established cell lines, primary cells are isolated directly from patient tissues and retain the morphological and functional characteristics of their tissue of origin; however, they have limited potential for self-renewal and differentiation. For decades, cell lines have provided valuable insight into tumour development and its underlying mechanisms; however, caution is needed when interpreting results from cell lines alone. Established and primary patient-derived cancer cells lack certain critical aspects, such as the effect of stromal cells, the TME, and phenotypic and genetic heterogeneity (Xu et al., 2018), which all contribute to cell proliferation, differentiation, and survival (Eke & Cordes, 2011). The assumption that *in*

vitro cell line responses have not been able to predict human responses has led to the development of new cancer models.

1.7.2 GSC Spheroids

In comparison to conventional 2D tumour cell cultures, 3D models of cancer stem cells incorporate the cellular heterogeneity of tumours, increase the predictability of drug responses, improve therapeutic response prediction, and thus serve as superior models for the development of novel anticancer drug targets (Saygin, Matei, Majeti, Reizes, & Lathia, 2019). GSC tumourspheres are models produced by symmetric and asymmetric divisions of patient-derived GSCs in a specific medium enriched with growth factors, such as epidermal growth factor (EGF), fibroblast growth factor (FGF)-2, and neuronal viability supplement B27 (Lee et al., 2006). These components, as well as the absence of serum, are required to maintain self-renewal and proliferation and preserve the genetic features detected in patient samples. Tumourspheres are characterized by an outer proliferative zone, an intermediate quiescent zone, and an inner necrotic core (Mehta, Hsiao, Ingram, Luker, & Takayama, 2012), which is observed at some distance from the presence of nutrients, metabolites, and oxygen and resembles the necrotic areas of GBs *in vivo* (Louis, 2006). Tumour cells within tumourspheres interact closely with one another, mimicking signalling pathways and communication that influence tumour growth, survival, and therapeutic responses in vivo (Hanahan & Coussens, 2012) and forming a physical barrier that obstructs and restricts drug delivery into the tumoursphere mass (Tannock, Lee, Tunggal, Cowan, & Egorin, 2002). Tumourspheres are a more accurate model than monolayer cultures; however, they still represent random collections of cells that lack ECM and do not organize into tissue-like structures (Torras, García-Díaz, Fernández-Majada, & Martínez, 2018). The lack of surrounding non-tumour cells, i.e. stromal cells, including astrocytes, neurons, endothelial cells, mesenchymal stem cells, brain-resident microglia, and infiltrated peripheral immune cells, hinders exploring their interactions with GSCs *in vitro*. Tumourspheres can be improved by co-culturing cancer and stromal cells in what are known as heterotypic spheroids. The inclusion of stromal cells in heterotypic cell models has been demonstrated to enhance cancer cell growth and influence intercellular signalling and gene expression. As a result, using a heterotypic 3D model may provide significant benefits for studying the effects of possible anticancer drugs in a system that more properly replicates the *in vivo* TME.

1.7.3 Organoids

Organoids are multicellular 3D structures with the capacity to self-organize and recapitulate the structure and function of the original organ (Klein, Hau, Oudin, Golebiewska, & Niclou, 2020). This is the basic definition of organoids, although there are different model types and approaches to their development. They can be prepared either from patient-derived adult stem cells from excised tumour tissue (T. Sato et al., 2011) or from pluripotent stem cells, including pluripotent embryonic stem cells and induced pluripotent stem cells (Clevers, 2016). In 2016, Hubert et al. generated patient-derived GBOs to study the heterogeneity and hypoxic gradient of tumours using a submerged culture system (Hubert et al., 2016). In this protocol, finely minced tumour specimens are embedded in a solid gel of ECM (Matrigel) to form 3–4 mm large organoids in the tissue culture medium, supplemented with EGF, FGF, and B27. These organoids formed in 2 months and could be cultured for over 1 year. GB organoids are characterized by rapidly proliferating cells on the edge of the organoid and highly resistant quiescent cancer stem cells in the hypoxic core with different molecular profiles. In 2018, Ogawa et al. constructed

cerebral organoids using induced pluripotent stem cells and embryonic stem cells and induced glioma carcinogenesis by CRISPR/Cas9 technology to disrupt the TP53 tumour suppressor and express oncogenic HRasG12V (Klein et al., 2020; Ogawa, Pao, Shokhirev, & Verma, 2018) Moreover, neoplastic cerebral organoids were established by Bian et al. (Bian et al., 2018) via recapitulating brain tumourigenesis by introducing oncogenic mutations or amplifications in cerebral organoids using transposon-mediated gene insertion and CRISPR/Cas9 technology. Unlike the previously described approach, induced pluripotent and embryonic stem cell organoids are 3D human tissues created by directed differentiation, self-morphogenesis, and intrinsically driven cell self-assembly, recapitulating human organogenesis *in vitro* (Papapetrou, 2016). Such organoids can contain multiple tissue cell types, including stroma and vasculature, unlike organoids developed from tissue-specific stem cells (Passier, Orlova, & Mummery, 2016).

A novel approach using human embryonic stem cell (hESC)-derived cerebral organoids and patient-derived GSCs to model tumour cell invasion was recently developed, i.e. a glioma cerebral organoid model. This system was shown to recapitulate the cellular behaviour of GB and to maintain genetic aberrations found in the original tumour (Linkous et al., 2019). In a very recent study, Jacob et al. (Jacob, Ming, & Song, 2020; Jacob, Salinas, et al., 2020) established patient-derived GB organoids (GBOs) that accurately recapitulate the molecular, genetic, and cell-type heterogeneity of parental tumours. Compared to other previous protocols of GBOs (Bian et al., 2018; Hubert et al., 2016; Ogawa et al., 2018), the authors dissected tumour tissues into approximately 1 mm fragments without the addition of ECM, EGF, or bFGF and cultured them on an orbital shaker for 1–2 weeks to generate 3D structures. These organoids contain heterogeneous populations of cellular subtypes and recapitulate tumour cell phenotypes, as confirmed by histopathology, single-cell RNA sequencing, and molecular profiling analysis. Moreover, GBOs develop a hypoxic gradient and retain vasculature and TME composition, which mimics the main features of GB (Jacob, Ming, et al., 2020; Jacob, Salinas, et al., 2020). In a very recent study, LeBlanc et al. (LeBlanc et al., 2022) developed a similar model, incorporating elements of the GB TME, defined as patient-derived explants. The authors demonstrated a similar degree of transcriptional heterogeneity compared to parental tumours. In addition to GBOs, patient-derived explants are a valuable model for exploring cellular heterogeneity and interactions between cancer cells and the TME, which may lead to the discovery of new potential treatments.

Chapter 2

Aim of Study, Objectives and Research Hypotheses

2.1 Aims and Objectives

This doctoral dissertation is divided into three parts. The first part relates to the establishment and biobanking of new *ex vivo* GB models. This part describes (A) the concept and techniques of biobanking and (B) its application in preclinical oncology for testing the efficacy of drugs to be used as therapeutics, such as cannabinoids. The second part considers the characterization of GBOs and the study of GB resistance to standard therapy. The third part is dedicated to the identification and characterization of the biomarker cathepsin X and its role in the GB TME.

Part I:

A. At the Department of Genetic toxicology and Cancer biology at the National Institute of Biology (NIB), we developed a comprehensive biobanking platform that includes sample collection of biospecimens from GB tumours and includes the generation of advanced patient-derived *ex vivo* tumour models, such as differentiated GB cells, GSCs, and GBOs. A complete biobanking strategy offers novel opportunities for basic translational and clinical research.

B. The major translational goal of the biobanking was to use the patient-derived GB cell lines *in vitro* to test the drug efficacy of cannabinoids. The establishment of GB cell lines offers a tool for screening patient-specific treatment strategies in terms of cell viability (cytotoxicity) and invasion.

Part II:

The TME represents the "soil" on which the "seeds" (cancer cells) depend on. In the most aggressive and deadly brain tumour, GB, the unique TME consists of stromal cells, such as neuronal and glial progenitor cells, neurons, astrocytes, oligodendrocytes, microglia, macrophages, endothelial cells, and mesenchymal stem cells. Standard and novel GB therapies, such as radiation and chemotherapy, also target and alter the TME. The success of cancer treatment depends on understanding the highly heterogeneous and immune-deficient TME. In recent years, we have seen great strides in developing cancer research models that represent the heterogeneity of the TME within and between tumours and

mimic the histological features, cell diversity, gene expression, and mutational profiles of associated parental tumours.
The main goal of this part of the dissertation was to set up an *ex vivo* model of GBOs from patient tumours that mimics the entire TME and thus enables more accurate studies. Such GBOs would provide a unique opportunity to understand GB resistance at the cellular and genetic levels, thereby significantly contributing to the discovery of new treatment approaches. We aimed to use a range of standard and state-of-the-art methods to investigate the changes in targeted gene expressions and the transformation of the GB TME in response to current standard therapy in clinically relevant GBOs. This was complemented by studies on patient-derived primary GB and GSC cell lines.

Part III:

In the third part of this dissertation, we investigated the abundance and potential role of the biomarker cathepsin X in the GB TME, focusing also on the regulation of its molecular target γ-enolase. We specifically investigated the localisation, expression level, and activity of cathepsin X in the GB TME. In addition, we investigated the therapeutic potential of selective irreversible and reversible cathepsin X inhibitors.

2.2 Research Hypotheses

Part I

A. Patient-derived GB cells, GSCs, and GBOs can be successfully established from a series of patient tumour samples with success rates of at least 80%, 30%, and 60%, respectively. They remain viable in culture through passaging and can be used for further analyses. Tumour tissues can be cryopreserved for the application of well-established mRNA analyses. We can confirm the expression of GSC and GB markers in patient-derived cell cultures and GBOs.
B. Patient-derived GB cell lines are appropriate models for screening natural compounds also in combination with chemotherapy.

Part II

A. The newly established *ex vivo* GBO model can grow in culture, retain elements of the TME, and recapitulate features of GB, such as preserving the heterogeneity of the original GB subtypes. The GBO microenvironment resembles that of the corresponding parental tumours.
B. Treatment of GBOs with standard therapy affects cell viability and invasion and the expression of markers of stem cells, cell differentiation, immunosuppression, epithelial-to-mesenchymal transition, DNA damage repair, cell cycle, and apoptosis. GBOs are more resistant to standard therapy compared to primary differentiated GB cells and GSCs.

Part III

A. Cathepsin X is upregulated in GB as compared to non-cancerous brain tissue. It is expressed in macrophages and microglia.
B. Cathepsin X is a prognostic factor for the survival of GB patients.
C. The enzymatic activity of cathepsin X is upregulated in GB tissues.
D. Cathepsin X colocalises with its target γ-enolase preferentially in GB-associated macrophages and microglia.

E. Potent irreversible and reversible selective cathepsin X inhibitors inhibits the viability of patient-derived GB cells as well as macrophages and microglia, cultured in conditioned media of GB cells and GSCs.
F. The γ-enolase peptide promotes proliferation of GB differentiated cells and GSCs.

Chapter 3

Materials and Methods

3.1 Chemicals

Primary antibodies were purchased from Abcam (Cambridge, UK). High-Capacity cDNA Reverse Transcription Kit and Universal Master Mix II with UNG were from Applied Biosystems (Thermo Fisher Scientific, Waltham, Massachusetts, USA). Primary antibodies were purchased from Atlas Antibodies (Bromma, Stockholms Lan, Sweden) and BioRad (Hercules, California, USA). DC™ Protein Assay was from BioRad (Hercules, California, USA). Other primary antibodies were from Cell Signaling Technology (Danvers, Massachusetts, USA). Xylene compound was from Chem-Lab (Zedelgem, Belgium). Matrigel matrix was purchased from Corning (NY, USA). Inhibitors AMS36 and Z7 (1-(2,3-dihydrobenzo[b][1,4]dioxin-6-yl)-2-((4-(o-tolyl)-4H-1,2,4-triazol-3-yl)thio) ethan-1-one) were provided by the Faculty of Pharmacy (Ljubljana, Slovenia). Assay Loading Reagent and DNA Sample Loading Reagent were from Fluidigm (South San Francisco, California, USA). DMEM/F-12, Hibernate™-A Medium, RPMI 1640 Medium, TrypLE Express, 2-mercaptoethanol ($HOCH_2CH_2SH$), Collagenase I, Collagenase II, Collagenase IV, FBS, N-2, PBS, trypsin–EDTA solution, GlutaMax were purchased from Gibco™ (Thermo Fisher Scientific, Massachusetts, USA). HyClone Dulbecco's Modified Eagle Medium (DMEM) with high glucose was from Hyclone (GE Healthcare, Chicago, IL, USA). ProLong Gold AntiFade reagent, bFGF, EGF, B-27 supplement w/o vitamin A, Hoechst 33342, Neurobasal Medium, primary and secondary antibodies were from Invitrogen (Life Technologies, Carlsbad, CA, USA). γ-Eno was synthesized by Biosynthesis (Lewisville, TX, USA). MycoAlert Mycoplasma Detection Kit was purchased from Lonza (Basel, Switzerland). 4 % Formaldehyde solution, Ethanol (C_2H_6O), Hydrogen peroxide (H_2O_2), Hydrochloric acid (HCl) and Sodium citrate ($Na_3C_6H_5O_7$) were from Merck (Darmstadt, Germany). Purified Δ9-tetrahydrocannabinol (THC), cannabidiol (CBD), and cannabigerol (CBG) extracts were provided by MGC Pharmaceuticals Ltd. (Ljubljana, Slovenia). The purity of the compounds was monitored by high-performance liquid chromatography. The concentration ranges in organic solvents (dimethyl sulfoxide (DMSO) for CBD and THC and ethanol for CBG) were as follows: THC (15674–17294 mg/mL), CBD (14367–14895 mg/mL), and CBG (5772–7369 mg/mL. Consecutive batches had similar purity levels. Annexin V-FITC Kit and propidium iodide solution were from Miltenyi Biotech (Bergisch Gladbach, Germany). RNase Inhibitor, 20 Units/Dl, 100 reactions was from Omega (La Chaux-de-Fonds, Switzerland). Cell Titer Glo 3D cell viability assay, MTS 3-(4,5-dimethylthiazol-2-yl)-5-(3-carboxymethoxyphenyl)-2-(4- sulfophenyl)-2H-tetrazolium salt and other secondary antibodies were from Promega (Madison, WI, USA). AllPrep DNA/RNA/Protein Mini Kit was purchased from Qiagen (Germantown, MD, USA). Primary antibodies were from R&D Systems (Minneapolis, Minnesota, USA). Fast probe

(biotium) Master Mix was from Roche (Basel, Switzerland). Heparin, Human insulin, L-glutamine, Penicillin/Streptomycin, 2-mercaptoethanol, 3,3',5,5'-tetramethylbenzidine (TMB) substrate, BSA (bovine serum albumin), Dimethyl sulfoxide (DMSO), glutaraldehyde ($C_5H_8O_2$), hexamethyldisilazane [(CH3)3Si]$_2$NH, methanol, methylcellulose, MTT 3-(4,5-dimethylthiazol-2-yl)-2,5-diphenyltetrazolium-bromide, Non-Essential Amino Acid (NEAA) Cell Culture Supplement, osmium tetroxide (OsO_4), phorbol 12-myristate 13-acetate (PMA), ribonuclease A solution, Temozolomide (TMZ) ($C_6H_6N_6O_2$), Triton X-100, and Tween 20 were purchased from Sigma-Aldrich (St. Louis, MO, USA). TATAA PreAmp GrandMasterMix was from TATAA Biocenter AB (Göteborg, Sweden). Pierce™ Peroxidase IHC Detection Kit, Mix primers & assays, MultiScribe® Reverse Transcriptase (50 U/µL), phosphatase inhibitors, Vybrant®Cell-Labeling solution, RBC lysis buffer and High-Capacity cDNA Reverse Transcription Kit were purchased from Thermo Fisher Scientific (Waltham, MA, USA).

3.2 Biobanking and Establishment of *ex vivo* GB Models

3.2.1 Established Cell Lines

The established GB stem cell lines NCH421k and NCH644 were obtained from CLS (Cell Lines Service GMBH, Eppelheim, Germany). Both cell lines were grown as floating spheres in complete Neurobasal Medium (Invitrogen, Life Technologies, Carlsbad, CA, USA) containing 2 mM L-glutamine, 1× penicillin/streptomycin (P/S) (both: Sigma-Aldrich, Misuri, USA), 1× B-27 (Invitrogen, Massachusetts, USA), 1 U/mL heparin (Sigma-Aldrich, Misuri, USA), 20 ng/mL bFGF and EGF (both: Invitrogen, Life Technologies, Carlsbad, CA, USA). All the cell lines were maintained at 37°C with 5% CO_2 and 95% humidity. Once these GSC spheres reached 200 µm in diameter, they were dissociated using TrypLE Express (Gibco, Thermo Fisher Scientific, Massachusetts, USA).

The established differentiated GB cell lines U87 and U373 were purchased from the American Type Culture Collection, and the T98 cell line was obtained from the European Collection of Cell Cultures (ECACC, Salisbury, UK). All of the cell lines were grown in high-glucose Dulbecco's Modified Eagle's Medium (DMEM) (Hyclone, GE Healthcare, Chicago, IL, USA) supplemented with 10% fetal bovine serum (FBS; Gibco, Thermo Fisher Scientific, Waltham, MA, USA), 2 mM L-glutamine (Sigma-Aldrich, Misuri USA), and 1× P/S (both: Sigma-Aldrich, Misuri, USA).

3.2.2 Patient Samples

Human tissue samples were obtained from patients with LGG (WHO grades I and II) and GB (WHO grade IV) operated at the Department of Neurosurgery, University Medical Centre Ljubljana, Slovenia. We also obtained tissue samples of nontumour brain tissue. Tumour diagnoses were determined using the standard histopathology protocols at the Institute of Pathology of the Medical Faculty, University of Ljubljana. The clinical data and tumour characteristics (histopathological and molecular data) were provided by the department of Neurosurgery and the Institute of Pathology of the Medical Faculty, University of Ljubljana, Slovenia. The study was approved by the National Medical Ethics Committee of the Republic of Slovenia (approval numbers 92/06/12, 0120-190/2018/4, and 0120-190/2018/26). Written informed consent was obtained from the patients and/or their authorized representatives in accordance with the Declaration of Helsinki (*Preamble WMA Declaration of Helsinki-Ethical Principles for Medical Research Involving Human Subjects*, n.d.).

3.2.3 Establishment of Primary GB Cell Lines

For the isolation of primary GB cells, fresh GB tumour tissue biopsies were minced with a scalpel in high-glucose Dulbecco's Modified Eagle's Medium (DMEM) (Hyclone, GE Healthcare, Chicago, IL, USA) supplemented with 10% fetal bovine serum (FBS; Gibco, Thermo Fisher Scientific, Waltham, MA, USA), 2 mM L-glutamine (Sigma-Aldrich, Misuri, USA), and 1× P/S (both: Sigma-Aldrich, St. Louis, MO, USA) and were seeded in six-well cell culture plates (Corning, New York, USA). Growing cells were detached with a 0.25% trypsin–EDTA solution (Gibco, Thermo Fisher Scientific, Waltham, MA, USA) and transferred to T25 or T75 cell culture flasks (Corning, New York, USA). For subsequent analyses, cells were grown after at least three passages. GB cells were analysed by qPCR for expression of GB cell marker *GFAP*.

For the isolation of primary GSCs, tumour tissue pieces were minced with a scalpel and digested in a digestion buffer (200 U/mL collagenase II and collagenase IV (both: Gibco, Thermo Fisher Scientific, Waltham, MA, USA)) in Neurobasal Medium (Invitrogen, Life Technologies, Carlsbad, CA, USA)). Cell suspensions were filtered using a cell strainer with 100 µm pores (BD Falcon, Corning, NY, USA). Single cells were collected and resuspended in complete Neurobasal Medium containing 2 mM L-glutamine (Sigma-Aldrich, Misuri, USA), 1× P/S (both: Sigma-Aldrich), 1× B-27 (Invitrogen, Life Technologies, Carlsbad, CA, USA), 1 U/mL heparin (Sigma-Aldrich), 20 ng/mL bFGF, and EGF (both: Invitrogen). GSCs were cultured as floating spheres in a non-treated cell culture flask (Sarstedt Inc., Nümbrecht, Germany). Once these GSC spheroids reached a diameter of 200 µm, they were dissociated using TrypLE Express (Gibco). The GSCs were analysed by qPCR for GSC markers such as *PROM1*, *SOX2*, *CD9, OLIG2* and *NOTCH*.

3.2.4 Establishment of GBOs

GBOs were established according to the protocol of Jacob et al. (Jacob, Salinas, et al., 2020). After transport in processing medium (Hibernate A (Gibco, Thermo Fisher Scientific, Massachusetts, USA), 1x GlutaMax (Gibco), 1x P/S (Gibco) on ice, patient-derived tumour tissue was washed with 1x PBS (Gibco) to remove blood and debris. Fresh processing medium was added, and the tumour tissue was cut into small pieces of approximately 0.5 to 1 mm using fine dissection scissors (Fine science tools, Foster City, USA). The tumour pieces were washed twice with 1x PBS (Gibco) and incubated in 1x RBC lysis buffer (Thermo Fisher Scientific, Waltham, MA, USA) for 10 min with gentle shaking at room temperature. After two washes in DMEM F-12 medium (Gibco), tumour pieces were distributed into ultra-low attachment 6-well culture plates (Corning, New York, USA) with 4 ml GBO medium containing 50% DMEM F-12 (Gibco), 50% Neurobasal (Gibco), 1X GlutaMax (Gibco), 1x NEAAs (Sigma-Aldrich), 1x P/S (Gibco), 1x N-2 supplement (Gibco), 1x B-27 supplement w/o vitamin A (Gibco), 1x 2-mercaptoethanol (Gibco), and 2,5 µg/mL human insulin (Sigma-Aldrich, St. Louis, MO, USA). The 6-well culture plates were placed on an orbital shaker rotating at 120 rpm in a sterile incubator at 37℃, 5% CO2, and 90% humidity. 75 % of the GBO medium was replaced every 48 h. Depending on tissue quality and characteristics, tumour pieces rounded within 1-2 weeks of culture. GBOs were generally used for experiments within 3-4 weeks. For longer cultivation, GBOs were cut into pieces of 200-500 µm diameter with fine scissors to prevent necrosis in the centre. Established GBOs were cryopreserved in GBO medium with Y-27632 and 10% Dimethyl sulfoxide (DMSO) and stored in biobank (Gliobank) in liquid nitrogen for further analysis.

3.3 *In vitro* Drug Testing Efficacy of Natural Compounds

3.3.1 Immunofluorescence of GSC Spheroids

The 3D GSC spheroids were washed with PBS, fixed in ice-cold methanol (Sigma-Aldrich, St. Louis, MO, USA) for 15 min at room temperature, and incubated for 15 min in 0.1% Triton X-100/1% FBS/PBS at room temperature 22℃, for membrane permeabilisation. The spheroids were stained for 30 min at room temperature with primary antibodies (Table 1).

Negative control staining was performed with the blocking peptides (Table 2), which bind specifically to the target antibody epitope at a 10-fold higher concentration than the primary antibodies. Spheroids were stained with secondary antibodies (Table 3) for 30 min at room T. For nuclear staining, the spheroids were incubated with Hoechst 33342 dye (1:1000, Invitrogen, Life Technologies, Carlsbad, CA, USA) for 5 min at room T. The spheroids were then mounted with ProLong Gold AntiFade reagent (Invitrogen, Life Technologies, Carlsbad, CA, USA) and analysed with a confocal microscope (Leica DFC 7000 T, Wetzlar, Germany).

Table 1: Table of primary antibodies used for immunofluorescent staining.

Primary Antibody	Manufacturer (catalog number)	Dilution
Rabbit polyclonal to Cannabinoid Receptor I	Abcam (ab23703)	1:200
Rabbit polyclonal to Cannabinoid Receptor I	Abcam (ab45942)	1:500

Table 2: Table of blocking peptides used for immunofluorescent staining.

Blocking Peptides	Manufacturer (catalog number)	Dilution
Cannabinoid Receptor I peptide	Abcam (ab50542)	1:80
Cannabinoid Receptor II peptide	Abcam (ab45941)	1:50

Table 3: Table of secondary antibodies used for immunofluorescent staining.

Secondary Antibody	Manufacturer (catalog number)	Dilution
Goat anti-Rabbit IgG (H+L) Cross-Adsorbed Secondary Antibody, Alexa Fluor 488	Invitrogen (A11008)	1:200

3.3.2 Immunocytochemistry

Immunohistochemistry was performed using antibodies against CB1 and CB2 (Table 1). Before incubation with antibodies, non-specific binding sites were blocked with 1% bovine serum albumin (BSA) with 2% goat serum in PBS overnight at 5–7°C. The sections were incubated with biotinylated secondary antibody (Table 4) followed by horseradish peroxidase-conjugated streptavidin (Cell Signaling Technology, Danvers, MA, USA). The sections were further incubated with 2,4-diaminobenzidine substrate (Thermo Fisher Scientific, Inc., Waltham, MA, USA) and counterstained with haematoxylin. To achieve high antibody specificity, we used CB1 and CB2 blocking peptides (Table 2) that bind

specifically to the target antibody epitope at a 10-fold higher concentration than the primary antibodies.

Table 4: Table of secondary antibodies used for immunocytochemistry.

Secondary Antibody	Manufacturer (catalog number)	Dilution
Goat anti-Rabbit IgG (H+L), HRP Conjugate	Promega (W4011)	1:200

3.3.3 Cell Viability Assay

Cell viability was determined with MTT assay, i.e., 3-(4,5-dimethylthiazol-2-yl)-2,5-diphenyltetrazolium-bromide (Sigma-Aldrich, St. Louis, MO, USA), for GB differentiated cells and with MTS 3-(4,5-dimethylthiazol-2-yl)-5-(3-carboxymethoxyphenyl)-2-(4-sulfophenyl)-2H-tetrazolium salt (Promega, Madison, WI, USA) for GSCs. Differentiated GB cells and GSCs were seeded onto 96-well plates at a density of 5000 and 8000 to 10000 cells/well, respectively. Cells were treated with different concentrations (0.16–50 µM) of the cannabinoids CBG, CBD, and THC alone. Samples contained the same amount of DMSO ($\leq$ 0.4%, v/v) for CBD and THC and ethanol (0.24%, v/v) for CBG under all of the treatment conditions. Cell viability was measured after 48 h of incubation by adding MTT or MTS reagent when spheroids were tested. All dose-response experiments were performed in triplicate, i.e., with three biological repeats. Absorbance was measured as the change in optical density (ΔOD 570/690 nm) using a microplate reader (Synergy™ HT, Bio-Tec Instruments Inc., Winooski, VT, USA). Cell viability and IC50 µM values were calculated using dose response curves, plotted using GraphPad Prism software. The factor of inhibitory concentration (FIC), which discriminates between the additive and synergistic effects of two drugs, was calculated using method number 2 from Deng et al. (Deng, Ng, Ozawa, & Stella, 2017), based on the concentrations at which the cannabinoids CBG and CBD produce half-maximal inhibition (IC50 µM values). Thus, the CBD concentration was fixed, and the dose-response curve of the inhibitory effects of CBG, added at serial (half log1) dilutions, was plotted. The IC50 of CBG (in the presence of the fixed CBD concentration) was then calculated using GraphPad Prism software. The FIC efficacy of the combination was calculated, and the following was defined: synergy (FIC $<$ 0.5), additivity (0.5 $<$ FIC $<$ 4), and antagonism (FIC $>$ 4). Statistical analyses were performed using GraphPad Prism software, using one-way ANOVA with Bonferroni's post-hoc test.

3.3.4 3D Tumour Spheroid Invasion Assay

Cells were labelled before 3D tumour spheroid invasion assay by Vybrant®Cell-Labeling solution (Thermo Fisher Scientific, Inc., Waltham, MA, USA) with the following spectral maxima: DiO excitation at 484 nm, and emission at 501 nm. The 1 mM stock solution was stored at −20°C. The U373 and T98 cells were removed from the culture dish using 0.1% trypsin (Sigma-Aldrich, St. Louis, MO, USA), and then counted. Next, 0.5×10^6 cells were incubated for 10 min at 37°C with a 5 µM dye solution in 1 mL of serum-free culture medium. After incubation, the cells were washed twice in PBS and resuspended in 1 mL of cell medium with serum. U87 dsRED cells and NCH421k GFP were labelled as described by Breznik et al. (Breznik, Motaln, Vittori, Rotter, & Turnšek, 2017). The GB cell lines T98, U87, and U373 were then seeded onto 96-well plates (5×10^3 cells/well; Corning, NY, USA) in high-glucose DMEM containing 4% methylcellulose, and NCH421k cells were seeded onto 96-well plates (5×10^3 cells/well; Corning, NY, USA) in complete Neurobasal

Medium (Invitrogen, Life Technologies) containing 2 mM L-glutamine, 1 × P/S, 1 × B-27 (Invitrogen, Life Technologies), 1 U/mL heparin (Sigma-Aldrich, St. Louis, MO, USA), 20 ng/mL bFGF and EGF (both from Invitrogen, Life Technologies), and 4% methylcellulose. The cells were centrifuged at 850× g for 60 min and incubated at 37°C and 5% CO_2 for four days (U87), two days (U373 and T98), and three days (NCH421k) to form one spheroid in each well. These spheroids were treated with CBG (10, 25, and 50 µM), CBD (2, 5, and 10 µM), and TMZ (100, 200, and 400 µM). The spheroids were then covered with 5 mg/mL Matrigel matrix (Corning, NY, USA). The invasion distance was measured after seven days for U87 cells and five days for U373 and T98 cells. We measured the extent of invasion with the fluorescence microscope NIKON-Eclipse Ti at 4× magnification. The invasion area, normalized to spheroid diameter, was determined by ImageJ software as described in Breznik et al. (Breznik, Motaln, Vittori, et al., 2017).

3.4 Characterization of GBOs from Patient Tumours and the Effect of Standard Therapy on Viability, Invasion and the Expression of Pre-specified Groups of Genes in GBOs

3.4.1 Immunofluorescence

GBOs were washed with 1x PBS (Gibco, Thermo Fisher Scientific, Waltham, MA, USA) and fixed in 4 % formaldehyde solution (Merck, Darmstadt, Germany) for 72 h at 4°C. At the Institute of Pathology, Medical Faculty, University of Ljubljana, the fixed GBOs were dehydrated and embedded in paraffin. Paraffin blocks were cut into 4 µm thick slices. Formalin-fixed paraffin-embedded sections on slides were deparaffinised in xylene (Chem-Lab, Zedelgem, Belgium) and rehydrated in ethanol (Merck, Darmstadt, Germany). Antigens were retrieved by heating in 10 mM sodium citrate buffer (pH 6.0) at 95 °C for 20 min. After cooling, GBO sections were blocked for 1 h at room temperature in 10% (v/v) FBS (Gibco, Thermo Fisher Scientific, Waltham, MA, USA) or normal goat serum (Sigma-Aldrich, St. Louis, MO, USA), 0.1% Triton X-100 (v/v) and 1% BSA (w/v) (both Sigma-Aldrich, St. Louis, MO, USA) in 1x PBS. Primary antibodies diluted in 1% BSA (w/v) in 1x PBS (Table 5) were added to the sections and incubated overnight at 4°C in a humidity chamber. The slides were then washed 2x in 0.5% BSA (w/v) in 1x PBS. Secondary antibodies diluted in 0.5% BSA (w/v) in 1x PBS (Table 6) were added to the slides and incubated for 1 h in a humidity chamber at room temperature. After washing with 1x PBS, nuclei were stained with Hoechst 33258 solution (Sigma-Aldrich; diluted 1:1000 in 1x PBS) for 5 min at room temperature. Slides were washed with 1x PBS and mounted in ProLong Gold AntiFade reagent (Invitrogen, Life Technologies, Carlsbad, CA, USA), cover slipped, and sealed with nail polish. Inverted fluorescent microscope (Nikon Eclipse Ti, Tokyo, Japan) and NIS-Elements, Nikon software were used to record fluorescence.

Table 5: Table of primary antibodies used for immunofluorescent staining.

Primary Antibody	Manufacturer (catalog number)	Dilution
Mouse monoclonal to SOX2	Abcam (ab171380)	1:50
Rabbit polyclonal to GFAP	Abcam (ab211271)	1:1000
Mouse monoclonal to Iba1	Abcam (ab15690)	1:200

Rabbit polyclonal to CD68	Atlas antibodies (HPA048982)	1:2500
Mouse monoclonal to CD44	BioRad (MCA2504)	1:100
Rabbit monoclonal to CD9	Cell signaling technology (13403)	1:200
Mouse monoclonal to CD31 (PECAM-1)	Cell signaling technology (3528)	1:1000
Rabbit polyclonal to CD105 (ENG)	Atlas antibodies (HPA067440)	1:1000

Table 6: Table of secondary antibodies used for immunofluorescent staining.

Secondary Antibody	Manufacturer (catalog number)	Dilution
Goat anti-Rabbit IgG (H+L) Cross-Adsorbed Secondary Antibody, Alexa Fluor 488	Invitrogen (A11008)	1:200
Goat anti-Mouse IgG (H+L) Cross-Adsorbed Secondary Antibody, Alexa Fluor 546	Invitrogen (A11003)	1:200

3.4.2 Real-Time Quantitative PCR

Tissue samples, GB cells, and GBOs (treated and non-treated) were snap frozen and stored in liquid nitrogen for further analysis. Total RNA was isolated using an AllPrep DNA/RNA/Protein Mini Kit (Qiagen, Germantown, MD, USA) according to the manufacturer's instructions; cDNA was generated from 1 µg of total RNA from each sample using a High-Capacity cDNA Reverse Transcription Kit (Thermo Fisher Scientific, Waltham, MA, USA). For the target-specific pre-amplification, mix of primers and assays (ThermoFisher Scientific, Table A.1 1) and TATAA PreAmp Grand MasterMix were used in a 10 µL reaction volume with 2 µL of pre-diluted cDNA (5x). Pre-amplification conditions were: pre-denaturation 60 s at 95°C and 1-step cycling, denaturation 15 s at 95°C, annealing 2 min at 60°C and extension 60 s at 72°C in a total of 14 cycles using a T100 thermal cycler (Bio-Rad Laboratories, California, USA). To evaluate the expression level of genes in our samples, RT-qPCR was performed. Fluidigm BioMark HD System RT-qPCR (Fluidigm Corporation, San Francisco, CA, USA) and 48.48 Dynamic Arrays IFC, where cDNA of 42 samples and 24 TaqMan Gene Expression assays (ThermoFisher Scientific, Table A.1 1), were mixed pairwise in nanoliter chambers to enable parallel analysis of 2304 reactions. The thermal cycling conditions included incubation at 50°C for 2 min, followed by 95°C for 10min and 40 cycles of 95°C for 15 s and 60°C for 60s. Visualization and analysis of the RT-qPCR results were performed using the Biomark Data Collection software, the Fluidigm RT-qPCR analysis software (both: Fluidigm Corporation), and the quantGenius software (Baebler et al., 2017), Relative copy numbers of cDNA were normalized to housekeeping genes *HPRT1* and *GAPDH*.

For PCR analysis, 22 GBOs and the corresponding parental tissues were analysed. For the studies on the effect of standard therapy on GBOs, 11 treated and non-treated GBOs and the corresponding parental GB tumour tissue were analysed. In addition, NCH421k and NCH644 GSC cell lines and differentiated primary GB cells (n = 3) and primary GSCs (n = 3) were analysed for relative mRNA expression of a pre-specified panel of markers (markers for the GB subtypes, markers for GSCs (*CD9, FUT4, ID1, PROM1, SOX2*, *OLIG-2* and *CD44*), genes involved in epithelial-to-mesenchymal transition (*STAT3, CDH1, CHI3L1, CD44*, and *SNAI1*), immunosuppression (*IDO1, IL6*), genes associated with immune cell populations within TME (*AIF1, CD16, CD68, FOXP3,* and *NCAM1*),

genes involved in DNA damage response and the cell cycle (*ATM, ATR, CDKN1A, CDKN2A, MDM2, CHEK1, mTOR* and *PIK3CA*) and cytokine signalling (*CCL2, CXCL12, CXCR4,* and *IL6*). GB samples and the corresponding clinical data are listed in Table A.1 2).

3.4.3 Gene Expression Data Analyses

3.4.3.1 Statistical Analysis

Paired t-test was used to compare the mean values between two related groups of samples (GBOs and tissues). Significance of gene expression among groups (treated/control) were evaluated on log2 transformed values (log2(treatment/control(DMSO)). One-way repeated measures ANOVA Multiple comparisons paired test was used to compare the expression level between treated and non-treated GBOs (GraphPad Software Inc., La Jolla, CA, USA). P-value annotation legend: * ≤ 0.05; ** ≤ 0.01; *** ≤ 0.001.

3.4.3.2 Pearson Correlation

The Pearson correlation coefficient was used to determine the associations within mRNA expression in GBOs and corresponding tissues. These correlation coefficients were represented in a heatmap, which is a two-way display of a data matrix where the individual cells are displayed as coloured rectangles. The colour of an individual cell is proportional to its position along a colour gradient. The dependence between mRNA expressions was evaluated using the Pearson correlation test. The p-values value below 0.05 was considered statistically significant. P-value annotation legend: * ≤ 0.05; ** ≤ 0.01; *** ≤ 0.001 (Table A.1 3).

Moreover, for a more structured visualisation of the correlation data within the mRNA expression, a clustering was carried out, which represents a grouping of data based on relationships among the variables. In particular, an agglomerative clustering was performed: at the beginning, we consider each data point as a stand-alone cluster and then repeatedly combine the two nearest clusters into larger clusters until we are left with a single cluster containing all data points. To obtain a criterion based on which the clusters are merged, we need to compute a measure of dissimilarity between the observations by using a distance measure between the latter, and a linkage criterion. In our case, we employed the average method as a linkage criterion, which defines the distance between groups as the average distance between each of the members; this method results in two groups having an equal influence on the final result. The euclidean distance is utilized as a distance metric. The resulting graph is the Dendrogram, which is plotted on top of the figure.

3.4.3.3 GB Subtyping

The fifteen selected genes, *COL1A2, COL1A, TGFB1, THBS1, DAB2, S100A4, P2RX7, STMN4, SOX10, ERBB3, ACSBG1, KCBF1, OLIG2, NOTCH1,* and *NFKB1* were used to cluster GB samples (tissues and cells) into four GB subtypes: mesenchymal (MES), proneural (PN), classical (CL), and mixed (MIX) (Behnan et al., 2016). We developed a decision tree-based model code for the differentiation of the various tissues according to tumour subtypes. The first point to be addressed was the normalisation of the data to be analysed. In order to make this tool as broad as possible, we decided to normalise using the 75th percentile (Q_3) of the training dataset. In particular, if the current value (x_i) is greater than Q_3, this value is replaced with 1. If the value is less than 0, it is replaced with 0. For all values between 0 and Q_3, it will be scaled based on Q_3.

$$f(x_i) = \begin{cases} 0, & x_i < 0 \\ \frac{x_i}{Q_3}, & 0 \le x_i \le Q_3 \\ 1, & x_i > Q_3 \end{cases}$$

Subsequently, a decision tree, a non-parametric supervised learning method, was used to differentiate between the four types of tumour classes, CL, MES, PN and MIX. However, decision trees are not able to generalise if the data are particularly complex, leading to overfitting. One of the ways to control overfitting is to set the maximum depth of the tree, which in our case was set to 2. An additional disadvantage of decision trees is the instability when the data changes and could lead to a totally different tree generation. Therefore, we reduced the dimensionality of the data. One of the most common methods for extracting features and reducing dimensionality is the principal component analysis (PCA). The PCA linearly rotates and scales the data matrix providing a new dataset without loss of information and maximizing variance. As a matter of fact, the first principal component is the one with the highest variance gradually descending to the last component. Moreover, the first two principal components are linearly independent. After performing PCA, it is therefore possible to choose the first principal components that contain the highest variance, thus reducing dimensionality, preserving the most information and eliminating data noise. Consequently, we created a new dataset with the first 3 principal components as features, from the initial 15. One of the criteria for separating decision trees, i.e. the function for measuring the quality of a division, is entropy, which is correlated with variance. A visualisation of the tree can be seen in the figure below (Figure 2).

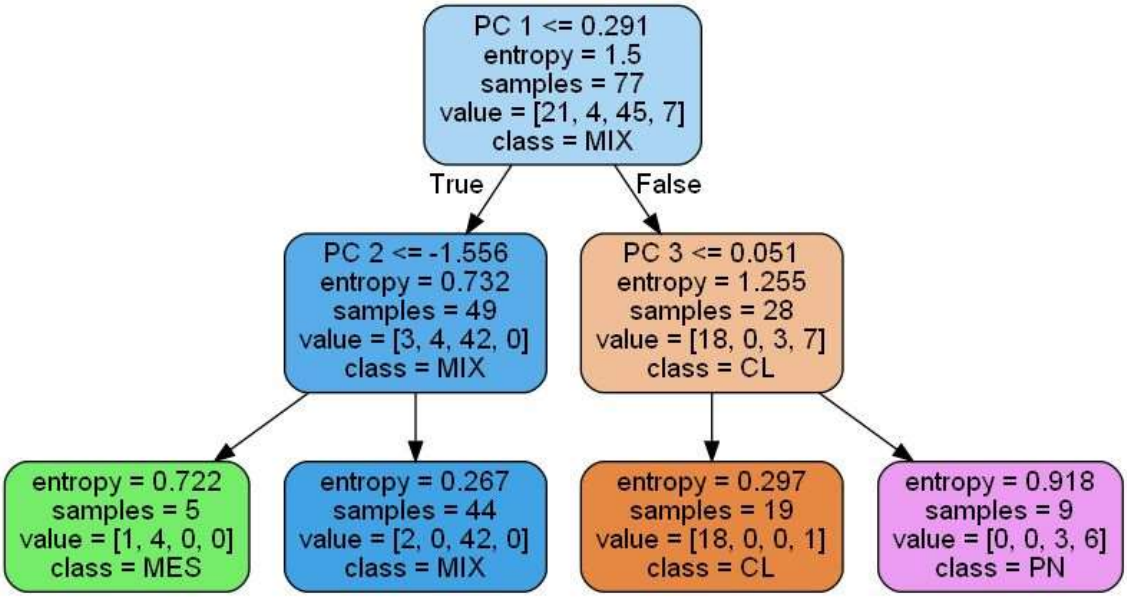

Figure 2: A visualisation of the decision tree for GB subtyping.

3.4.4 Organoid Viability Assay

GBOs (non-irradiated or irradiated with a single dose of 10 Gy) were added to individual wells of a 24-well plate (Corning, New York, USA) with 200 µL of GBO medium per well. GBOs were then cultured for one week on an orbital shaker rotating at 120 rpm within a 37°C, 5% CO2, and 90% humidity sterile incubator in GBO medium containing either 50 µM TMZ (Sigma-Aldrich, Misuri, USA), or DMSO (Sigma-Aldrich, Misuri, USA) vehicle

control. The medium containing fresh drug was replaced every 48 h. For a given treatment, GBOs were treated in triplicate. The Cell Titer Glo 3D cell viability assay (Promega, Madison, WI, USA) was used to assess cell viability according to manufacturer's instructions.

3.4.5 Organoid Invasion Assay

GBOs (non-irradiated or irradiated with a single dose of 10 Gy) were placed in individual wells of a U-bottom 96-well plate (VWR). GBO medium was removed and 100 µl of 30% Matrigel (Corning, NY, USA) in GBO medium with or without 50 µM TMZ (Sigma-Aldrich, St. Louis, MO, USA) was added per well. GBO invasion was imaged after 24h or 48h on inverted microscope (Nikon Eclipse Ti, Tokyo, Japan) and NIS-Elements, Nikon software. Images were analysed in ImageJ. Invasion was quantified either by counting the number of invasive cells (for GBOs exhibiting single-cell invasion) or by measuring the invasion area (for GBOs exhibiting collective invasion). The number of invasive cells or the invasion area were normalised to average GBO diameter to account for differences in sizes of GBOs.

3.4.6 Scanning Electron Microscopy

For scanning electron microscopy (SEM), GBOs were fixed with 2.5% glutaraldehyde in PBS for 1 h at 37 °C and postfixed with 1% aqueous osmium tetroxide (OsO4) for 3 h at room temperature. After washing with deionized water, GBOs were dehydrated in an ascending concentration series of ethanol and air-dried in hexamethyldisilazane (HMDS). Dry samples were attached to aluminum holders using conductive silver paste and sputter coated with platinum. Imaging was performed using a JSM-7500F field emission scanning electron microscope (JEOL).

3.4.7 Apoptosis Assay

Assessment of apoptosis induced by standard therapy (TMZ, IR, or combination) in GBOs was performed by flow cytometry. Six GBOs for one condition were irradiated with a single dose of irradiation (IR; 10 Gy) or/and subjected to daily treatment with 50 µM TMZ for one week. GBOs were then enzymatically dissociated with TrypLE and Collagenase I solution in a 2:1 ratio and washed with 1× PBS. Early/late apoptotic cells were detected by staining with Annexin-V-FITC (Miltenyi Biotech, Bergisch Gladbach, Germany) for 15 min in the dark at room T and with 1 µg/mL propidium iodide solution (100 µg/mL; Miltenyi Biotech, Bergisch Gladbach, Germany). Stained cells were analysed with a flow cytometer (MACSQuant Analyzer, Miltenyi Biotec Bergisch Gladbach, Germany) and analysed with FlowJo™ v10.8 Software (BD Life Sciences, New Jersey, USA). DMSO was used as a negative control.

3.5 Up-regulation of Cathepsin X in GB: Investigation of Selective Inhibitors and its Target γ-enolase

3.5.1 GB and Astrocyte Cell cultures

GB stem cell line NCH421k was obtained from CLS (Cell Lines Service GMBH, Eppelheim, Germany). NCH421k cells were grown as floating spheres in complete Neurobasal Medium (Invitrogen, Life Technologies, Carlsbad, CA, USA). All the cell lines were maintained at

37°C with 5% CO2 and 95% humidity. Once these GSC spheres reached 200 µm in diameter, they were dissociated using TrypLE Express (Gibco).

NIB 140 cells were primary patient-derived GB cells obtained from freshly resected tumour biopsies of the GB patients operated at University Medical Centre Ljubljana and grown in monolayers in cell culture flasks as described above. All the cell cultures were tested for mycoplasma contamination using a MycoAlert Mycoplasma Detection Kit (Lonza, Basel, Switzerland).

Human astrocytes were purchased from ScienCell Research Laboratories (Carlsbad, CA, USA) and cultured in Astrocyte Medium (ScienCell) supplemented with 2% FBS (ScienCell), 1% astrocyte growth supplement (ScienCell), and 1% P/S (ScienCell).

3.5.2 Microglia and Macrophage Cell Cultures

Mouse microglial BV-2 cells were a generous gift from Dr. Alba Minelli (University of Perugia, Perugia, Italy). BV-2 cells were cultured in DMEM (Sigma-Aldrich) supplemented with 10% FBS (Gibco), 2 mM L-glutamine, 1× P/S (Sigma-Aldrich). The cells were maintained at 37°C in a humidified atmosphere of 95% air and 5% CO2. Confluent cells were subcultured twice or thrice weekly using 0.25% trypsin. Human THP-1 monocytes were obtained from ATCC (American Type Culture Collection: TIB-202) and grown in suspension in advanced RPMI (Gibco, Thermo Fisher) supplemented with 10% (v/v) FBS in a humidified, 37°C, 5%CO2 incubator. THP-1 cells were kept at a minimum density of 3×10^5 cells/mL and passaged when reaching 8×10^5 cells/mL. For differentiation, phorbol 12-myristate 13-acetate (PMA) (Sigma-Aldrich) was added to a final concentration of 100 nM. After 48 h, the PMA-supplemented medium was removed, the cells were washed with PBS and treated with GB and GSC-conditioned media for further analysis.

3.5.3 Patient samples

The collecting procedure of patient GB samples and other human specimens is described in Chapter 3.2.2.

3.5.4 Primary GB Cells

For cathepsin X biomarker analysis, the establishment of primary GB cells from patient samples was performed as described in Section 3.2.3.

3.5.5 Cell coculture Models

To test the effect of soluble factors secreted by GB, differentiated THP-1 or BV-2 cells were cultured in the complete medium and treated for 48 h with the supernatants of patient-derived GB cells (NIB140) and GSCs (NCH421k) in the absence or presence of cathepsin X inhibitors AMS36 and Z7 (1.5–20 µM) and the γ-Eno peptide (20–100 nM). After transfer of the GB cell- and GSC-conditioned media, the cells were examined for cell viability and proliferation index.

3.5.6 Real-Time Quantitative PCR

Tissue samples were frozen and stored in liquid nitrogen for further analysis. The procedure for qPCR analysis is described in Section 3.4.2. For PCR analysis, 43 de novo GB, five recurrent GB (GB rec), 14 LGG, and 16 non-tumour brain (N) samples were analysed. In addition, differentiated GB cells (n=17) and GSCs (n=6) were isolated from GB tumour biopsies to analyse the relative mRNA expression of cathepsin X. Gene Expression assays

(Thermo Fisher Scientific, Inc., Waltham, MA, USA) are listed in Table A.2.1. GB samples and the corresponding clinical data are listed in Table A.2 2.

3.5.7 Gene Expression Data Analyses

3.5.7.1 GB Subtyping

GB samples (tissues and cells) were clustered into four GB subtypes: mesenchymal (MES), proneural (PN), classical (CL), and mixed (MIX) as described in Section 3.4.3.3.

3.5.7.2 Differentially Expressed Genes among the GB Samples

Differences in the mRNA expression levels of cathepsin X between the GB samples (tissues and cells) and the previously defined GB subtypes (mesenchymal—MES, proneural—PN, classical—CL, and MIX—mixed) were analysed. To minimize the effect of genes with low expression, we first removed them from the analysis by placing the Ct values > 40 as zero. We plotted boxplots to visually assess the differences and variability of the cathepsin X gene expression and then assessed the potential difference between sample types and subtypes using analysis of variance (to determine the homogeneity of variance) followed by Tukey's post hoc tests. The analyses were conducted in R version 4.0.3.

3.5.7.3 Survival Analysis

Cox proportional hazards regression was calculated to assess survival in the GB sample cohorts of different groups. High and low cathepsin X expression groups were determined based on the median expression of cathepsin X. All the analyses were performed in R software version 4.0.3. Logrank test was used to evaluate the statistically significant difference.

3.5.8 Immunofluorescence

Formalin-fixed and paraffin-embedded tissue sections from six GB (*de novo*, WHO grade IV) patients and one nontumour brain tissue were prepared at the Institute of Pathology and used for immunofluorescence analyses (Table A.2.3.). Immunofluorescence procedure is described in Section 3.4.1. A panel of primary and secondary antibodies are listed in Table 7 and Table 8. Confocal imaging was performed using a confocal microscope (SP8 TCS) and the LAS X Life Sciences software (both: Leica, Wetzlar, Germany) at 100× and 200× magnification. Negative control staining was performed in the absence of the primary antibodies.

Table 7: Table of primary antibodies used for immunofluorescent staining.

Primary Antibody	Manufacturer (catalog number)	Dilution
Goat polyclonal to cathepsin X	R&D System (AG934)	1:200
Mouse monoclonal to Iba1	Abcam (ab15690)	1:200
Rabbit polyclonal to CD68	Atlas antibodies (HPA048982)	1:2500
Mouse monoclonal to SOX2	Abcam (ab171380)	1:50
Rabbit polyclonal to CD133	Abcam (ab19898)	1:100

Rabbit polyclonal to GFAP	Abcam (ab211271)	1:1000
Mouse monoclonal to γ-enolase (NSE-P1)	Santa Cruz Biotechnology (sc-21738)	1:250
Mouse monoclonal to γ-enolase (NSE-P2)	Santa Cruz Biotechnology (sc-21737)	1:250
Mouse monoclonal to γ-enolase (D-7)	Santa Cruz Biotechnology (sc-376375)	1:250

Table 8: Table of secondary antibodies used for immunofluorescent staining.

Secondary Antibody	Manufacturer (catalog number)	Dilution
Donkey anti-goat IgG (H+L) Highly Cross-Adsorbed Secondary Antibody, Alexa Fluor Plus 488	Thermo Fisher Scientific (A32814)	1:200
Donkey anti-mouse IgG (H+L) Highly Cross-Adsorbed Secondary Antibody, Alexa Fluor Plus 647	Thermo Fisher Scientific (A32787)	1:200
Donkey anti-rabbit IgG (H+L) Highly Cross-Adsorbed Secondary Antibody, Alexa Fluor Plus 546	Thermo Fisher Scientific (A10040)	1:200
Donkey anti-mouse IgG (H+L) Highly Cross-Adsorbed Secondary Antibody, Alexa Fluor Plus 546	Thermo Fisher Scientific (A10036)	1:200

3.5.9 Protein Extraction from GB Tissues and Nontumour Brain Tissues

For analysis of the protein levels of cathepsin X and its activity, tissues were homogenised in ice-cold lysis buffer (0.05 M sodium acetate, pH 5.5, 1 mM EDTA, 0.1 M NaCl, 0.25% Triton X-100) supplemented with a cocktail of phosphatase inhibitors (Thermo Fisher Scientific), then sonicated and centrifuged at 15,000× g at 4°C for 15 min to collect the supernatant. Total protein concentration was determined with DC™ Protein Assay (Bio-Rad, Hercules, CA, USA). All the samples were kept at −70°C until they were used for analysis.

3.5.10 Cathepsin X Activity

Cathepsin X activity was measured in tissue lysates and cell lysates with cathepsin X-specific intramolecular quenched florigenic substrate Abz–Phe–Glu–Lys(Dnp)–OH synthesized by Jiangsu Vcare Pharmatech Co. (China). An aliquot of 50 µg of the lysate proteins was incubated at 37°C, followed by measurement of cathepsin X activity using 10 µM Abz–Phe–Glu–Lys(Dnp)–OH. The fluorometric reaction was quantified at 37°C at an excitation wavelength of 320 nm and emission wavelength of 420 nm on a microplate reader (Tecan Safire2). The results are presented as a change in fluorescence as a function of time ($\Delta F/\Delta t$), and cathepsin X activity was expressed relative to the control.

3.5.11 ELISAs

The protein levels of cathepsin X and γ-enolase in tissue lysates were determined using ELISA assay. For the cathepsin X protein levels, microtiter plates were coated with equal aliquots of goat polyclonal anti-cathepsin X antibody (RD Systems, Minneapolis, Minnesota, USA) in 0.01 M carbonate/bicarbonate buffer, pH 9.6, at 4°C After blocking with 2% BSA in PBS, pH 7.4, for 1 h at room temperature, the samples with equal protein amounts (50 µg) or cathepsin X standards (0–65 ng/mL) were added. Following 2 h incubation at 37 °C, the wells were washed and filled with a mouse monoclonal anti-cathepsin X 3B10 antibody conjugated with horseradish peroxidase (HRP) in a blocking buffer. Mouse monoclonal 3B10 antibodies were prepared from a mouse hybridoma cell line as reported (Kos et al., 2005). After a further 2 h incubation at 37°C, 200 µL/well of 3,3',5,5'-tetramethylbenzidine (TMB) substrate (Sigma-Aldrich) in 0.012% H_2O_2 was added. After 15 min, the reaction was stopped by adding 50 µL/well of 2 µM H_2SO_4. The amount of protein was determined by measuring the absorbance at 450 nm using a microplate reader (Tecan Safire2), and the concentration of cathepsin X was calculated from the standard calibration curve. To measure active γ-enolase, microtiter plates were coated with equal aliquots of the protein in 0.01 M carbonate/bicarbonate buffer, pH 9.6, at 4°C. After blocking with 2% BSA in PBS, pH 7.4, for 1 h at room temperature, a mouse antibody against C-terminal γ-enolase (Santa Cruz Biotechnology) suitable for detecting its active form was added. Following 2 h incubation at 37°C, the wells were washed and filled with an anti-mouse antibody conjugated with HRP. After further 2 h incubation at 37°C, 200 µg/well of a TMB substrate in 0.012% H_2O_2 was added. After 15 min, the reaction was stopped by adding 50 µL of 2 µM v H_2SO_4. The amount of cleaved substrate was determined by measuring the absorbance at 450 nm, and the protein levels of cathepsin X and γ-enolase were expressed relative to those in non-treated cells (control).

3.5.12 Cathepsin X Inhibitors and γ-enolase C-Terminal Peptide

The irreversible selective inhibitor of cathepsin X, AMS36, was synthesized according to the modified procedure of Sadaghiani et al. (Sadaghiani et al., 2007). The selective reversible inhibitor Z7 (1-(2,3-dihydrobenzo[b][1,4]dioxin-6-yl)-2-((4-(o-tolyl)-4H-1,2,4-triazol-3-yl)thio) ethan-1-one) was obtained from in-house compound library screening and was synthesized as described (Sadaghiani et al., 2007). The C-terminal 30-amino-acid sequence of human brain γ-enolase (γ-Eno) was synthesized by Biosynthesis (Lewisville, TX, USA), here defined as the γ-enolase peptide (AKYNQLMRIEEELGDEARFAGHNFRNPSVL). The use of the concentration range of cathepsin X inhibitors and the γ-Eno peptide was based on previous studies (Pečar Fonović et al., 2013, 2017).

3.5.13 Cell Viability Assay

MTS [3-(4,5-dimethylthiazol-2-yl)-5-(3-carboxymetoxyphenyl)-2-(4-sulfophenyl)-2H-tetrazolium] colorimetric assay was used to measure viability of GB cells. NIB140 (5×10^3) and NCH421k (8×10^3) cells were seeded into wells of a 96-well microplate (Thermo Fisher Scientific), and after overnight incubation, they were treated with a range of concentrations of cathepsin X inhibitors (Z7 and AMS36; 0.1–20 µM) and the γ-enolase peptide (20–100 nM) for 48 h. DMSO (final concentration, 0.25%; Sigma-Aldrich) and the culture medium were used as solvent controls for cathepsin X inhibitors and the γ-enolase peptide, respectively. The MTS reagent (Promega, Madison, WI, USA) was then added to the wells of a 96-well microplate and, after incubation, absorbance of formazan was measured at 490

nm on a Synergy Mx microplate reader (Biotek, Winooski, VT, USA). Cell viability (%) was determined as the ratio of absorbance obtained in the presence of the tested compound to that in the solvent alone. Three independent experiments with three replicates per treatment were performed.

3.5.14 Cell Proliferation Assay

A CellTrace Cell Proliferation kit with the CellTrace CFSE reagent (Invitrogen, Life Technologies, Carlsbad, CA, USA) was used to determine cell proliferation. CFSE fluorescent dye stably incorporates into the cells, and the CFSE content of a cell is divided approximately by half each time the cell divides. By measuring CFSE-labeled cell fluorescence, cell proliferation can be determined. GB cells were stained with the CellTrace CFSE reagent at a concentration of 1 µM in a cell suspension according to the manufacturer's protocol. NIB140 (20×10^3) and NCH421k (10×10^3) CFSE-labeled cells were seeded into 24-well culture plates (Corning), respectively. After overnight incubation, the cells were treated with a range of concentrations of cathepsin X inhibitors (Z7 and AMS36; 5–20 µM) and the γ-enolase peptide (20–100 nM) for 48 h. DMSO (final concentration, 0.25%; Sigma-Aldrich) and the culture medium were used as solvent controls for cathepsin X inhibitors and the γ- enolase peptide, respectively. Temozolomide (TMZ; Sigma-Aldrich) in a concentration of 100 µM was used as the positive control. The cells were harvested using TrypLE Express (Gibco), and the mean fluorescence intensities of the cells were measured in the B1 channel using a MACSQuant Analyzer 10 flow cytometer and MACSQuantify Software V3 (both: Miltenyi Biotec, Bergisch Gladbach, Germany). The obtained data were analysed in FlowJo software V10 (Becton Dickinson, Franklin Lakes, NJ, USA). The mean fluorescence intensity of CFSE reagent staining was normalized to the solvent control. Three independent experiments with two replicates per treatment were performed.

3.5.15 Statistical Analyses

Tukey's post hoc test, one-way ANOVA test with Dunnett's multiple comparison, unpaired t-test with Welch's t-correction, and multiple t-test followed by a two-stage linear step-up procedure of the Benjamini, Krieger, and Yekutieli correction were used to perform statistical analyses in GraphPad Prism software (GraphPad Software Inc., La Jolla, CA, USA) version 8. p-values < 0.05 were considered to indicate significant differences. P-value annotation legend: * ≤ 0.05; ** ≤ 0.01; *** ≤ 0.001, **** $p \leq 0.0001$.

Chapter 4

Results

4.1 PART I:

A: Biobanking and Establishment of GBOs

After surgical resection, a part of the tumour tissue was immediately transported to the Institute of Pathology, Faculty of Medicine, University of Ljubljana, Slovenia, for histopathological and molecular examination. The other part was immediately transported to NIB, Slovenia, where it was used for biobanking as part of the Glioma and Trans-Glioma project (started in 2011), to which we added differentiated GB cells and GSCs. During this PhD research, we also added new *ex vivo* models, GBOs. Part of tumour tissue was snap frozen and stored in liquid nitrogen containers. Fresh tumour tissues were used for the establishment of patient-derived GBOs and primary GB cell lines, including differentiated GB cell lines and GSCs. Procedures for collection and storage of biological material have been developed in accordance with the best practice guidelines. Research and clinical data, including neuroclinical, histopathological, and oncological data, were deposited in the online GlioBank, using SciNote software. Neuroclinical data were provided by the Department of Neurosurgery at the University Medical Centre Ljubljana, Slovenia. Diagnosis confirmation and histopathological and molecular data of tumours were provided by the Institute of Pathology at the Faculty of Medicine, University of Ljubljana. The oncological data, such as treatment data, were provided by the Institute of Oncology, Ljubljana, Slovenia. The description of specimen storage and research data were provided by NIB, Ljubljana, and the Medical Faculty of Ljubljana (Figure 3).

We obtained approval by the National Medical Ethics Committee of the Republic of Slovenia (approval numbers 92/06/12, 0120-190/2018/4, and 0120-190/2018/26) for collecting, processing, and performing research on patient tumour tissue, and corresponding personal data. All patients and/or their authorized representatives signed written informed consent in accordance with the Declaration of Helsinki (*Preamble WMA Declaration of Helsinki-Ethical Principles for Medical Research Involving Human Subjects*, n.d.).

From January 2018 to September 1, 2022, a total of 177 GB tumour samples were included in GlioBank. Each sample was first taken from the core region of the tumour (named core), according to the enhancement area on an image guidance (MRI) navigation system. The second sample was taken from the invasive edge or margin (named rim) of the initial sample and was defined by the 5-aminolevulinic-acid fluorescence-positive area beyond the enhancement, according to the image guidance navigation system. GB samples were further processed for the establishment of primary differentiated GB cells (Figure 4A), GSCs (Figure 4B), and GBOs (Figure 4C), with success rates of 49%, 34%, and 69%,

respectively (Table 9). GB cells, GSCs, and GBOs remained viable in culture through passaging and were cryopreserved for further analyses. GB cells and GSCs were examined for the expression of GSC and GB differentiation markers. Primary patient-derived GB cells expressed low levels of stem cell markers and high levels of the differentiation marker *GFAP*. By contrast, GSCs expressed higher levels of the GSC markers *SOX2, PROM1, CD9, OLIG2*, and *NOTCH1*, and lower levels of *GFAP* marker than GB cells (Figure 5). Based on our analysis, we use the markers SOX2 and OLIG-2 to identify GSCs because their expression in GSCs is significantly different from GB cells.

The data included in GlioBank, such as neurosurgical, neuroclinical, oncological, histopathological, and research data, are presented in Table 10.

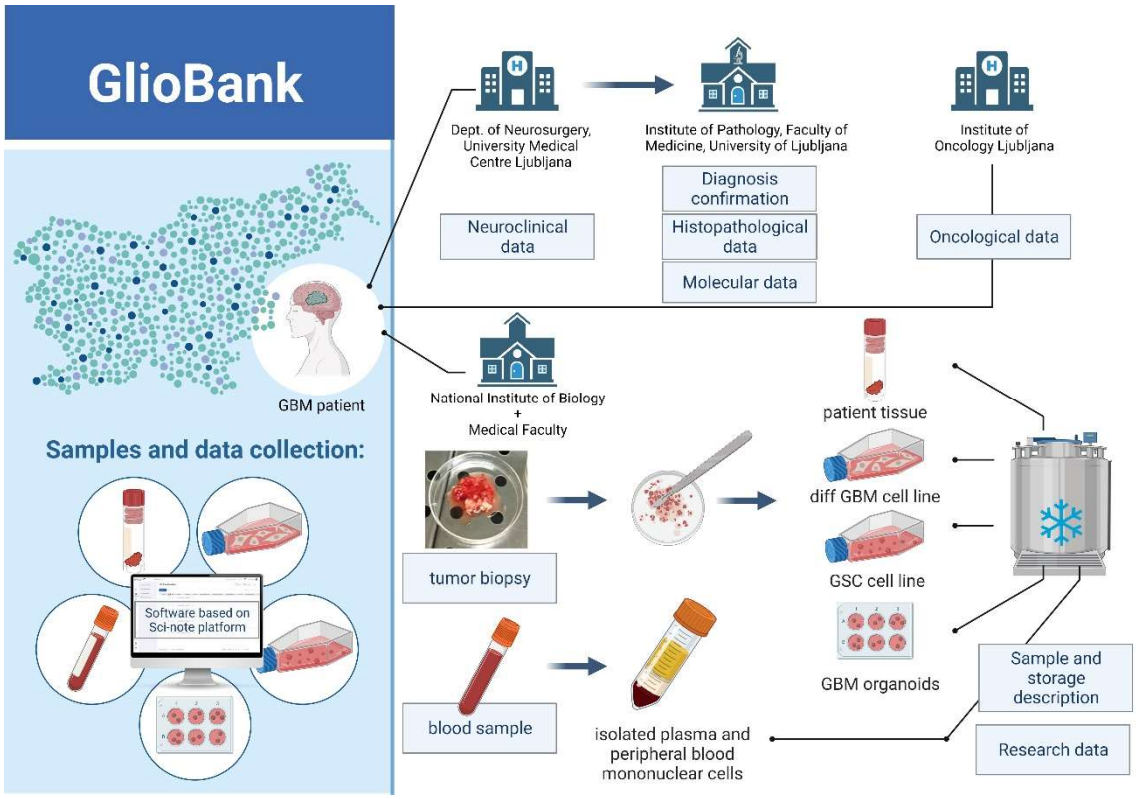

Figure 3: Schematic representation of the GlioBank translational platform, established in 2011.GlioBank is a collection of biological samples as well as neurological and clinical data (provided by the Department of Neurosurgery), histopathological and molecular data (provided by the Institute of Pathology), and oncological data (provided by the Institute of Oncology). Tumour tissues were collected at the time of surgery and stored in tissue banks. Part of the tissue was further processed for the establishment of differentiated GB cells, GSCs and GBOs. Legend: GB-glioblastoma, GSCS-glioblastoma stem cells, GBOs-glioblastoma organoids.

Table 9: Biological materials stored in GlioBank (included from January 18, 2018, to September 1, 2022).

Biological material	Quantity	Success rate	Storage temperature
Tissues			
LGG (grade I and II)	21	n.d.	liquid nitrogen
Grade III	14	n.d.	liquid nitrogen

Gliosarcoma	15	n.d.	liquid nitrogen
GB (rim and core)	177	n.d.	liquid nitrogen
Tissue-derived samples (from rim and core)			
GB cells	72	49%	-80°C or liquid nitrogen
GSCs	31	34%	-80°C or liquid nitrogen
GBOs	40	69%	-80°C or liquid nitrogen

GBOs are included from May 2020 to September 2022. Legend: LGG-low grade glioma, GB-glioblastoma, GSCs-glioblastoma stem cells, GBOs-glioblastoma organoids, n.d.-not defined.

Table 10: Clinical and research data that are included in GlioBank.

Type of data	Data
Neurosurgical and neurological data	Patient´s gender and age, *de novo* tumour or recurrence, steroid treatment, comorbidities, tumour location, edema, necrosis, extent of tumour surgical removal, pre- and post-surgical karnofsky performance status, neurological outcome after tumour removal, complications after surgery
Oncological data	Overall survival, progression-free survival, treatment after surgery and neoadjuvant treatment (radiotherapy, temozolomide, other experimental therapy), pre- and post-operative/treatment tumour volume, second line treatment
Histopathological data	Tumour type and grade; *ATRX* loss; *MGMT* methylation status; mutations in genes *TP53, IDH1/2, EGFR, TERT, PTEN, CDKN2A/CDKN2B, BRAF, KRAS, CDK4, MET, KIT, PDGFRA* and *PIK3CA*, chromosomal aberrations (co-deletion of 1p/19q and others)
Research data	Storage information; subtype (PN, CL, MES, or MIX) determined based on mRNA expression of genes: *ACSBG1, COL1A1, COL1A2, DAB2, ERBB2, KCNF1, NFKB1, NOTCH1, OLIG2, P2RX7, S100A4, SOX10, STMN4, TGFB1,* and *THBS1;* mRNA expression of biomarkers: *AIF1, ALYREF, ATR, ATM, CCL2, CCR3, CCL5, CCR5, CD3D, CD3E, CD3G, CD9, CD44, CD68, CDKN2A, CDKN1A, CDH1, CHI3L1, CHEK1, CXCR4, CXCL12, FCGR3A, FOXP3, FUT4, GFAP, ID1, IDO1, IL6, MDM2, MTOR, NCAM1, PIK3CA, PROM1, SNAI1, SOX2, STAT3, TRIM28, TUBB3, TUFM,* and *VIM*

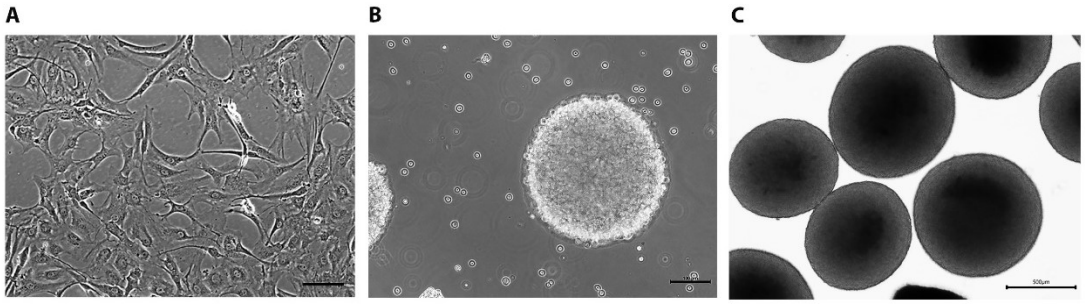

Figure 4: Patient-derived GB models. Representative images of differentiated GB cells (A), GB stem cells (GSCs) (B), and GB organoids (GBOs) (C). Scale bars: 100 µM (A, B) and 500 µM (C).

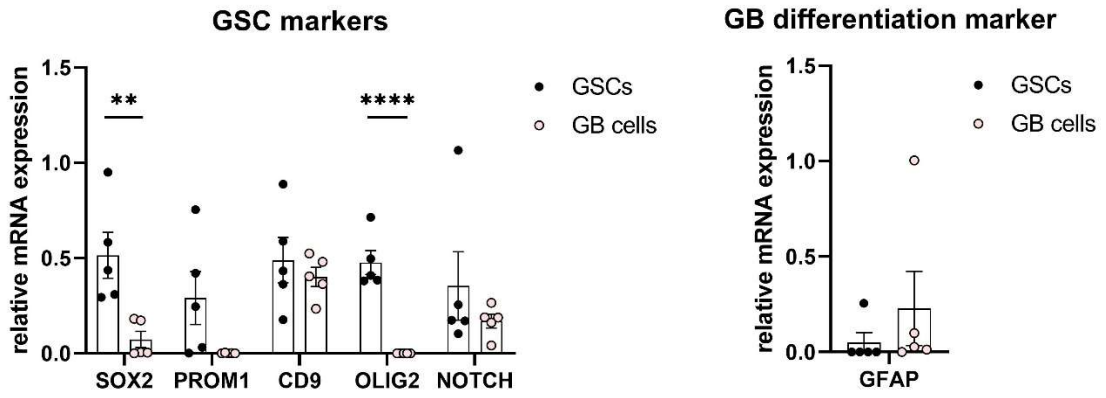

Figure 5: mRNA levels of several GSC and GB cells markers in primary GSCs and GB cells. mRNA expression of GSC and GB markers *SOX2, PROM1, CD9, OLIG2*, *NOTCH,* and *GFAP* were determined by RT-qPCR in GSCs (n=5) and GB cells (n=5), normalized to the housekeeping genes *HPRT1* and *GAPDH*, and analysed with quantGenius software (Baebler et al., 2017). Data are presented as mean ± S.E.M. Statistical analyses were performed with GraphPad Prism software using an unpaired t-test (**$p < 0.01$, **** $p < 0.0001$).

Biological material from our biobank has been used in various research projects. We have used patient-derived GB and GSC cell lines as models for screening natural compounds also in combination with chemotherapy.

4.1.1 CB1 and CB2 Cannabinoid Receptors are Highly but Differentially Expressed in Patient GB Cells

We aimed to determine whether the two major cannabinoid receptors, CB1 and CB2, are expressed in our established and primary GSC cell lines, as their expression in GB has been confirmed in other studies (Galve-Roperh et al., 2013; Ligresti et al., 2016; Zhu et al., 2000). We have confirmed that both receptors are strongly but differentially expressed in GB cells, indicating wide variability among patients in this regard (Figure 6A and 6B).

Furthermore, we have shown that both CB1 and CB2 receptors are also expressed at different levels in all GSCs (Figure 6B).

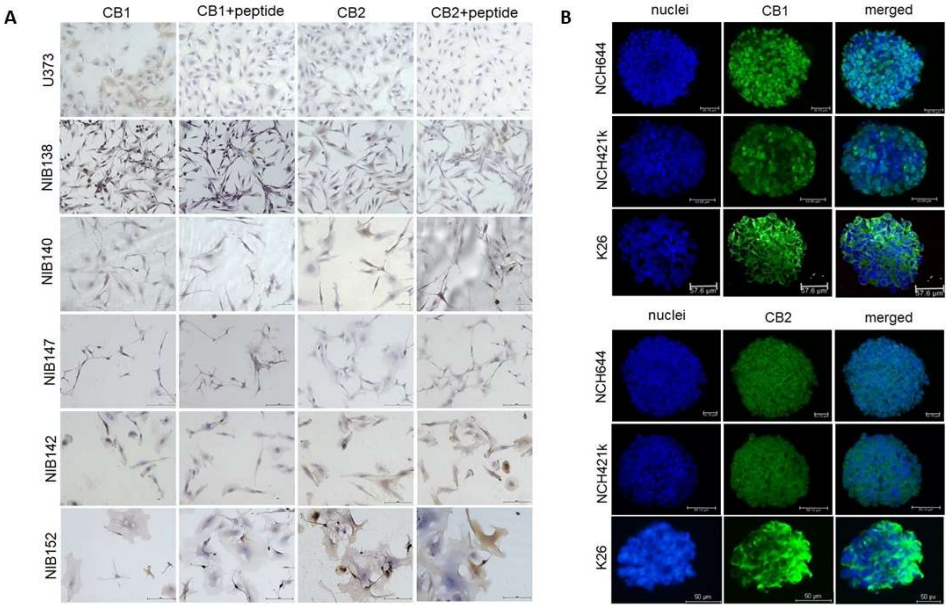

Figure 6: CB1 and CB2 receptors are differentially expressed in GB cells and GSCs. (A) Immunocytochemical staining of CB1 and CB2 receptors (brown) in established cell lines and differentiated GB cells from patient tumour samples. Cell nuclei were stained with haematoxylin (blue). CB1 or CB2 peptides in combination with primary antibodies were used as negative controls. Scale bars: 50 µm. (B) Immunofluorescence staining of CB1 and CB2 receptors in the spheroids of two established and one patient-derived GSC cell line, K26. Cell nuclei were stained with Hoechst (blue), and the receptors CB1 and CB2 were stained with Alexa Fluor 488 (green). Scale bars: 50 µm. NCH644/NCH421k are established GSC cell lines, NIBXXX and KXX are primary patient-derived differentiated GB cell and GSCs.

4.1.2 The Cannabinoids CBG, CBD, and THC Affect the Viability of Primary GB Cells and GSCs

We used GB *ex vivo* models from our biobank to test the efficacy of using cannabinoids as therapeutics. We investigated the effects of cannabigerol (CBG), cannabidiol (CBD), and tetrahydrocannabinol (THC) on the viability of GSCs and differentiated GB cell lines by using mitochondrial dehydrogenase activity MTT and MTS assays after 48 h of treatment of spheroid cultures. The viability of both GB cell lines and GSCs was significantly reduced by all three cannabinoids (Figure 7). In two established and eight primary patient-derived GB cell lines, CBG reduced GB cell viability in a concentration range of 22–32 µM (IC50 28.1 ± 1.1 µM), similarly as THC (IC50 27.9 ± 1.8 µM). In the same cell lines, CBD was significantly more cytotoxic than CBG and THC with an IC50 of 22.0 ± 2.1 µM. In GSCs, IC50 values were 59 ± 15 µM (CBG), 20 ± 4 µM (CBD), and 23 ± 3 µM (THC) and were of the same magnitude as in GB lines. Overall, CBD had the strongest inhibitory effect on the viability of both GB cells and GSCs (Table 11). Our quantitative results confirmed previous findings on the effects of CBD and THC on GB cell viability (Torres et al., 2011) and also show a novel effect on GSC viability. Furthermore, our results show that CBG reduces the viability of GB and GSC lineages with similar efficacy as CBD and THC.

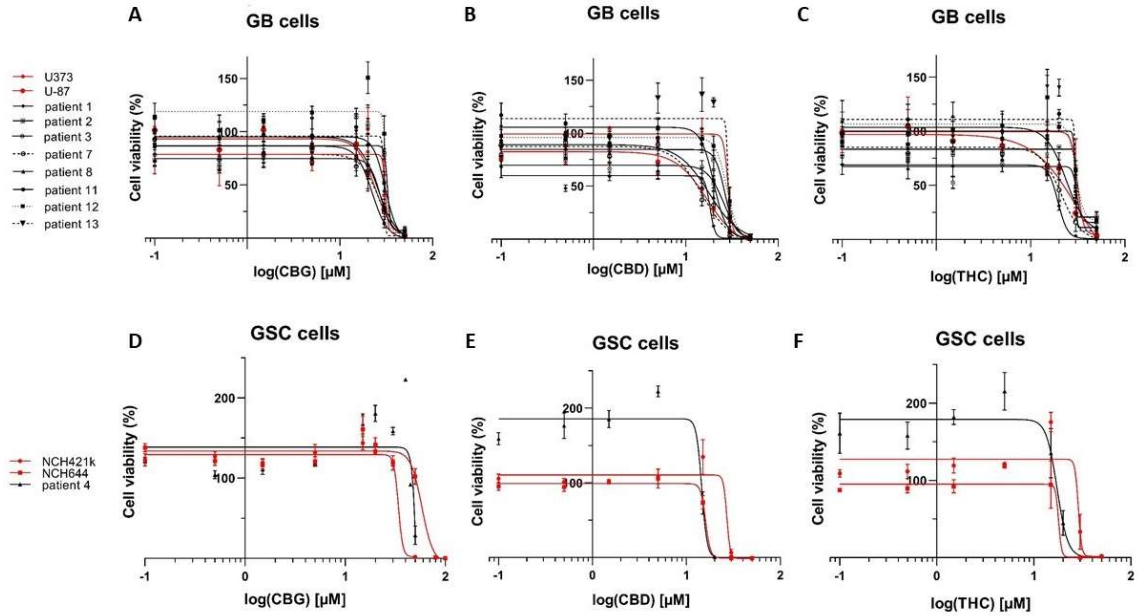

Figure 7: Cannabinoids reduce GB cell and GSC viability. CBG (A, D), CBD (B, E), and THC (C, F) decrease the viability of differentiated GB cells and GSCs. IC50 curves of cell viability measured by MTT assay (y-axis) and different CBG, CBD, and THC concentrations increasing in the range of 0.1–50 µM (x-axis log scale) for established GB cells (U87 and U373) (A, B, C; red lines) and primary patient-derived GB cells (A, B, C; black lines) are presented. Established GSC lines NCH421k and NCH644 (D, E, F; red lines) and primary patient-derived GSCs (D, E, F; black line) after 48 h of cannabinoid treatment. Data are presented as mean values ± S.E.M. (n=3–5 independent biological experiments, each in technical triplicate). Vehicles comprised ≤ 0.1% (v/v) DMSO for THC and CBD and 0.24% (v/v) ethanol for CBG.

Table 11: The inhibitory effects of CBG, CBD, and THC on the viability of GB cells and GSCs, estimated as IC50 [µM].

Cell lines (GB)	**CBG [µM]**	**CBD [µM]**	**THC [µM]**
U87	24.2	17.4	25.5
U373	31.1	29.7	34.9
NIB138	22.3	18.3	19.5
NIB140	32.0	26.7	29.9
NIB142	27.4	25.9	34.4
NIB160	26.3	15.0	21.1
NIB167	25.6	12.6	23.7
NIB180	30.8	20.1	29.6
NIB182	31.6	28.1	30.2
NIB185	29.8	28.8	30.0
Mean ± S.E.M.	28.1±1.1	22.2±2.1	27.9±1.8
Stem cell lines (GSCs)	**CBG [µM]**	**CBD [µM]**	**THC [µM]**

NCH644	58.3	15.9	22.3
NCH421k	34.0	27.9	28.7
K26	84.8	14.6	17.4
Mean ± S.E.M.	**59.0±14.7**	**19.5±4.2**	**22.8±3.3**

IC50 values (in μM) for CBG-, CBD-, and THC-treated GB cells and GSCs were calculated from the half maximal inhibitory effects on GB and GSC viability using GraphPad Prism software, as described by Deng et al. (Deng et al., 2017) and in detail in the Methods. Each value represents the mean of three independent biological assays (individual S.E.M. values are shown in Figure 7). U87/ U373 (red) are established differentiated GB cells, NCH644/NCH421k (red) are established GSC cell lines, NIBXXX and KXX are primary patient-derived differentiated GB cell and GSCs.

4.1.3 The Effects of CBG, CBD, and TMZ on GB Cell and GSC Invasion

Invasion is an important feature of GB that can also be targeted to improve treatment responses. Therefore, we examined the inhibitory effects of the two cannabinoids with the 3D spheroid invasion assay. The GB lines U87, U373, and T98 were treated with increasing concentrations of CBD and CBG, with responses varying below IC50 concentrations. We demonstrated that CBD and CBG at concentrations above 10 μM significantly inhibited invasion by 50–70% (Figure 8A, 8B, 8C), particularly of U87 cells in this experimental setup. Overall, CBD appears to be a less potent inhibitor of cell invasion than CBG in all differentiated cell lines. No statistically significant decrease in cell invasion was observed in the GSC line NCH421k after CBD treatment alone. However, invasion was significantly inhibited by almost 50% by the 3:1 CBD:CBG combination (Figure 8D).

In addition, the effect of CBD and CBG on cell invasion in 3D cultures was compared to that of the chemotherapeutic agent TMZ, which reduced U87 cell invasion by approximately 50% at both 100 μM and 400 μM. However, under the same conditions, 10 μM CBG inhibited U87 cell invasion by 90%, showing stronger efficacy than TMZ. By contrast, 50 μM CBG only inhibited U373 cell invasion by 50%, while 100 and 400 μM TMZ inhibited U373 cell invasion by 60% and 80%, respectively (Figure 8B). Both CBG and TMZ at the highest concentrations (50 μM and 400 μM) inhibited the invasion of T98 cells by 70% (Figure 8C). In GSC line NCH421k, CBG, CBD, and TMZ treatments alone did not reduce cell invasion. However, the CBD:CBG combination significantly inhibited GSC invasion. Conversely, TMZ actually increased GSC invasion (Figure 8D).

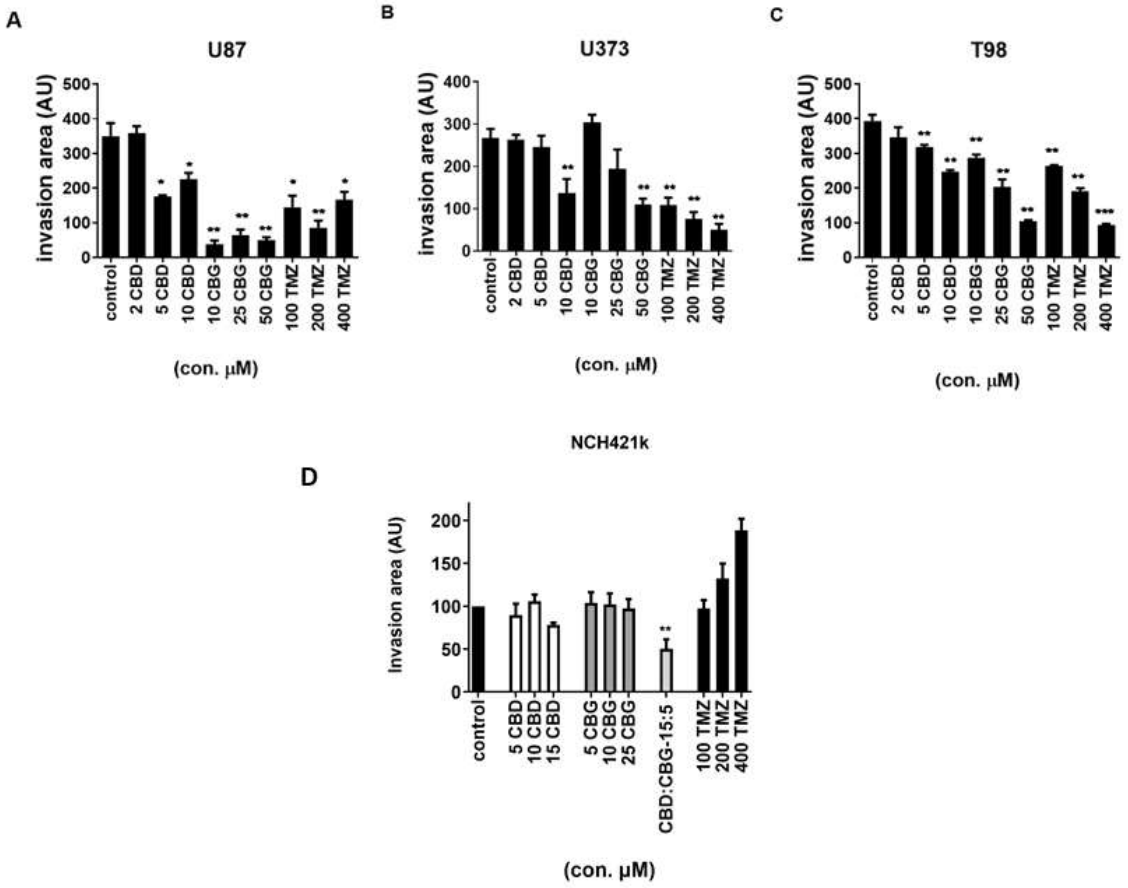

Figure 8: The effect of CBD and CBG on the invasion of GB cells and GSCs. Spheroids were treated with CBG (10, 25, and 50 µM), CBD (2, 5, and 10 µM), and TMZ (100, 200, and 400 µM). Invasion distance was measured after 5 days in Matrigel using the fluorescence microscope NIKON Eclipse Ti Series at 4x magnification. Invasion area was normalized to spheroid diameter as determined using ImageJ software. CBG and TMZ inhibited cell invasion in all three GB cell lines. In GSC line NCH421k, no significant decrease in cell invasion was observed after CBD, CBD, or TMZ treatment alone. However, the combination of CBD:CBG at a ratio of 3:1 significantly inhibited invasion by almost 50% (D). Data are presented as mean ± S.E.M. of five to six independent experiments. Statistical analyses were performed with GraphPad Prism software using a one-way Anova test (*$p < 0.05$, **$p < 0.01$, and ***$p < 0.001$). U87, U373 and T98 are established GB cell lines and NCH421k is established GSC line.

4.2 PART II: *Ex Vivo* GBOs Translate Novel Therapeutic Discoveries Tailored to Individual Patient Tumours

4.2.1 Organoids Grow in Culture and Retain Characteristics of the Parental Tumour

GB tumours are extremely resistant to standard-of-care treatments that include IR and chemotherapy. Studying the effects of GB standard therapy, IR and TMZ, in the context of the TME is only possible with the GBO model. GBOs were established from freshly resected patient tumour tissues according to the protocol of Jacob et al. (Figure 9A) (Jacob,

Salinas, et al., 2020). The success of GBO establishment and growth rate was highly dependent on the quality and characteristics of the original tumour tissues (Figure 9A, 9B). The success rate for establishing GBOs derived from GB tissues in our study was 69%. By immunofluorescent staining of selected cell type-specific markers, we confirmed that stromal cells of the TME are preserved within GBOs in culture (Figure 10A). Macrophages, microglia, and endothelial cells were detected among differentiated GB cells and GSCs. In general, the abundance of stromal cells in GBOs reflected their abundance in patient tumour tissue, although significant differences were sometimes observed between individual GBOs from the same patient, reflecting intra-tumour heterogeneity. To prevent gradual loss of the stromal cell types (Jacob, Salinas, et al., 2020), GBOs used for experiments were never older than 3–4 weeks. We also evaluated basal cytokine secretion in GBOs and patient-derived GB cells from the same patient. GBOs secreted several cytokines, of which many are associated with tumour growth, chemoattraction, angiogenesis, immunosuppression, and resistance to therapy. These included IL-6, IL-8, CCL2 (= MCP-1), CXCL12 (= SDF-1α), CCL5 (= RANTES), M-CSF (= CSF1), ENA-78 (CXCL5), and VEGF. In addition, cytokines such as IL -6, ENA-78, and VEGF, all of which are associated with TME, were released by GBOs but not GB cells (Figure 10B).

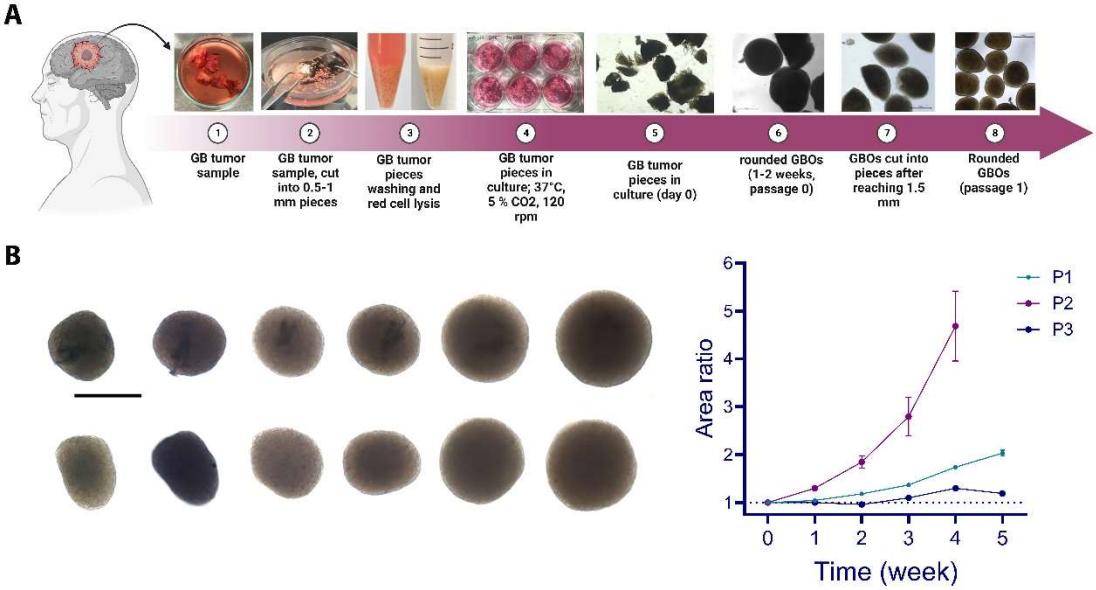

Figure 9: Overview of the procedures used to generate GBOs from resected tumour tissue. (A) Schematic representation of the main steps for generating GBOs from resected tumour tissue, created with bioRender.com. (B) Viable organoids grow in culture for five and more weeks. Quantification of GBO growth over time by calculating the ratio of the measured 2D area at each time point to the 2D area at time point 0 for individual GBOs in culture. Data represent mean values ± S.E.M. (n = 3 GBOs per sample; sample: patient (P)).

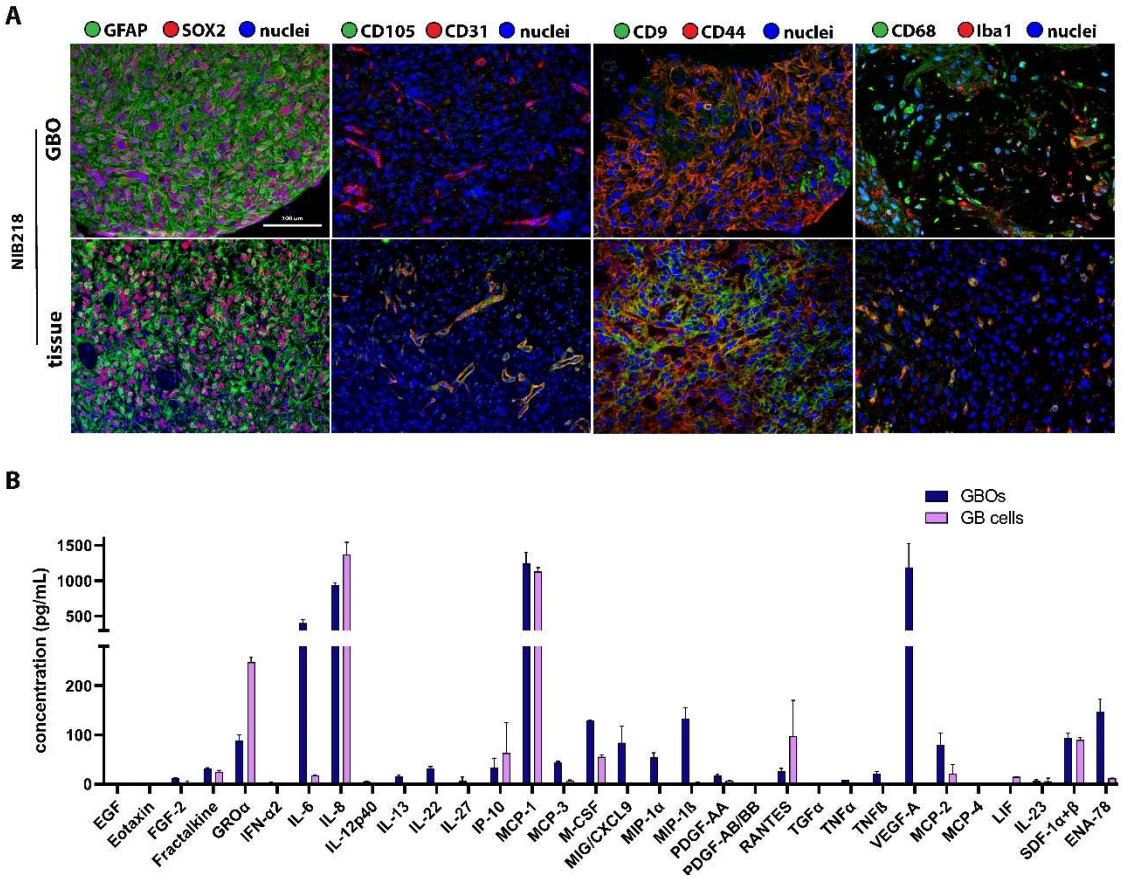

Figure 10: Immunofluorescence characterization of the GBOs and cytokine secretion. (A) Immunofluorescence characterization of the GBO tumour microenvironment. GBOs express different markers of the tumour microenvironment, including markers of GSCs (SOX2, CD9, and CD44), differentiated GB cells and astrocytes (GFAP), macrophages and microglia (CD68 and Iba1), and vasculature (CD31 and CD105). Representative images from a tissue sample from one patient are shown. Scale bar: 100 µm. (B) Cytokines and growth factors are secreted by GBOs. Cytokine levels [pg/ml] in GBO/GB cell culture medium measured by Human Cytokine/Chemokine 71-Plex Discovery Assay® Array (HD71).

4.2.2 Organoids Reflect the Gene Expression Profile of the Parental Tumour

To compare gene expression patterns between tissues and matching GBOs, we selected genes that encode GSCs (*CD9, FUT4, ID1, PROM1, SOX2*, *OLIG-2,* and *CD44*); genes involved in epithelial-to-mesenchymal transition (*STAT3, CDH1, CHI3L1, CD44*, and *SNAI1*), immunosuppression (*IDO1* and *IL6*), DNA damage response and the cell cycle (*ATM, ATR, CDKN1A, CDKN2A, MDM2, CHEK1, mTOR,* and *PIK3CA*), and cytokine signalling (*CCL2, CXCL12, CXCR4,* and *IL6*); and genes associated with immune cell populations within the TME (*AIF1, CD16, CD68, FOXP3,* and *NCAM1*). Moreover, based on the expression values of 12 subtype-specific genes according to Behnan et al., and three more genes based on in-house gene expression analyses, we classified GB tumour tissues and matching GBOs into four GB subtypes: MES, PN, CL, and mixed (MIX). The PN subtype was classified based on the genes expression levels of *OLIG2, P2RX7, STMN4, SOX10, NOTCH*, and *ERBB3*. The CL subtype was classified based on the genes

expression levels of *NFKB1*, *ACSBG1*, *S100A4*, and *KCNF1*. The MES subtype was classified based on the genes expression levels of *DAB2, TGFB1, THBS1, COL1A2*, and *COL1A1*.

A subset of 22 organoids from the corresponding tumour tissues of 17 patients were screened for the above gene groups by RT-qPCR. We then performed a statistical comparison of the gene expression profiles in the GBOs and corresponding tissue samples. The Pearson correlation coefficient was used to determine the associations in mRNA expression. We found similar correlation patterns in both groups, suggesting that the GBOs preserve the transcriptional characteristics of their tissue of origin. A correlation heat map of GBOs (Figure 11A) and tissues (Figure 11B) identified four distinct clusters of correlated genes. In both GBOs and tissues, cluster 1 consists of genes related to GSCs, DNA damage responses, and cell cycle progression. There is also a subset of genes belonging to the group of genes involved in epithelial-to-mesenchymal transition, PN, and CL subtype. Cluster 2 consists of genes that determine PN subtype; cluster 3 consists of genes associated with MES subtype, and a proportion of genes belonging to the GSC group and cytokine signalling; and cluster 4 consists of genes associated with cytokine signalling and genes related to the immune cells of the TME. For example, PN-related genes (marked with ochre squares) are grouped together in both samples (GBOs and tissues) and form a cluster in the heatmap. These results suggest that patient-derived GBOs reflect the transcriptional profile of the original tumours.

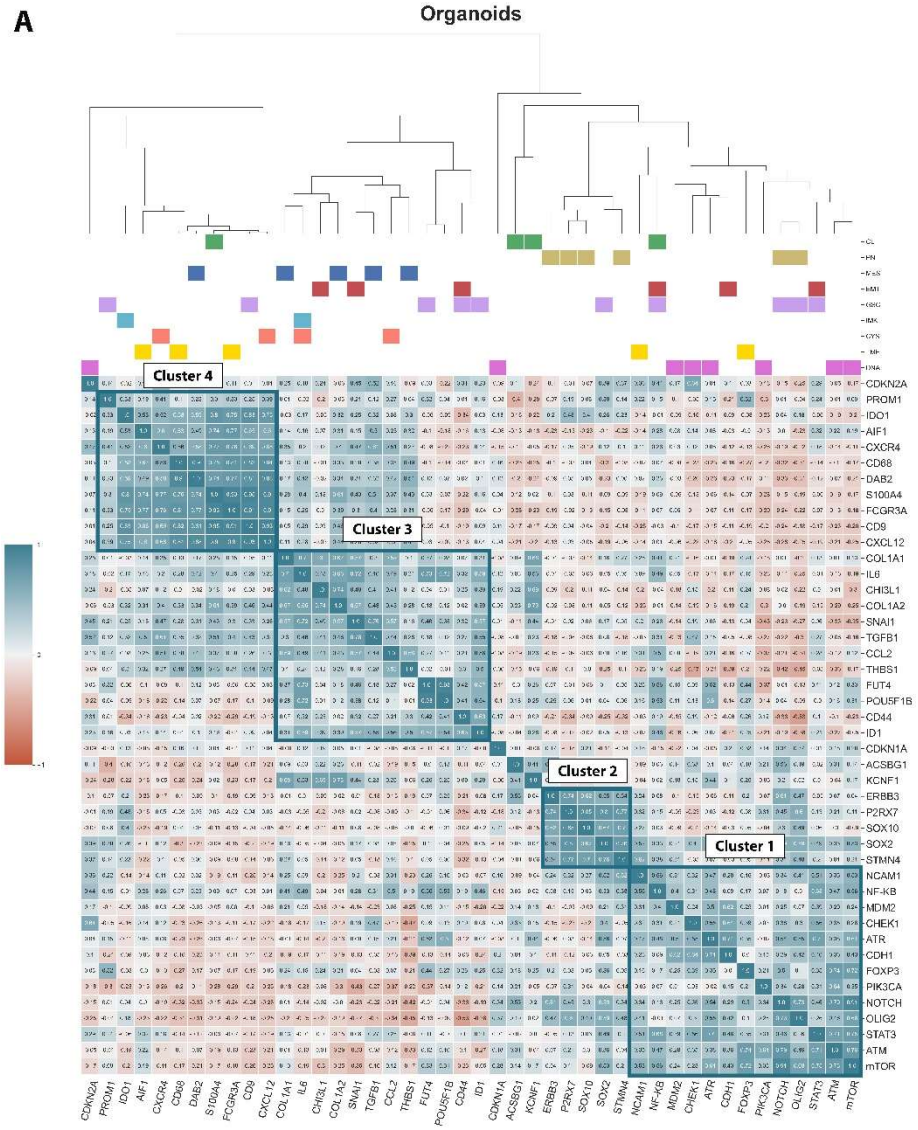
A
Organoids
Cluster 4
Cluster 3
Cluster 2
Cluster 1
CDKN2A
PROM1
IDO1
AIF1
CXCR4
CD68
DAB2
S100A4
FCGR3A
CD9
CXCL12
COL1A1
IL6
CHI3L1
COL1A2
SNAI1
TGFB1
CCL2
THBS1
FUT4
POU5F1B
CD44
ID1
CDKN1A
ACSBG1
KCNF1
ERBB3
P2RX7
SOX10
SOX2
STMN4
NCAM1
NF-KB
MDM2
CHEK1
ATR
CDH1
FOXP3
PIK3CA
NOTCH
OLIG2
STAT3
ATM
mTOR

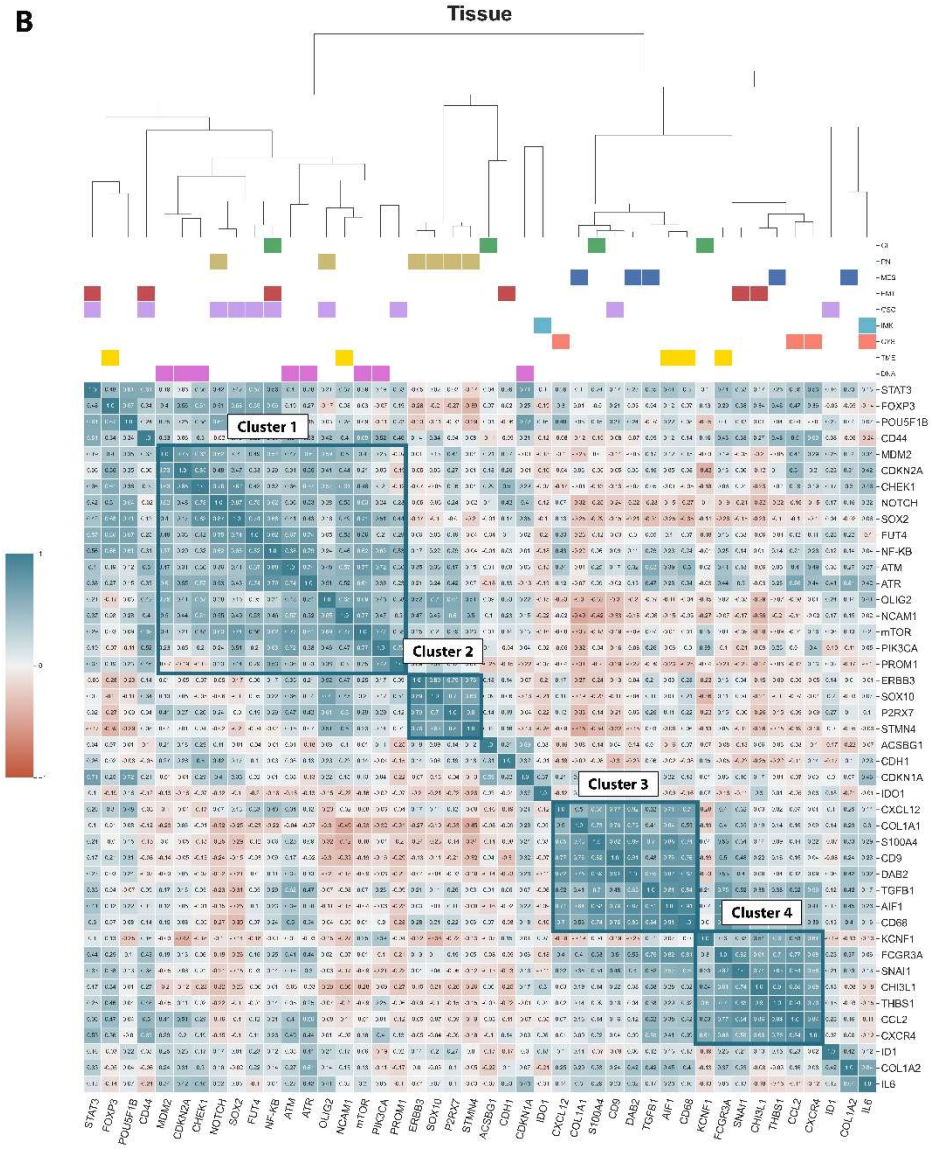

Figure 11: Correlation matrix heatmaps of the gene expression profiles in GBOs and and corresponding tumour tissues.. The heatmaps represent correlation matrixes between mRNA expression in (A) organoids and (B) tissues. Pearson correlations between gene expressions in (A) organoids samples (n_O=22) and (B) corresponding tissues (n_T=22) are displayed. These correlation coefficients are represented in heatmaps, two-way displays of a data matrix in which individual cells are displayed as coloured rectangles. The colour of an individual cell is proportional to its position along a colour gradient. The colour key indicates the correlation values between genes: blue, positive correlation; red, negative correlation. For a more structured visualization of the correlation data within the mRNA expression, clustering was carried out, i.e. grouping of data based on relationships among variables. All the features can be divided into four groups (clusters). In both organoids and tissues, cluster 1 mostly consists of genes related to GSCs (violet squares) and genes involved in DNA damage responses and the cell cycle (pink squares); cluster 2 consists of genes determining the PN subtype (ochre squares); cluster 3 consists of genes determining the MES subtype (blue squares) and genes involved in cytokine signalling (orange squares); and cluster 4 consists of genes involved in cytokine signalling (orange squares) and immune cells of the TME (yellow squares).We also selectively compared gene expression groups between GBOs and the corresponding tumour tissues. The estimation plots show that gene

expression remains stable in most cases and is not significantly different. Major changes were observed in the expression of TME-related genes, e.g. the *AIF1*, *FCGR3A* (CD16), and *NCAM1* genes are significantly different, consistent with the fact that the TME becomes underrepresented in GBO cultures (Figure 12). For other groups of genes, we only found significant changes in the gene expression for some genes from each group. For example, between GBOs and corresponding tissues, the gene expressions of *S100A4, STMN4,* and *COL1A1* differed in the CL, PN, and MES subtype groups, respectively (Figure A.1.1.). *CXCR4* gene expression differed in the group of cytokines, and *CDKN1A*, *CHEK1,* and *PIK3CA* gene expressions slightly differed in the group of DNA damage response and cell cycle (Figure A.1.2.).

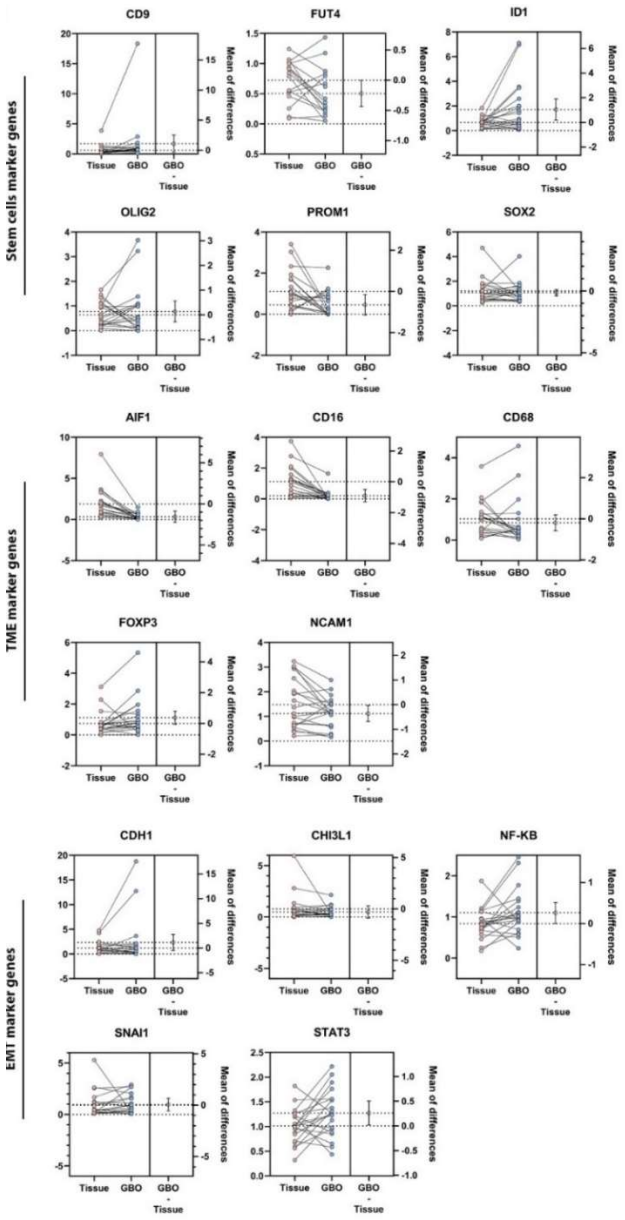

Figure 12: Comparisons of selective gene expressions between GBOs and corresponding tumour tissues. Differences in the expressions of markers of stem cells, the TME, and epithelial-to-mesenchymal transition are presented. The paired mean difference between tissue and GBO is shown in the estimation plots. Both groups are plotted on the left axes as a scatter graph showing individual values: each paired set of the individual patient is

connected by a line. Statistical analyses were performed with GraphPad Prism software using Paired t-test The paired mean difference is plotted on the right axis, and the 95% confidence interval is indicated by the error bars.

According to the TCGA data portal, GBs can be classified based on bulk RNA-seq analyses into the three subtypes PN, CL, and MES, which are associated with specific genomic alterations (Verhaak et al., 2010). These results are promising, as they suggest that each tumour could be treated by targeting distinct abnormal signalling pathways. Based on the expression of the specific genes described above, samples were assigned to one of these subtypes, and whether the subtype was maintained in the GBO model compared to the corresponding tumour tissue was assessed. In 60% of the GBO-tissue pairs, the subtype was retained (marked in bold in Table 12). In addition, we observed that, in most cases (73% for GBOs and 60% for tissues), samples exhibit a mixture of all molecular genetic subtypes, i.e. the MIX subtype. Thus, we can conclude that GBOs and tissues, in most cases, have a MIX subtype, which reflects the heterogeneity of tumours.

Table 12: TCGA subtype comparison between 22 GBOs and corresponding tumour tissues.

Patient	**GBO subtype**	**Tissue subtype**
NIB211_C	PN	MIX
NIB213_C	MES	MIX
NIB214_REC	**CL**	**CL**
NIB215_C	**MIX**	**MIX**
NIB216_C	MIX	MES
NIB218_R	**PN**	**PN**
NIB218_C	MIX	PN
NIB219_REC	**MIX**	**MIX**
NIB220_R	MIX	PN
NIB220_C	**MIX**	**MIX**
NIB225_C	**MIX**	**MIX**
NIB227_R	**MIX**	**MIX**
NIB228_REC	**MIX**	**MIX**
NIB231_C	**MIX**	**MIX**
NIB232_R	**MIX**	**MIX**
NIB235_C	MIX	MES
NIB237_C	MES	MIX
NIB239_C	MIX	MES
NIB240_C	**PN**	**PN**
NIB240_R	**MIX**	**MIX**
NIB246_R	MIX	PN
NIB246_C	**MIX**	**MIX**

Matching subtypes between GBOs and tissues are emphasized in bold. NIBXXX, patient ID; C, core; R, rim; REC, recurrent GB.

4.2.3 Standard GB Therapy Alters the Surface-Associated Cells But Not the Viability or Invasion of GBOs

To study how IR and chemotherapy affects tumours, we mimicked therapy *in vitro* on the GBO model. GBOs were irradiated with a single dose of IR (10 Gy) and exposed to daily treatment with 50 µM TMZ for 1 week. The overall effects of the treatment were assessed on GBOs from six GB patients using Cell-Titer Glo 3D viability assay (Figure 13A). Partial responses (i.e. decreases in viability) were observed in GBOs from two patients; however, overall, GBO viability was not significantly affected by IR and TMZ.

We also studied the effects of IR and TMZ on GB invasion, which is one of the main obstacles in successfully treating GB. We set up an invasion assay of GBOs embedded in Matrigel and monitored the invasion of GBOs into the 3D matrix after 48 h. None of the treatments (IR, TMZ, or their combination) had a significant effect on GBO invasion (Figure 13B).

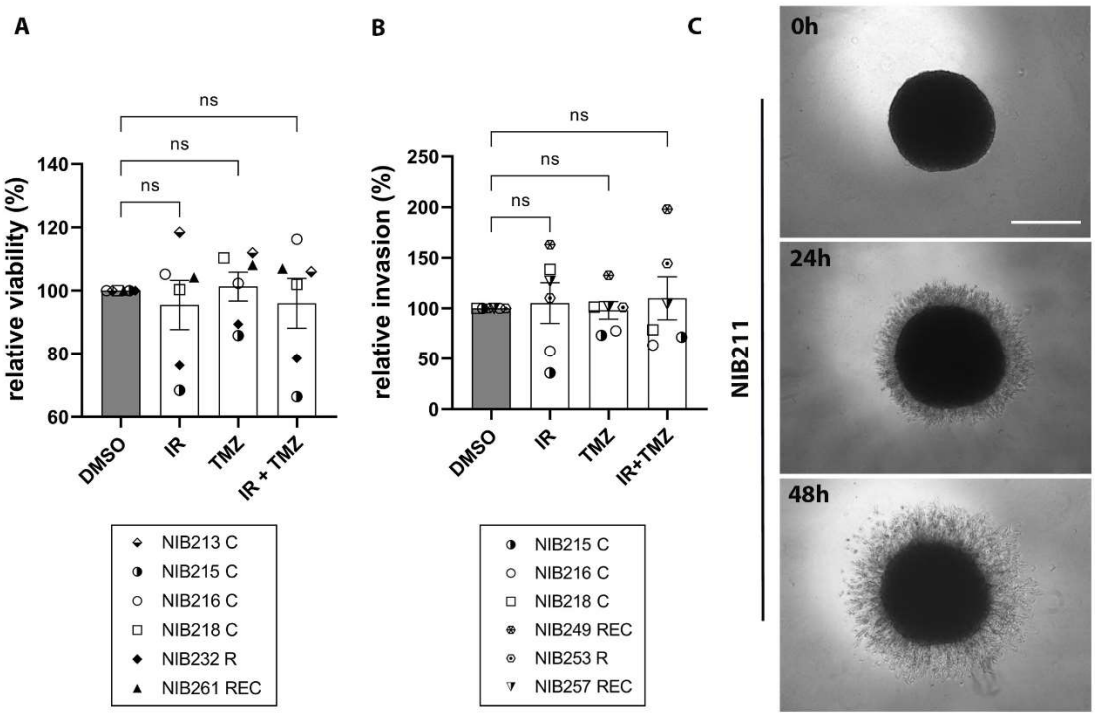

Figure 13: Treatment with IR and TMZ does not significantly affect GBO viability or invasion in Matrigel. (A) The effect of IR (10 Gy, single dose), TMZ (50 µM, daily 1 week), and their combination on GBO viability, which was measured with Cell-Titer Glo 3D assay. Data are presented as means ± S.E.M. of five patient samples. (B) The effect of IR (10 Gy, single dose), TMZ (50 µM), and their combination on GBO invasion in Matrigel, which was quantified 48 h after treatment. Data are presented as mean values ± S.E.M. of six patient samples. Statistical analyses were performed with GraphPad Prism software using the one-way repeated measures ANOVA test. (C) Representative images for one condition (TMZ treatment) after 24 and 48 h are shown. Scale bar: 500 µm. Legend: NIBXXX, patient ID; C, core; R, rim; REC, recurrent GB.

The morphology of GBOs and the effects of standard therapy on GBO surfaces were studied with SEM. Low-magnification SEM images show a compact round structure with a granular surface of NIB211 GBOs (Figure 14A). At a higher magnification, the granular structure is shown to be caused by protruding cells (Figure 14B) that possess numerous astrocyte-like long protrusions (arrows; Figure 14C).

Treatment with 50 µM TMZ and 10 Gy IR did not alter the overall shape of NIB211 organoids (Figure 14D), but fewer protruding cells were visible at GBO surfaces at higher magnification (Figure 14E) and with shorter protrusions (Figure 14F). Moreover, numerous cells lost their membrane integrity due to apoptosis or necrosis (Figure 14F).

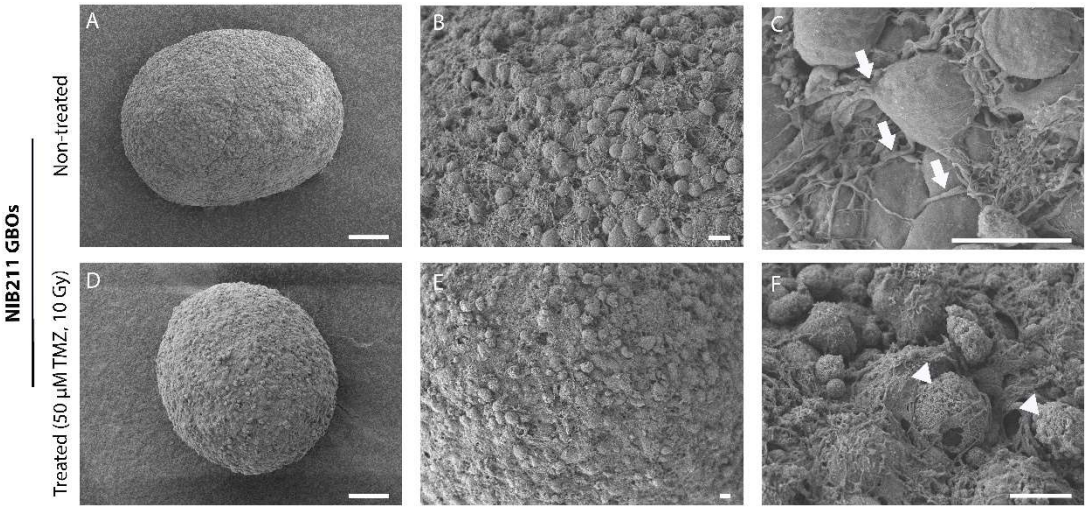

Figure 14: Scanning electron microscopy (SEM) of NIB211 GBOs. SEM images of non-treated (A–C) and TMZ- and IR-treated (D–F) GBOs at low (A, D), medium (B, E), and high magnification (C, F). Both non-treated and treated GBOs are round and compact, whereas the granular aspect at high magnification appears to be caused by protruding cells at the GBO surface that possess high numbers of long protrusions (arrows in C). Treatment with TMZ and IR resulted in necrotic cells that lost their membrane integrity (arrowheads in F) and most of their protrusions (F).

Based on the SEM results, we further tested whether standard treatment induces cell death via early and late apoptosis in GBOs from two different patients (NIB232_R and NIB279_C). GBOs were treated as described in section 4.2.3. Significant changes in the percentage of cells in early and late apoptosis were observed after treatments. In both patients, IR, TMZ, and the combination of both treatments increased the percentage of apoptotic cells in GBOs by 7%, 6%, and 5%, respectively. This suggests that the observed effect on apoptosis was attributed to a small percentage of cells on the GBO surfaces (Figure 15).

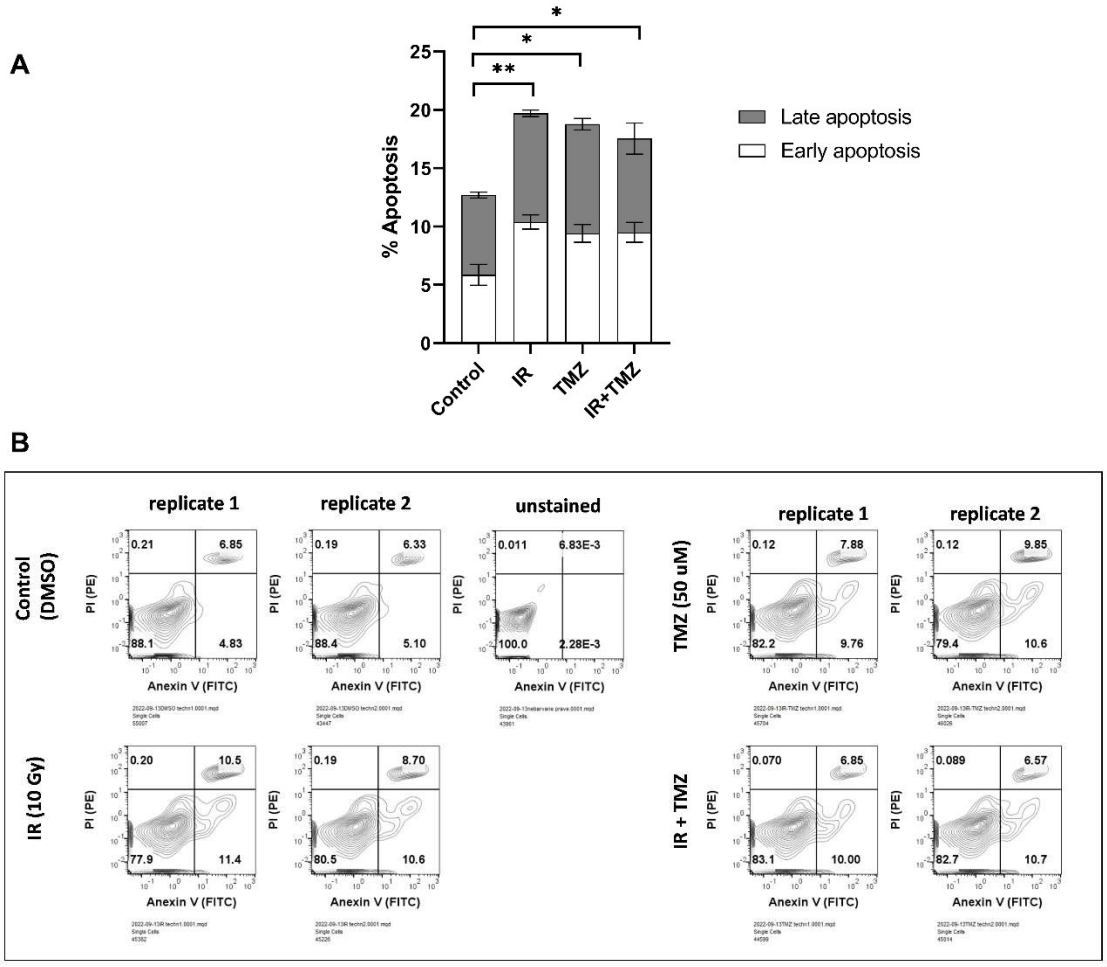

Figure 15: The determination of apoptosis in GBOs by flow cytometry. GBOs (n_O=2 for each condition) were irradiated with a single dose of IR (10 Gy) and exposed to daily treatment with 50 µM TMZ for 1 week. (A) The percentage of cells in early and late apoptosis after TMZ and IR treatment (mean ± S.E.M.). (B) After GBO dissociation, cells were labelled with Annexin-V-FITC (x-axis) and propidium iodide (PI) (y-axis) and analysed by flow cytometry. Dot blots represent the results from GBOs from one patient. Statistical analyses were performed using GraphPad Prism software, using ordinary one-way ANOVA test (*p < 0.05, **p < 0.01).

4.2.4 The Effect of Standard Therapy on the Expression of Selected Genes in GB Cell Models

To evaluate the effect of standard therapy on GBOs at the level of gene expression, we analysed the expression patterns of individual genes associated with GSCs, immune cells, epithelial-to-mesenchymal transition, cytokines, DNA damage response and cell cycle and subtype gene signatures. We exposed 10 GBOs from 11 patients to a single dose of IR (10 Gy) and a weekly treatment with 50 µM TMZ. In total, 44 genes were assessed, and changes in their expression after TMZ, IR treatment or the combination of IR with TMZ treatment, were observed (Figure 16). Four genes *MDM2*, *CDKN1A*, *ATM* and *ATR*, all involved in DNA damage responses, the cell cycle, and the p53 pathway, were significantly upregulated in GBOs after treatment (Figure 16B). TCGA subtyping of non-treated and treated GBOs

revealed no changes in subtypes after treatment. Most GBOs represent a mixture of all genetic subtypes (MIX) (Table 13).

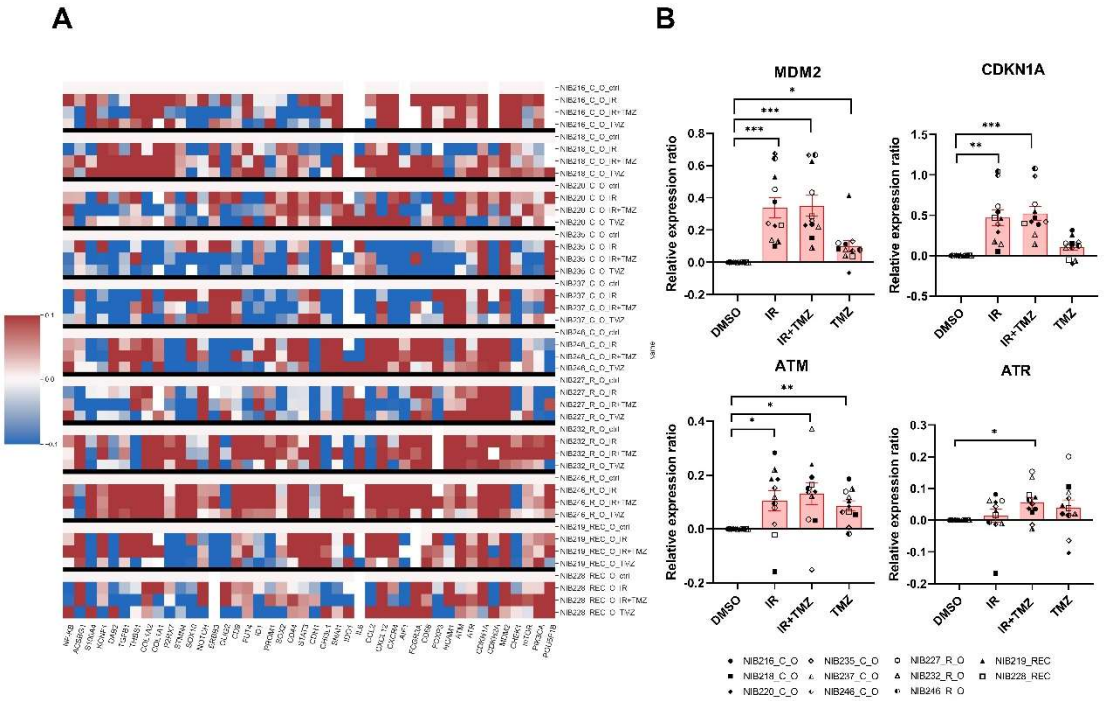

Figure 16: A heatmap of relative gene expression ratios in treated GBOs and upregulation of DNA damage response and cell cycle genes. A)In total, 11 patient samples (n_O=11) were used. Relative gene expression ratios in GBOs treated with IR (10 Gy, single dose), TMZ (50 µM, 1 week), or the combination of IR and TMZ are presented as downregulation in blue and upregulation in red. The baseline expression is represented in white. The tested genes are provided below, and the GBOs and treatments are provided on the right side of the heatmap. B) *CDKN1A*, *MDM2, ATM and ATR* genes are upregulated in GBOs treated with TMZ, IR or IR and TMZ. Data are presented as mean values ± S.E.M. of 11 patient samples (n_O=11). Significance of gene expression among groups were evaluated on log2 transformed values (log2(treatment/control(DMSO)). Statistical analyses was performed with GraphPad Prism software using the one-way repeated measures paired ANOVA test. Data are presented as mean values ± S.E.M. (* $p < 0.05$, ** $p < 0.01$, *** $p < 0.001$). Legend: NIBXXX, patient ID; C, core; R, rim; REC, recurrent GB.Table 13: TCGA subtype comparison between non-treated and treated GBOs.

Patient	Control	IR	TMZ	IR+TMZ
NIB216_C	MIX	MIX	MIX	MIX
NIB218_C	MIX	MIX	MIX	MIX
NIB219_REC	MIX	MIX	MIX	MIX
NIB220_C	MIX	MIX	MIX	MIX
NIB227_R	MIX	MIX	MIX	MIX
NIB228_REC	MIX	MIX	**MES**	MIX
NIB232_R	MIX	MIX	MIX	**CL**
NIB235_C	MIX	MIX	MIX	MIX

NIB237_C	**MES**	MIX	MIX	MIX
NIB246_R	MIX	MIX	**MES**	MIX
NIB246_C	MIX	MIX	MIX	MIX

Subtypes different than MIX are displayed in bold. NIBXXX, patient ID; C, core; R, rim; REC, recurrent GB.

4.2.5 Gene Expression in GBOs, Differentiated GB Cells, and GSCs in Response to Therapy

To compare the effect of standard therapy on GB cells, GSCs, and GBOs at the gene level, patient-derived GB cells (n=5) and GSCs (n=5) were subjected to a single dose of IR (2 Gy) and a 48 h treatment with 50 µM TMZ. In contrast to GBOs, significant upregulation of *CD44, MTOR, THBS1* and *ATM* genes was observed in GSCs. *OLIG2* gene was downregulated after IR and TMZ combined treatment. In differentiated GB cells, *TGFB1* was downregulated and *ATR* was upregulated after treatment (Figure 17).

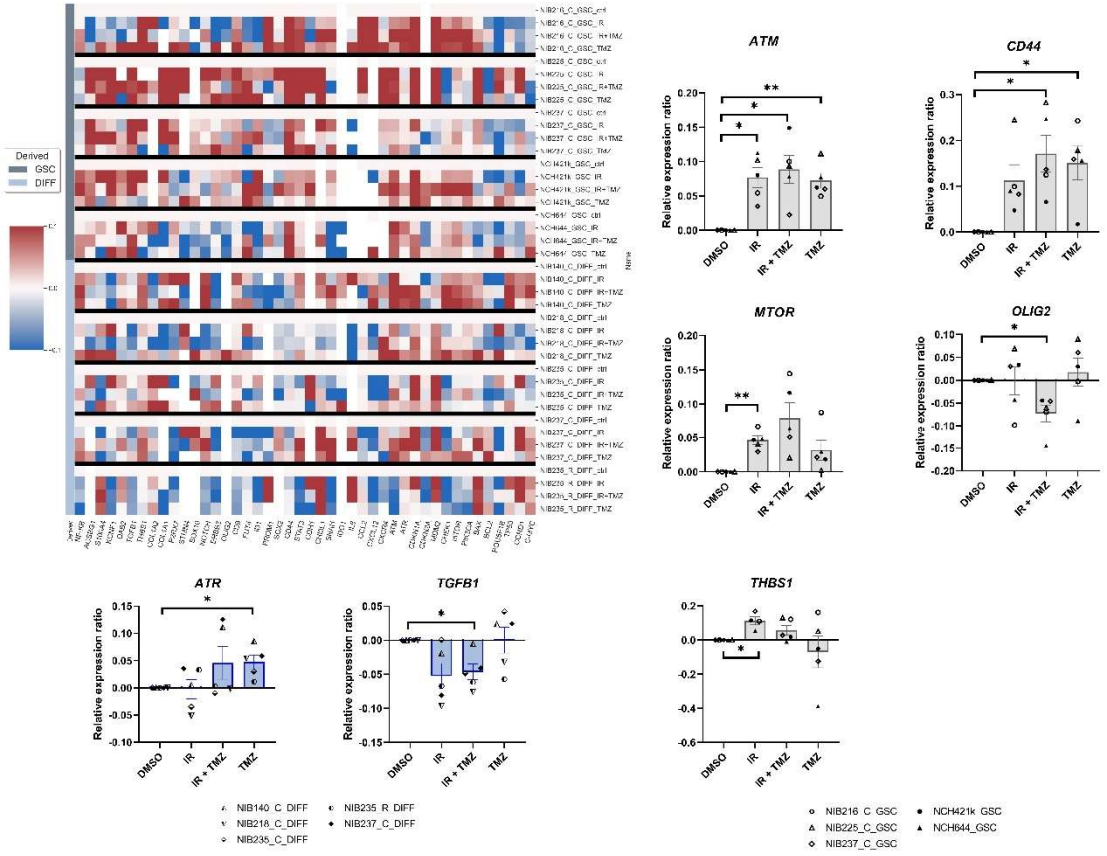

Figure 17: A heatmap of relative gene expression levels in treated GB cells and GSCs and deregulation of different genes. Relative gene expression ratios in treated cells with IR (2 Gy, single dose), TMZ (50 µM, 48 h), or combination (IR+TMZ) are presented as downregulation in blue and upregulation in red. The baseline expression is represented in white. The tested genes are shown below, and cell and treatment types are shown on the right. GSCs (n_{GSCs}=5) and differentiated GB cells (DIFF) (n_{DIFF}=4) are shown in grey and blue, respectively. In GSCs (n=5), treatment with IR, TMZ, or IR and TMZ combined increased *CD44*, *MTOR, THBS1* and *ATM* and decreased *OLIG2* gene expression (bar charts in grey). In differentiated GB cells (n=5), treatment with IR and TMZ combined

decreased *TGFB1* and treatment with TMZ increased *ATR* gene expression. Significance of gene expression among groups were evaluated on log2 transformed values (log2(treatment/control(DMSO)). Statistical analyses was performed with GraphPad Prism software using the one-way repeated measures paired ANOVA test. Data are presented as mean values ± S.E.M. * $p < 0.05$, ** $p < 0.01$. Legend: NIBXXX, patient ID; C, core.

4.2.6 Cathepsin X in the GB TME

4.2.6.1 The Expression and Enzymatic Activity of Cathepsin X are Upregulated in GB Tissues

Cathepsin X gene expression was examined in low-grade glioma tissues (LGGs), GBs, nontumour brain tissues, and primary GB cells and GSCs derived from GB tissues. Cathepsin X mRNA expression was highest in recurrent GB tissue, followed by *de novo* GB and LGG tissue. Compared to recurrent and *de novo* GB tissues, nontumour brain tissues exhibited significantly lower cathepsin X mRNA expression (Figure 18A). Compared to GSCs, normal astrocytes and GB cells exhibited higher cathepsin X mRNA expression (Figure 18B). In addition, we examined cathepsin X mRNA expression in the four GB subtypes MES, PN, CL, and MIX. All GB subtypes expressed the cathepsin X gene, with the subtype MIX expressing the lowest levels. The only significant difference in cathepsin X expression between subtypes was between CL and MIX (Figure 18C). In our study of 48 GB patients, cathepsin X median gene expression levels did not correlate with GB patient overall survival (Figure 19).

Cathepsin X protein levels between GB and nontumour brain tissue were analysed using ELISA. Cathepsin X protein levels did not differ between groups; however, a trend towards higher cathepsin X protein levels in GB was observed (Figure 20A). By contrast, the enzymatic activity of cathepsin X was significantly higher in GB tissue compared to nontumour brain tissue (Figure 20B).

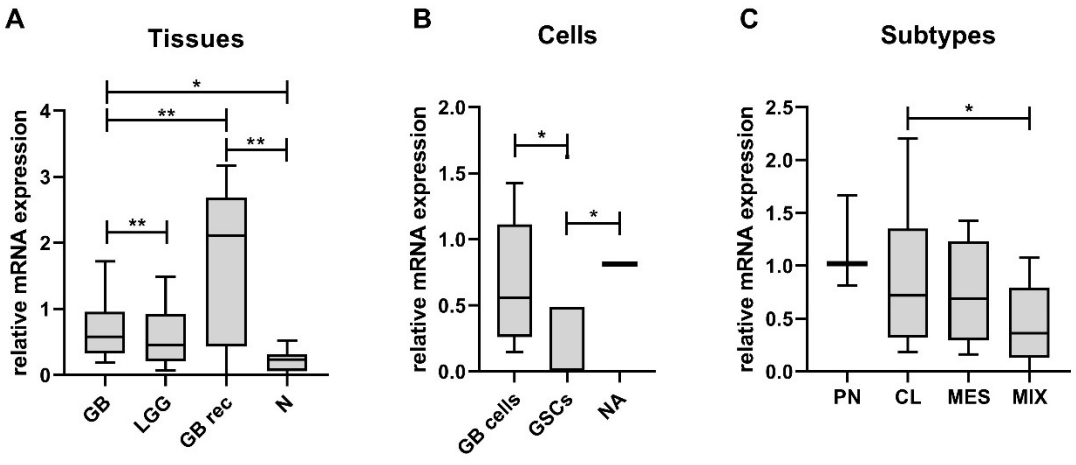

Figure 18: Cathepsin X mRNA expression. Cathepsin X gene expression levels were increased in *de novo* GB tissues (n=43) and recurrent GB (GB rec, n=5) compared to LGG (n=14) and nontumour brain tissues (N, n=16). (B) Cathepsin X gene expression levels were highest in primary GB cells (n=17), followed by normal astrocytes (NA, n=1) and GSCs (n=6). (C) Cathepsin X mRNA was expressed in classical (CL, n=18), proneural (PN, n=3), mesenchymal (MES, n=17), and mixed (MIX, n=25) GB subtypes. Data are presented as mean values ± S.E.M. * $p < 0.05$, ** $p < 0.01$.

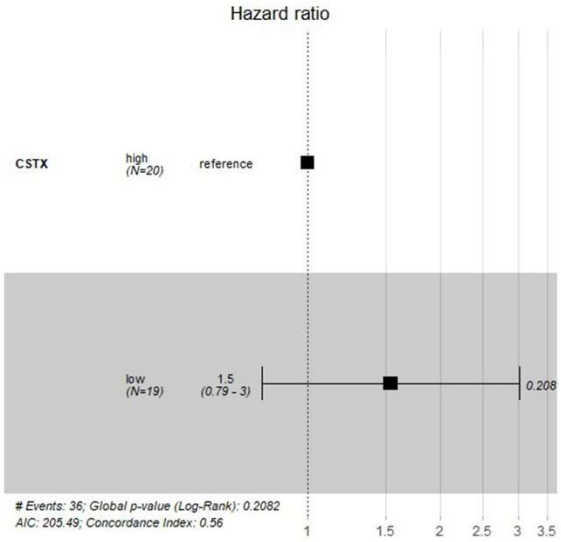

Figure 19: Relative cathepsin X mRNA expression levels were not associated with the overall survival of GB patients. Forest plot model showing the association between cathepsin X mRNA levels (low and high) and overall survival of GB patients with confidence interval of 95%. Cox proportional hazard regression was calculated to assess survival in GB sample cohorts of different groups. Log-rank test was used to evaluate statistically significant differences.

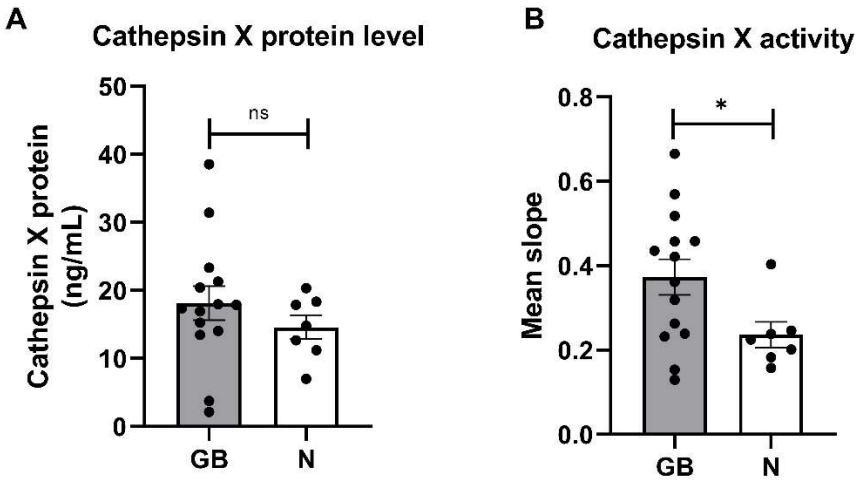

Figure 20: Cathepsin X protein levels and activity. (A) Cathepsin X protein levels did not differ between GB tissues (n=14) and nontumour tissues (N, n=7). (B) Cathepsin X enzyme activity was significantly higher in GB tissues (n=14) compared to nontumour tissues (N, n=7). Data are presented as mean values ± S.E.M. * $p < 0.05$.

4.2.6.2 Macrophage- and Microglia-Specific Localisation of Cathepsin X in GB Tissues

We detected high cathepsin X levels in GB sections. To determine which cells express cathepsin X, we performed immunofluorescence analysis. We used CD68 and Iba1 as biomarkers for immune cells in GB tissues, mainly macrophages and microglia, respectively, because cathepsin X is known to be expressed in immune-like cells. GFAP was used as an astrocytic marker, and SOX2 and CD133 were used as GSC biomarkers. The cellular localisation of cathepsin X in GB was determined by immunofluorescence staining of tissue sections from four GB patients (Figures 21, A.3) and of two nontumour brain tissue sections (Figures 22, A.3). Cathepsin X mostly localised within cells of the innate immune system, i.e. macrophages and microglia (markers CD68 and Iba1), and was also expressed in some GFAP-, SOX2-, and CD133-positive cells. Localisation of cathepsin X in CD68-positive and Iba-1-positive cells in nontumour brain tissue (NB) is also shown (Figure 22).

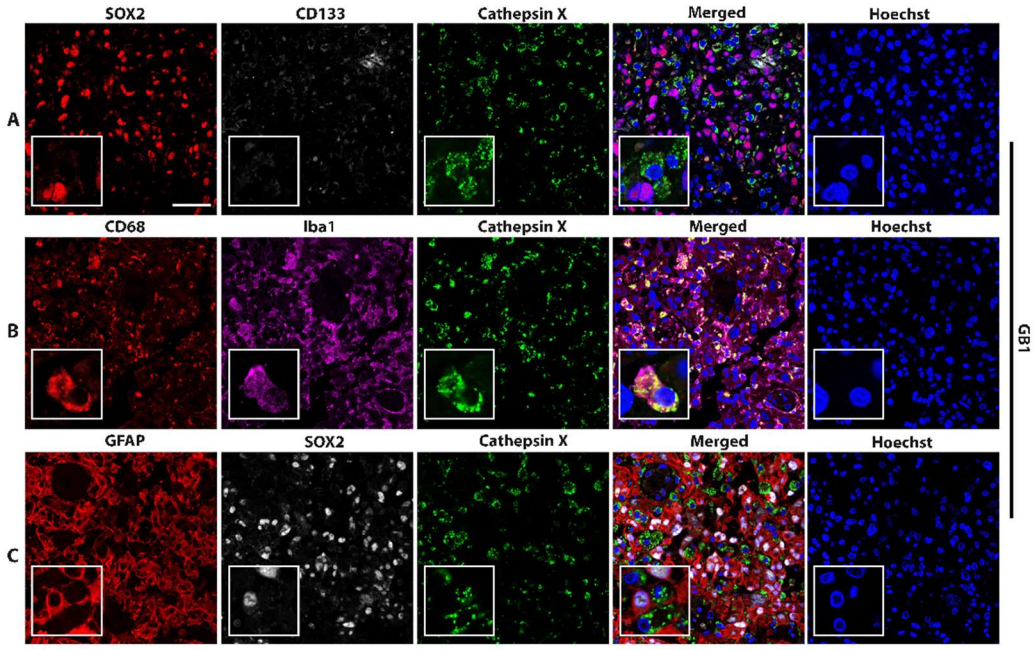

Figure 21: Expression and cell-specific localisation of cathepsin X in GB tissue. Representative images of triple immunofluorescence staining of cathepsin X (green) and markers of (A) GSCs (SOX2 (red) and CD133 (grey)), (B) macrophages (CD68 (red)) and microglia (Iba1 (purple)), and (C) GB cells and astrocytes (GFAP (red)) and GSCs (SOX2 (grey)) are shown. Cell nuclei were stained with Hoechst 33258 (blue). Scale bar: 50 µm.

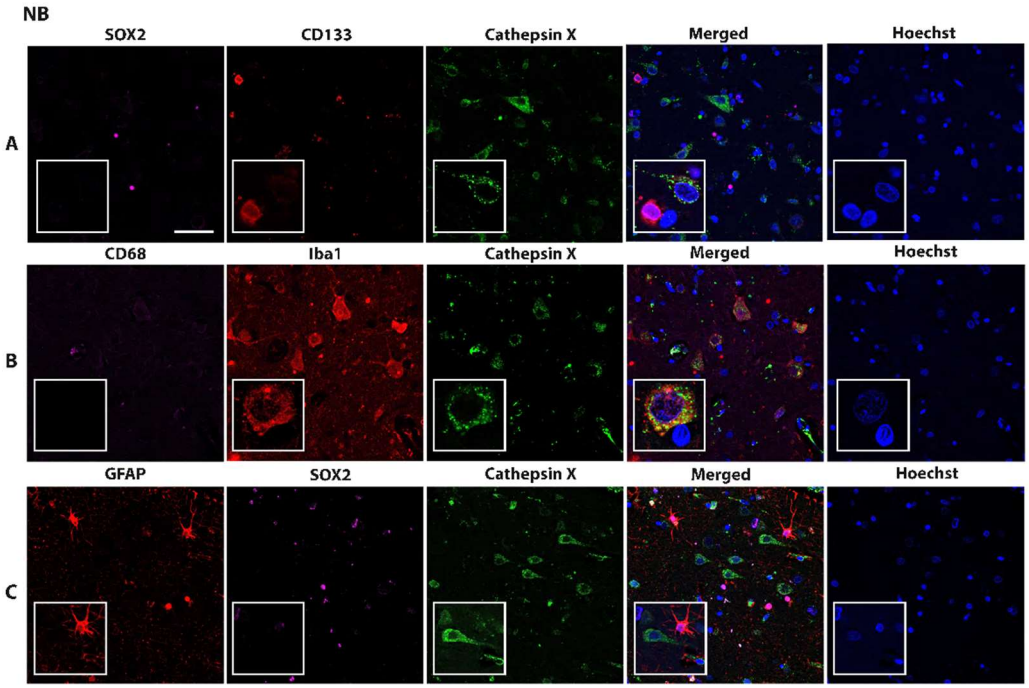

Figure 22: Localisation of cathepsin X in nontumour brain tissue (NB). Representative images of triple immunofluorescence staining of cathepsin X (green) and markers of (A) GSCs (SOX2 (purple) and CD133 (red), (B) macrophages (CD68 (purple)) and microglia (Iba1 (red), and (C) GB cells and astrocytes (GFAP (red)) and GSCs (SOX2 (purple) are shown. Cell nuclei were stained with Hoechst 33258 (blue). Scale bar: 50 µm.

4.2.7 The Role of Cathepsin X in GB and the Effects of Cathepsin-X-Selective Inhibitors

4.2.7.1 Cathepsin X Inhibition Decreases the Viability of Primary Patient-Derived GB Cells and GB-Stromal Cells

First, GB cell viability and proliferation were examined after 48 h of treatment with two selective cathepsin X inhibitors: irreversible inhibitor AMS36 and reversible inhibitor Z7. The effects of these inhibitors were tested on both the primary patient-derived GB cells NIB140 and GSCs NCH421k. AMS36 decreased the viability of NIB140 cells by up to 45%, and Z7 by up to 20%, as compared to the vehicle control (0.25% DMSO) (Figure 23A). Similarly, AMS36 and Z7 reduced NIB140 cell proliferation, as shown by the CFSE staining assay. Increased cell CFSE fluorescence intensity indicates decreased cell proliferation in cell culture. CFSE-labeled NIB140 cells showed an increased mean CFSE fluorescence intensity of 5% in the presence of AMS36 and Z7 compared to controls (Figure 24A). Conversely, the inhibitors did not alter NCH421k cell proliferation (Figure 24B).

We then tested the effects of cathepsin X inhibitors AMS36 and Z7 on macrophages and microglia that were exposed to soluble factors secreted by GB cells and GSCs. We used coculture models where we collected media from NIB140 and NCH421k cells and transferred the conditioned media to PMA-differentiated THP-1 cells (macrophages) and BV-2 cells (microglia) in the presence of increasing concentrations of cathepsin X inhibitors. AMS36 (at the highest concentrations tested) inhibited the viability of THP-1 macrophages treated with NIB140/NCH421k-conditioned medium (Figure 23B). AMS36 and Z7 exerted stronger effects on the cell viability of BV-2 microglial cells treated with NIB140/NCH421k-

conditioned media. AMS36 decreased viability by up to 60% at the highest concentrations (5–20 µM), whereas Z7 also showed an effect at lower concentrations in both BV-2 cells (Figure 23C).

To test the effects of cathepsin X inhibitors on GB cell invasion, a 3D cell invasion assay was performed. All the tested inhibitors inhibited NIB140 cell invasion by up to 20%. Z7 inhibited NCH421k cell invasion by up to 20% (Figure 25).

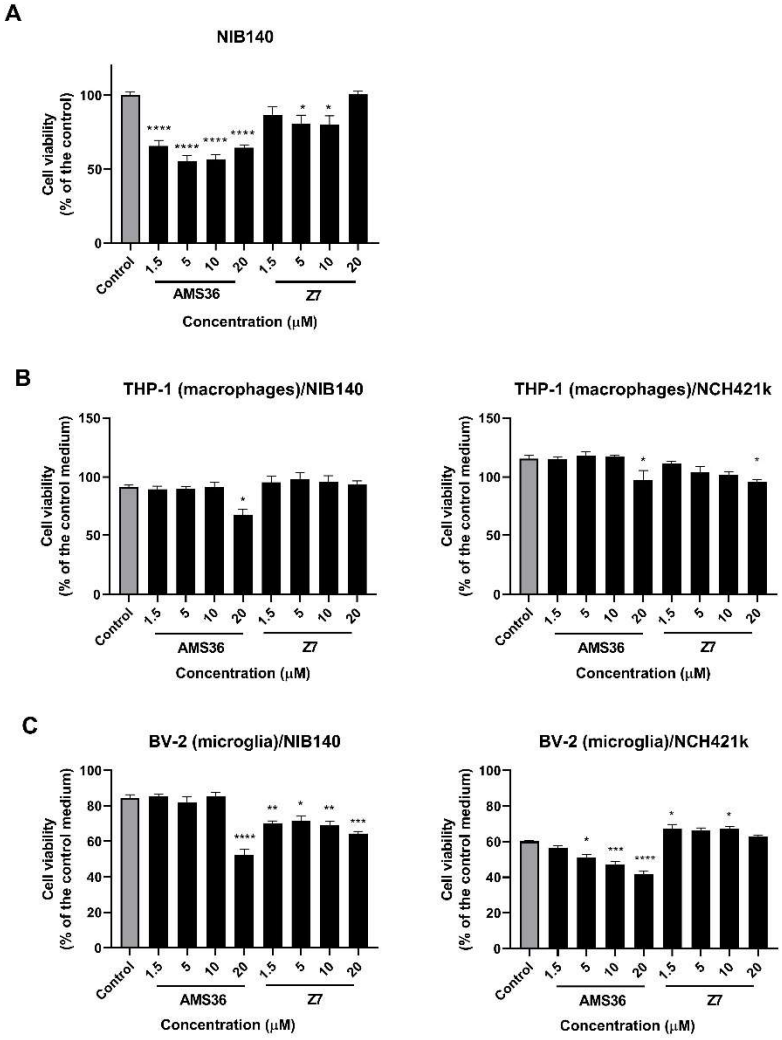

Figure 23: The effects of the cathepsin X inhibitors AMS36 and Z7 on the viability of GB cells and GB-associated cells. GB cells NIB140 (A), differentiated macrophage THP-1 cells (B), and BV-2 microglial cells (C) exposed to NIB140- and NCH421k-conditioned media were treated with AMS36 and Z7 at different concentrations. Cell viability was then assessed using the MTS assay. DMSO (0.25%) was used as a control. The control medium was a blank GB cell/GSC medium without soluble molecules secreted from GB cells/GSCs. Data are presented as mean values ± SEM. * $p < 0.05$, ** $p < 0.01$, *** $p < 0.001$, and **** $p < 0.0001$.

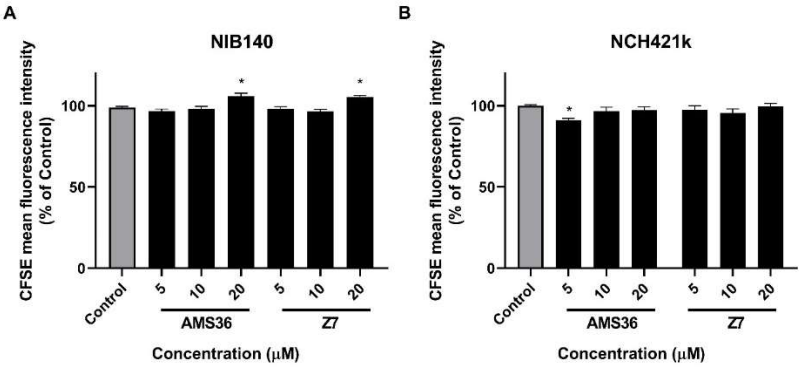

Figure 24: The effects of the cathepsin X inhibitors AMS36 and Z7 on the proliferation of NIB140 GB cells and NCH421k GSCs. NIB140 and NCH421k cells were treated with AMS36 and Z7 at different concentrations. Cell proliferation was assessed by CFSE staining and flow cytometry. The inhibitors did not alter cell proliferation, except AMS36 and Z7 at the highest concentration used for NIB140 GB cells and AMS36 at the lowest concentration used for GSCs. DMSO (0.25%) was used as a control. Data are presented as mean values ± S.E.M. Statistical analyses were performed with GraphPad Prism software using one-way ANOVA – Dunnett's multiple comparisons test (* $p < 0.05$).

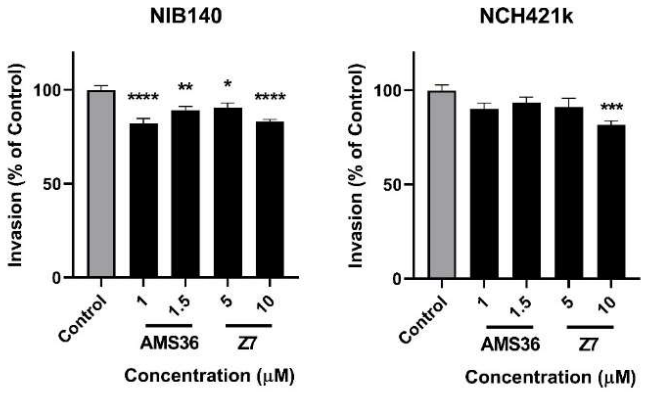

Figure 25: The effects of cathepsin X inhibitors on the invasion of GB cells and GSCs. All tested inhibitors inhibited NIB140 cell invasion by up to 20%. Z7 impaired NCH421k cell invasion by up to 20%. Control means DMSO (0.25%). Data are presented as mean values ± S.E.M. Statistical analyses were performed with GraphPad Prism software using the one-way ANOVA – Dunnett's multiple comparisons test (* $p < 0.05$, ** $p < 0.01$, *** $p < 0.001$, and **** $p < 0.0001$).

4.2.7.2 Interplay between Cathepsin X and γ-enolase in GB Tissues

Neuron-specific enolase, or γ-enolase, is aberrantly expressed in GBs (Chai et al., 2004; "Expression of ENO2 in Cancer. The Human Protein Atlas.," n.d.) and is a molecular target of cathepsin X, which cleaves the C-terminal amino acids L433 and V432 of γ-enolase (Figure 26 A-1) (Nataša Obermajer et al., 2009). To gain insight into the role of cathepsin X in GB, we explored the possible interaction of cathepsin X and its target γ-enolase in GB tissues. To test whether both proteins colocalise, we used three different primary antibodies against γ-enolase: D-7 that is specific for the epitope between amino acids 41–73 near the N-terminus, NSE-P2 that is specific for the internal region (amino

acids 271–285; to detect total γ-enolase), and NSE-P1 that is specific for amino acids 416–433 in the C-terminal region (to detect intact active γ-enolase) (Figure 26). Partial or no colocalisation of cathepsin X and γ-enolase was observed when using the antibodies that recognize the N- or C-terminus of γ-enolase (Figure 27A). However, noticeable colocalisation of cathepsin X and γ-enolase was observed when the primary antibodies against the internal region of γ-enolase were used.

Because of different colocalisation patterns, we next determined the protein levels of the intact active form, which is the C-terminally noncleaved form of γ-enolase, and the total form of γ-enolase in GB tissues. The protein levels in GB tissues measured using "in-house" ELISA were significantly lower for the intact active form of γ-enolase compared to total γ-enolase (both the intact active form and cleaved γ-enolase). Additionally, the protein level of noncleaved γ-enolase was significantly lower in GB tissues compared to nontumour brain tissues (Figure 27B). Results of immunofluorescence staining and ELISA suggested that upregulated cathepsin X activity in GB tissues may regulate the protein level of the intact active end of γ-enolase in GB by cleaving the C-terminus of γ-enolase (Figure 27). To further explore the type of cells in which cathepsin X and γ-enolase colocalise, we conducted triple immunofluorescence staining to detect colocalisation in immune-like cells in GB tissues. The analysis revealed that cathepsin X and γ-enolase colocalised in CD68-positive cells (Figure 28).

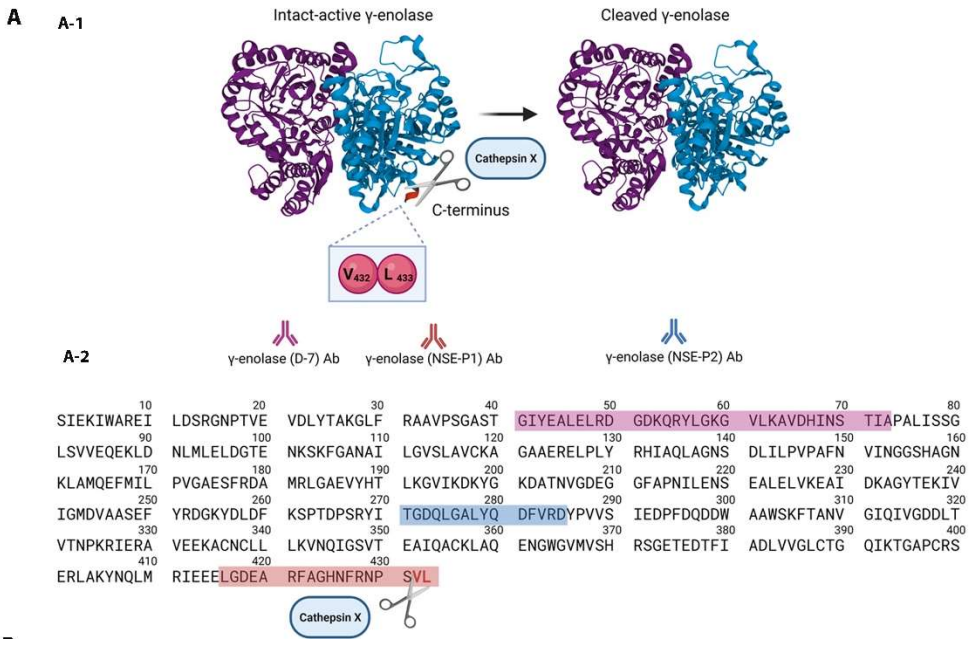

Figure 26: Cathepsin X cleavage of γ-enolase A structure of the γ-enolase dimer and cleavage of C-terminal amino acids by cathepsin X (A-1). Three different primary antibodies against γ-enolase were used: A γ-enolase (D-7) antibody specific for the epitope between amino acids 41–73 near the N-terminus (purple amino acid sequence), a γ-enolase (NSE-P2) antibody against the internal region (amino acids 271–285, blue amino acid sequence), and a γ-enolase (NSE-P1) antibody against amino acids 416–433 in the C-terminal region (red amino acid sequence) (A-2). Total γ-enolase was detected using the NSE-P2 antibody, whereas the intact active form was detected using the NSE-P1 antibody. Image was created with Mol*Viewer (Sehnal et al., 2021) based on RCSB PDB (rcsb.org)

ID 1TE6 (Chai et al., 2004) and with BioRender.com.

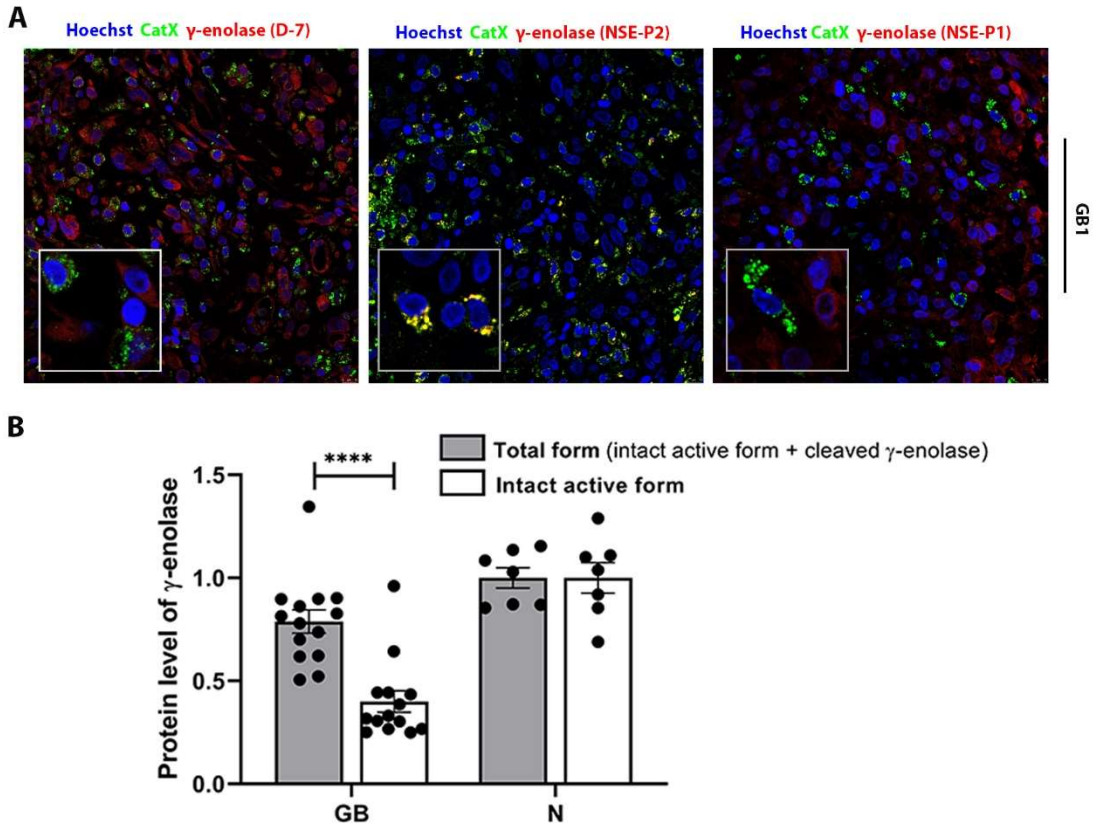

Figure 27: Double immunofluorescence staining of cathepsin X and γ-enolase. (A) No or partial colocalisation of cathepsin X and γ-enolase was observed. Colocalisation was observed with NSE-P2, suggesting that cathepsin X colocalises mainly with cleaved γ-enolase. The cell nuclei were stained with Hoechst 33258 (blue). Scale bar: 50 µm. (B) Significantly lower levels of the intact active form of γ-enolase were observed in GB tissues compared to the nontumour brain tissue control (N). Protein levels of both forms of γ-enolase in GB and nontumour brain tissues were obtained by means of ELISA. The bars represent mean values ± S.E.M. (n = 14 for GB and n = 7 for N). **** $p < 0.0001$.

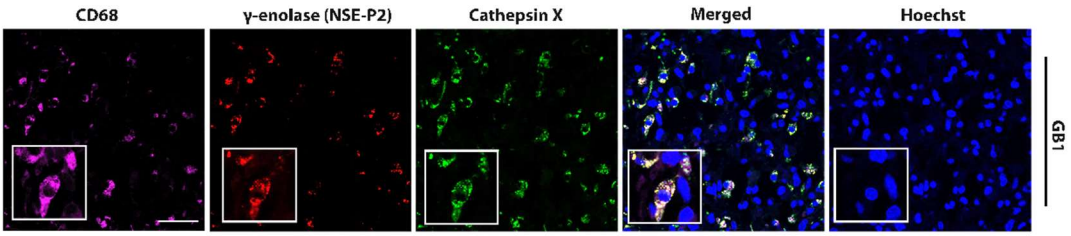

Figure 28: Colocalisation of cathepsin X and γ-enolase in CD68-positive cells in GB tissues. Representative images of triple immunofluorescence staining for cathepsin X (green), γ-enolase NSE-P2 (red), and CD68 (a marker of macrophages and microglia; purple) show overlapping expression of cathepsin X and γ-enolase NSE-P2 in CD68-positive cells. The cell nuclei were stained with Hoechst 33258 (blue). Scale bar: 50 µm.

4.2.7.2.1 Proliferation of GB Cells, GSCs, and GB-Associated Cells Affected by the γ-enolase Peptide

As we observed significantly reduced levels of the intact active form of γ-enolase in GB tissues, and as the peptide mimicking the intact C-terminal end of γ-enolase promotes proliferation of neuronal cells (Hafner, Obermajer, & Kos, 2011, 2012) we were interested in whether intact active γ-enolase plays a functional role in the proliferation of cancer cells, macrophages, and microglia. Cells were treated with a range of concentrations of the γ-enolase peptide (γ-Eno), which mimics the C-terminal end of γ-enolase, for 48 h, and cell proliferation was evaluated afterwards using CFSE staining. First, proliferation of both GB cells NIB140 and GSCs NCH421k increased after treatment with the γ-Eno peptide (Figure 29A). γ-Eno decreased the mean fluorescence intensities of CFSE-stained NIB140 and NCH421k cells by up to 8% and 7%, respectively. Second, γ-Eno increased the proliferation of microglial BV-2 cells grown in the NCH421k-conditioned media by up to 15% but did not affect the proliferation of differentiated THP-1 macrophages grown in NIB140/NCH421k cell-conditioned media (Figure 29B, 29C). Treatment with the highest concentration of γ-Eno decreased invasion of NIB140 and NCH421k cells by 15% and 25%, respectively (Figure 30)

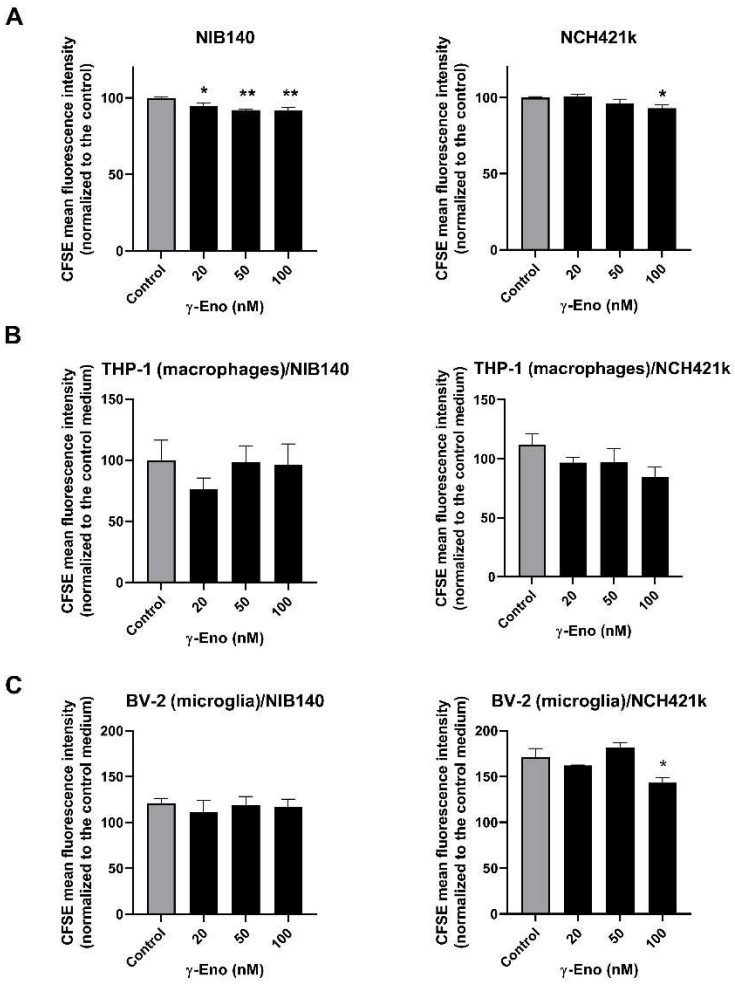

Figure 29: The effects of the γ-enolase peptide (γ-Eno) on the proliferation of GB cells, GSCs, and GB-associated cells. GB NIB140 cells, NCH421k GSCs (A), differentiated THP-1 macrophage cells (B), and BV-2 microglial cells (C) exposed to the NIB140- and

NCH421k-conditioned media were treated with increasing concentrations of γ-Eno. Cell proliferation was evaluated using CFSE staining and flow cytometry. The control means blank GB cell/GSC medium without the addition of γ-Eno (A) or blank GB cell/GSC medium without soluble molecules secreted from GB cells/GSCs and without the addition of γ-Eno (B, C). Data are presented as mean values ± S.E.M. * $p < 0.05$, ** $p < 0.01$.

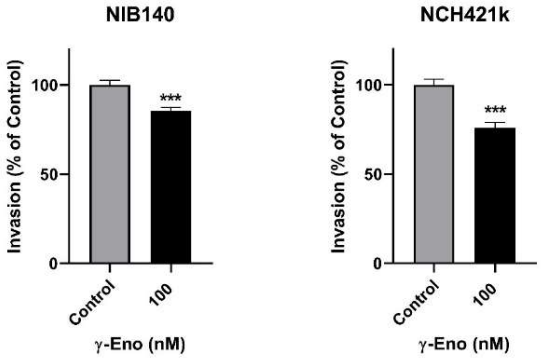

Figure 30: The effects of γ-enolase peptide (γ-Eno) on the invasion of GB cells and GSCs. Treatment with the highest concentration of γ-Eno peptide decreased the invasion of NIB140 and NCH421k cells by 15% and 25%, respectively. Control means blank GB cell/GSC medium without the addition of γ-Eno peptide. Data are presented as mean values ± S.E.M. Statistical analyses were performed with GraphPad Prism software using the one-way ANOVA – Dunnett's multiple comparisons test (* $p < 0.05$, ** $p < 0.01$, *** $p < 0.001$, and **** $p < 0.0001$).

Chapter 5

Discussion

5.1 Biobanking and *Ex Vivo* GB Models

As the most aggressive and common primary brain tumour in adults, GB responds poorly to standard therapy. Biobanks represent an invaluable collection of biological samples and associated clinical information that can help in improving our understanding of GB biology, identifying new diagnostic and prognostic biomarkers of therapy resistance, and developing new personalized treatment approaches. To date, several glioma biobanks have already been developed worldwide (Aibaidula et al., 2015; Bregy et al., 2015; Clavreul et al., 2019; Kong et al., 2018). At the Department of Genetic Toxicology and Cancer biology of the NIB, a biobanking strategy for GB samples and data collection has been set up to accelerate the discovery of GB biomarkers and their consecutive translation into clinical practice. The SciNote software platform, which was recently developed by the lab digitalization company Biosistemika, was used for the online GlioBank. GlioBank contains: 1) biological samples (tissues, cells, organoids, and plasma and peripheral blood immune cells) and 2) corresponding clinical data (e.g. karnofsky performance status, extent of surgical resection, age at diagnosis, sex, overall survival, progression-free survival, and therapy data) and molecular data (e.g. gene and protein expression and common genetic markers). For this doctoral dissertation, a total of 227 glioma samples were collected in this GlioBank, of which 177 GB samples were further processed to establish primary differentiated GB cells, GSCs, and GBOs, with success rates of 49%, 34%, and 69%, respectively. GB cells, GSCs, and GBOs remained viable in culture and were cryopreserved for further analysis. Expression of GSC and GB differentiation markers were regularly examined in GB cells and GSCs. As expected, primary GB cells from patients expressed low levels of stem cell markers but high levels of the differentiation marker *GFAP*. By contrast, GSCs expressed higher levels of GSC markers (*SOX2, PROM1, CD9, OLIG2*, and *NOTCH1*) and lower levels of differentiation marker (*GFAP).*

5.2 *In Vitro* Drug Testing of Natural Compound Efficacy

The work regarding cannabinoids in this dissertation has been successfully incorporated into the establishment of the GlioBank pipeline at NIB as an important pillar for further preclinical oncological studies, specifically for testing the efficacy of cannabinoids as potential therapeutics. The cannabinoids THC, CBD, and CBG are terpenophenolic compounds from the cannabis plant that are being proposed for combination therapy with standard GB treatment. Numerous studies have shown that the combination of CBD and THC induces autophagy-dependent necrosis (Nabissi et al., 2015) and apoptosis via ceramide-accumulation or ROS activation, and exerts anti-invasive effects on GB

(Dumitru, Sandalcioglu, & Karsak, 2018). THC and CBD have already been used in clinical trials alone or in combination with the chemotherapeutic agent TMZ. The combination of these two cannabinoids has been shown to reduce the psychotropic effects of THC, as CBD is a negative allosteric modulator of the CB1 receptor, antagonising THC-mediated adverse downregulation of anti-tumour immunity (Zhu et al., 2000). Similar to CBD, CBG has no intoxicating or psychotropic effects, which is why a number of studies have focused on its involvement in various diseases (Zalman & Bar-Sela, 2017). Using a similar approach, combining the two agents for targeting GB cells, we have studied the effects of cannabinoids, specifically CBG and CBD (without THC as a psychoactive substance and also in combination with chemotherapy) on GB progression, including GB proliferation and invasiveness.

The presence of GSCs in GB has been shown to be related to tumour resistance and recurrence. GSCs generally express high levels of DNA damage repair proteins and ATP-binding cassette transporters and are thus more resistant to radiotherapy and chemotherapy, representing an important target for new treatment approaches. Cannabinoids bind to cannabinoid receptors, which are present on tumour cells, as part of the endocannabinoid system (Mackie, 2008). This triggers biochemical signalling in GB cells that inhibits proliferation and cell viability (Galve-Roperh et al., 2013). It has been previously shown that CB1 and CB2, two important cannabinoid receptors, are present in neural stem/progenitor cells and control their self-renewal, proliferation, and differentiation (Galve-Roperh et al., 2013). We were the first to demonstrate that GSCs highly express both receptors, CB1 and CB2, and that they are also expressed in differentiated GB cell lines (Lah et al., 2021). Moreover, CB1 and CB2 expressions differ among patients, and therefore we expected different treatment responses, which may also be explained by the presence of other nonspecific ionotropic receptors involved in cannabinoid signalling, as discussed by De Petrocellis et al. (De Petrocellis et al., 2017). Next, in a cohort of nine patient-derived GB cell lines, three differentiated GB cell lines, and three GSC lines, we tested the effects of pure CBG on cell viability compared to the effects of THC and CBD. CBG decreased GB cell viability in a concentration range (mean IC50 value = 28.1 μM) comparable to that of THC (mean IC50 value = 27.9 μM), whereas CBD was much more cytotoxic. This is consistent with a study on breast cancer (Ligresti et al., 2006), in which the authors found that pure CBG was less effective than CBD. However, another study showed that CBG was more cytotoxic than CBD in melanoma and oral cavity carcinoma (Cascio, Gauson, Stevenson, Ross, & Pertwee, 2010).

We further investigated whether combined therapy of cannabinoids with the chemotherapeutic agent TMZ affects GB invasion, which is an important feature of GB progression. Several other studies (Afrin et al., 2020; Pisanti et al., 2017) have shown that CBD has an anti-invasive effect on cancer cells, including GB. CBD has been shown to reduce GB cell invasion using organotypic brain slices (Soroceanu et al., 2013). In addition, Solinas et al. (Solinas et al., 2013) showed that GB cell invasion was reduced after CBD treatment by downregulating the enzymes Matrix metallopeptidase 9 (MMP-9) and Metalloproteinase inhibitor 4 (TIMP-4), which are associated with tumour invasion. We were the first to show that subtoxic doses of CBG reduce invasion of both GB cells and GSCs, which have superior resistance to current treatment options and cause GB recurrence. We compared the effects of CBD, CBG, and TMZ on cell invasion. CBG generally had a stronger effect on the invasion of GB cells but not GSCs. The combination of CBG and CBD at a molar ratio of 1:3 was required to significantly inhibit GSC invasion.

In this study, using patient-derived *in vitro* models, we demonstrated the potential use of cannabinoids as anticancer drugs, particularly for overcoming GSC resistance to cytotoxic agents and inhibiting GB cell invasion. The combination of CBG and CBD, each at subcytotoxic concentrations, resulted in additive effects on reduced cell viability that

were sufficient to replace the use of THC. Thus, because of the psychotropic effects of THC, which are particularly harmful to GB patients with neurological abnormalities associated with tumour growth, THC-containing formulations are unnecessary and should be avoided.

5.3 *Ex Vivo* GBOs Translate Novel Therapeutic Discoveries Tailored to Individual Patient Tumours

Patient-derived cancer cells are valuable tools in basic research and pre-clinical studies. For a long time, differentiated GB cells and GSCs have been used to study GB and have provided important insights into the biology of the disease. However, tumours are not only composed of cancer cells but represent a complex ecosystem of diverse cells and other elements of the TME (Gimple et al., 2022). Therefore, more sophisticated models that represent the complexity and heterogeneity of tumours are needed. Recently, 3D organoid cultures of human tumour tissue have emerged as a representative platform for *in vitro* modelling of cancer heterogeneity and interactions with the TME. Organoids are multicellular 3D tissue constructs that recapitulate the original organ-like architecture and its functionality *in vitro* (de Souza, 2018). There are several approaches to creating organoids, from pluripotent embryonic stem cells and induced pluripotent stem cells (Clevers, 2016) to adult stem cells and resected tumour tissue (T. Sato et al., 2011), all of which have the ability to self-organize and self-renew.

The main goal of this part of the dissertation was to set up an *ex vivo* model of GBOs that mimics the entire TME and enables more accurate research studies. Among the various types of organoids, we have successfully generated GBOs following Jacobs's protocol (Jacob, Ming, et al., 2020; Jacob, Salinas, et al., 2020). GBOs can be grown with high efficiency from patient tumour tissues, potentially enabling patient-specific drug testing and the development of individualized treatment regimens. A key aspect of this method is preventing the dissociation of tumour tissue to single cells and maintaining native cell-cell contacts, which allow the formation and development of GBOs in the absence of exogenous growth factors (e.g. EGF and bFGF), serum, and ECM. Thus, GBOs retain properties similar to the parental tumour.

We established GBOs from multiple patient tumours, either from the tumour's invasive edge or core or from recurrent tumours. The success rate was 69%, which is notably higher than that of differentiated GB cells and GSCs, with success rates of 49% and 34%, respectively. We have shown that GBOs retain the cellular composition and diversity of the TME observed in primary tumours, such as GSCs, differentiated GB cells, astrocytes, macrophages, microglia, and vasculature. In addition, cytokines that are associated with TME were released only by GBOs and not GB cells. This demonstrates that communication through cytokines and growth factors is present within GBOs. Moreover, we have explored and compared the transcription profiles of GBOs and their corresponding parental tissues.

At the gene expression level, we identified four distinct clusters of correlated genes that were similar in both sample groups, i.e. GBOs and parental tissues. Cluster 1 consists of genes related to GSCs, cell cycle, and DNA damage response. This is in accordance with a previous study that showed that GSCs exhibit higher expression and activity of DNA damage response proteins, which contribute to higher resistance to radiotherapy (Ahmed et al., 2015). Cluster 2 consists of genes determining the PN subtype of GB according to the TCGA classification. Cluster 3 contains genes for the MES subtype, genes involved in cytokine signalling, and genes encoding GSCs. Cluster 4 contains genes involved in cytokine signalling and genes determining immune cells of the TME. Cytokines in GB are involved

in attracting immune cells from the periphery to the tumour site and play an immunosuppressive role, thus contributing to tumour progression (Novak et al., 2020; Yeo, Brown, Gargett, & Ebert, 2021).

Our correlations indicate similar patterns between patient-derived GBOs and parental tissues, suggesting that GBO models preserve the same transcriptomic profile as GB tissues. In-depth selective gene expression comparisons showed that gene expression remains stable in most cases. For example, marker genes of stem cells and genes involved in epithelial-to-mesenchymal transition do not significantly differ between GBOs and their corresponding tissues. However, major changes were observed in the expression of genes encoding immune cells, e.g. *AIF1, FCGR3A*, and *NCAM1*, likely reflecting the loss of immune cells in GBOs upon culturing for longer periods (Jacob, Salinas, et al., 2020).

The previously discovered transcriptional subtypes MES, PN, and CL represent one level of heterogeneity of GB tumours that is based on bulk expression analysis (Behnan et al., 2016; Verhaak et al., 2010). We determined the subtypes of GBOs and their corresponding tumour tissues and tested whether the subtypes were preserved. Our analysis showed that in 60% of GBO-tissue pairs, the subtype is retained. We could not confirm our hypothesis that the subtype is retained in most GBO-tissue samples, although 60% is indeed very high in the case of GB. This can be explained by the fact that part of the tissue is used for RNA tissue analysis and the other part of the tissue is used for GBO generation and subsequent RNA analysis, reflecting the tumour's spatiotemporal diversity. It should also be noted that some components of the media for proliferation and viability of cultured GBOs may affect the expression of classification genes, resulting in a subtype shift. In addition, we found that in most cases (73% for GBOs and 60% for tissues), the samples reflected a mixture of all molecular genetic subtypes, which we referred to as a mixed subtype (MIX), reflecting high heterogeneity within the tumour.

The recent study by Neftel et al. (Neftel et al., 2019) using single cell RNA sequencing described four distinct cellular states within GB tumours, namely astrocyte-like, neural progenitor cell-like, oligodendrocyte progenitor cell-like, and mesenchymal-like states. The authors were able to deconvolute the cellular states of the TCGA GB subtypes based on the transcriptional programmes that define each cellular state. They found that CL and MES subtypes are predominantly composed of cells in astrocyte-like and mesenchymal-like states, whereas PN subtypes are enriched by cells in the developmental neural progenitor cell-like and oligodendrocyte progenitor cell-like states (Neftel et al., 2019). Thus, GB subtype analysis confirmed the plasticity of GB subtypes and raises further questions regarding the maintenance of GB transcriptional subtypes and cell states at different stages of tumour development. Further research is needed to determine the translational potential of novel subtypes and the impact of existing treatment options on the spectrum of cell states that promote GB. Future determination of these cell states in GBOs, rather than subtyping, would therefore help us understand how transitions between cell states differ in different patient populations and how therapies may alter state transitions.

We aimed to investigate the changes in targeted gene expressions and the transformation of the GB TME in response to current standard therapy in clinically relevant GBOs, which was complemented by studies in patient-derived primary GB and GSC cell lines. GBOs from two out of the six patients responded with decreased cell viability, but overall, there was no significant response in GBO viability after standard therapy. Similarly, two of the six patients responded with decreased cell invasion to standard therapy, but again, the overall effect of IR and TMZ on cell invasion was not observed in our GBO model. A similar result in terms of therapeutic responses in some patients, but not others, was shown by Jacob et al. (Jacob, Salinas, et al., 2020) who clearly demonstrated that responses of GBOs correlated with clinical responses of patients.

By contrast, some changes on the GBO surfaces were observed after GBO exposure to standard treatment. We observed that TMZ and IR did not change the shape of GBOs, but at higher magnification, numerous cells on the surfaces of GBOs lost their membrane integrity, indicating apoptosis or necrosis. Based on the SEM results, we further tested whether standard treatment induces cell death via early and late apoptosis in GBOs established from two different patients. After therapy, there were small but significant changes in the proportion of cells in early and late apoptosis. In both patients, IR increased the proportion of apoptotic cells by 7%, whereas TMZ and the combined IR and TMZ increased the proportion of apoptotic cells by 6% and 5%, respectively.

Next, we investigated the effects of standard therapy on gene expression levels by analysing genes associated with GSCs, immune cells in the TME, cytokines, GB subtypes, the epithelial-to-mesenchymal transition, DNA damage responses, and cell cycle in GBOs. Overall, no major changes in gene expression were observed after treatment with TMZ, IR, or both. Out of 44 different genes, four genes *MDM2*, *CDKN1A, ATM* and *ATR,* all involved in DNA damage response*,* were significantly upregulated in GBOs after treatment with IR, TMZ or IR and TMZ combined. E3 ubiquitin-protein ligase MDM2 (mouse double minute 2 homolog protein) is an important negative regulator of the tumour suppressor p53 (Hou, Sun, & Zhang, 2019). The encoded protein can target p53 protein for proteasomal degradation via its E3 ubiquitin ligase activity, preventing p53 from regulating target genes involved in cell cycle arrest, apoptosis, senescence, DNA repair, or metabolism (Bourdon et al., 2005). *MDM2* overexpression has been found in a variety of different cancers and is associated with chemo- and radioresistance in human malignancies (Hou et al., 2019). Previously, the MDM2-p53 negative feedback regulatory pathway was shown to contribute to TMZ resistance in glioma cells (A. Sato et al., 2011). The authors demonstrated that MDM2 inhibition leads to p53 activation and consequently MGMT downregulation. Thus, decreased enzymatic activity leads to increased cell sensitivity to chemotherapeutic agents (A. Sato et al., 2011), indicating an important role of MDM2 in the development of chemotherapy resistance. Moreover, MDM2 has also been linked to radiation sensitivity in hepatocellular carcinoma cells (Koom et al., 2012).

Cyclin-dependent kinase inhibitor 1A (CDKN1A), also known as p21/Cip1, plays an important role in regulating cell cycle progression in G1. *CDKN1A* expression is tightly regulated by the p53 protein, which mediates p53-dependent cell cycle arrest in G1. Acquired resistance mechanisms have been previously demonstrated in lung cancer (Zamagni et al., 2020). The chemotherapeutic agent cisplatin induced DNA damage that led to cell cycle arrest and apoptosis. Tumour cells responded to therapy by upregulating genes involved in DNA damage repair, including *CDKN1A*. *CDKN1A* overexpression caused cells to adopt a more aggressive phenotype capable of overcoming cell blockade, senescence, and apoptosis (Zamagni et al., 2020). *ATM* (ATM serine/threonine kinase) and *ATR* (*ATR* serine/threonine kinase) are also important mediators of the DNA damage response by inducing cell cycle arrest and facilitating DNA repair through downstream signaling (Weber & Ryan, 2015), both involved in therapeutic resistance in GB (Frosina, Marubbi, Marcello, Vecchio, & Daga, 2019).

In this doctoral dissertation, we showed that in the GBO model, standard therapy did not affect cell viability or invasion, possibly due to upregulation of genes involved in DNA damage repair, leading to acquired chemo- or radio-resistance.

In addition, we compared the effects of standard therapy on GSCs and differentiated GB cells. Our gene expression analysis indicates changes in gene expression patterns after treatment with IR and IR in combination with TMZ. In contrast to GBOs, we observed four other genes that were upregulated in GSCs. *CD44*, a well-known marker for GSCs and the MES GB subtype (which plays an important role in tumour initiation and progression), was upregulated, suggesting that GSCs initially enriched with a PN signature transition to

a more aggressive MES subtype after IR (Minata et al., 2019). Two other genes, *mTOR* (mammalian target of rapamycin) and *ATM*, both involved in the DNA damage response, were also upregulated in GSCs after treatment. Moreover, *OLIG2* gene, GSCs marker was downregulated after combined treatment. By contrast, *ATR* was upregulated in differentiated GB cells after TMZ treatment, and *TGFB1* (transforming growth factor beta-1) was downregulated after treatment with IR and TMZ. We have shown that differentiated GB cells and GSCs respond to therapy differently, with a different combination of genes compared to GBOs.

GBOs definitely show huge potential for applications linked to brain tumour research. But are these models really good system for pre-clinical/clinical studies? Compared to traditional 2D and 3D cell models that represent uniform cancer cell populations grown in conditions that promote clonal selection and expansion over several passages, GBOs retain cellular diversity, heterogeneity, and transcriptional profiles of their parental tumours. This enables studying dynamic interactions of cancer cells with the TME that consists of stromal cells and ECM. The only restriction is the limited time that immune and endothelial cells can be maintained within GBOs. To overcome this limitation, GBOs can be optimized by co-culturing with immune or other stromal cells. For the purpose of basic research to study genetic contributions to the disease, Jacob et al. (Jacob, Ming, et al., 2020; Jacob, Salinas, et al., 2020) stated that GBOs may also be subjected to genetic alterations such as overexpression, shRNA/siRNA knockdowns, and CRISPR-mediated knockouts.

The procedure for establishing GBOs does not require cell dissociation and therefore preserves native cell-cell interactions and histological characteristics of the tumour tissue. Jacob et al. (Jacob, Ming, et al., 2020; Jacob, Salinas, et al., 2020) and our group demonstrated that GBO establishment requires a short generation time and has high success rates, enabling the evaluation of possible therapeutics for personalized medicine approaches. GBOs can be generated within 2–4 weeks after surgery, which enables testing targeted therapies *in vitro* before initiating treatment in patients. We demonstrated that GBOs can be established from either the tumour's rim or core or recurrent tumours. Several previous studies using patient-derived models have focused on samples only from tumour cores. This is the region most likely to be resected by the neurosurgeon. Conversely, non-resectable GB cells with other molecular and phenotypic characteristics, such as a higher capacity for infiltrative growth at the invasion edge, are responsible for GB recurrences (Minata et al., 2019). Therefore, with this approach of establishing GBOs from the invasive edge of the tumour, we may contribute to the development of novel therapies that eradicate the seed for GB recurrence.

GBOs provide a promising tool for advanced preclinical medicine but are less useful for high-throughput screening because of their complexity and a lack of a standardization protocol. Nevertheless, this complexity and similarity to tumours *in vivo* could limit the need for animal experimentation and decrease the likelihood of false-positive results. In the end, despite some of the shortcomings of GBOs, these models can reshape the way we approach personalized care and may accelerate the implementation of clinically effective treatments that significantly improve patient outcomes.

5.4 The Abundance and Potential Role of the Novel Prognostic Biomarker Cathepsin X in the GB TME

We investigated the abundance and potential role of the biomarker cathepsin X in the GB TME, focusing on the regulation of its molecular target γ-enolase. We studied the localisation, expression level, and activity of cathepsin X in the GB TME as well as the

therapeutic potential of selective irreversible and reversible cathepsin X inhibitors (Majc et al., 2022).

Cathepsins are proteases from the cysteine family that act as intracellular/lysosomal enzymes of rather distinct specificities and are overexpressed in GB. We found upregulated cathepsin X expression levels in recurrent and *de novo* GB tissues compared to less malignant low-grade gliomas and nontumour brain tissues. This confirms a previous observation that increased cathepsin X expression correlates with advanced tumour stages in a variety of malignancies, including prostate, colon, pancreatic, and neuroendocrine cancers (Akkari et al., 2014; Krueger et al., 2005; Nägler et al., 2004; Vizin, Christensen, Nielsen, & Kos, 2012).

In our study, we confirmed increased protein expression and significantly higher activity of cathepsin X in GB. This indicates that cathepsin X could be a new target for specific inhibitors, suggesting new possibilities for the treatment of this disease. We used Z7 (Pečar Fonović et al., 2017) as a selective, reversible, and non-toxic inhibitor, and AMS36 as a selective irreversible inhibitor of cathepsin X (Hafner Pišlar, Zidar, Kikelj, & Kos, 2014; Sadaghiani et al., 2007). By selectively inhibiting cathepsin X, we found that it enhances the viability and proliferation of patient-derived GB cells but does not affect GSCs. We also demonstrated the role of cathepsin X in promoting cell invasion, which is consistent with previous studies that demonstrated that cathepsin X is involved in cell signalling in cancer and promotes cancer cell adhesion, migration, and invasion (Akkari et al., 2014; Kos et al., 2015; N. Obermajer et al., 2009; Pečar Fonović et al., 2013). However, the molecular mechanisms underlying these effects are still not well understood.

Next, we discovered increased cathepsin X expression in GB cells, TAMs and microglia in GB tissues, which is consistent with previous research on other cancer types showing that cathepsin X is produced in the TME by both cancer cells and TAMs, influencing cellular crosstalk, cancer proliferation, and invasion (Akkari et al., 2014). In GB, TAMs and microglia play an important role in regulating GB development, invasion, angiogenesis, and treatment resistance (Glass & Synowitz, 2014; Quail & Joyce, 2017; L. B. Wang et al., 2021; Zhou et al., 2015). We showed that cathepsin X inhibition reduced the viability of macrophages and microglia cultivated in conditioned medium of GB cells and GSCs, indicating a function for cathepsin X in the survival of tumour-supporting TAMs and microglia. Inhibiting cathepsin X prevented the growth of GB cells and immune cells that support tumours, such as macrophages and microglia. To investigate the effects of cathepsin X inhibitors on cancer and immune cells, more sophisticated tumour models that preserve the immune compartment, such as organoids or animal models, are required.

γ-enolase is a specific target of cathepsin X in brain cells. It is involved in enhanced aerobic glycolysis and cell proliferation. γ-enolase is overexpressed in neurogenic and neuroendocrine tumours (Tapia et al., 1981) and GB tissues, as shown in our study and by others (Yan et al., 2011). High γ-enolase levels are associated with increased aerobic glycolysis, proliferation, and survival of cancer cells (Vizin & Kos, 2015; Yan et al., 2011). Another catalytic site, which is not involved in aerobic glycolysis, is the intact C-terminal region of γ-enolase, responsible for neurotrophic activity that promotes neuronal development, survival, and differentiation (T. Hattori, Ohsawa, Mizuno, Kato, & Kohsaka, 1994; Tatsuya Hattori, Takei, Mizuno, Kato, & Kohsaka, 1995; Takei et al., 1991). In our study, we observed that the γ-Eno peptide mimicking the C-terminus of γ-enolase increased the proliferation of GB cells, GSCs, and GB-associated immune cells *in vitro*. γ-enolase pro-survival function is thought to be regulated by cathepsin X. We also discovered a link between cathepsin X and C-terminal γ-enolase cleavage during GB progression. We found increased cathepsin X activity in GB tissues associated with lower levels of the intact active form of γ-enolase. In nontumour brain tissues, the levels of both intact active and total γ-enolase were comparable. Moreover, cathepsin X colocalised with total γ-enolase in GB

tissues, particularly in TAMs and microglia. We demonstrated that cathepsin X cleaves the C-terminal end of γ-enolase in GB in contrast to nontumour tissue, in which we observed only the intact form of γ-enolase and lower cathepsin X protein levels and activity.

Cathepsins are potent prognostic biomarkers of GB patient survival (Habič et al., 2021; Lah et al., 2006; Levicar et al., 2002) Although we showed that cathepsin X, through its selective suppression, increases the viability of GB cells and GB-associated macrophages and microglia and the proliferation and invasion of GB cells, high cathepsin X levels did not correlate with the survival of GB patients in this study. This may be because cathepsin X can interact with and cleave a variety of molecules involved in various other cellular processes (Kos et al., 2015). Conversely, cathepsin X also has anticancer effects, as it cleaves the C-terminal end of γ-enolase and presumably neutralizes the proliferative effects of intact active γ-enolase on GB cells, GSCs, and especially tumour-associated microglia.

However, the basic mechanism of γ-enolase activity and its modulation by cathepsin X in the pathophysiology of GB needs to be further investigated. Particularly, whether cathepsin plays a promotive or inhibitory role in GB progression remains to be elucidated.

Chapter 6

Conclusions

In this doctoral dissertation, we have 1) contributed to the establishment of the Slovenian biobank containing glioma samples, GB cell models, and corresponding clinical data, 2) tested cannabinoid extracts on GB cell models and showed their potential cytotoxic and anti-invasive properties in GB, 3) established GBOs that mimic the patient's TME to model and explore the therapeutic resistance of GB to standard therapy, and 4) revealed the role of cathepsin X in GB progression.

First, the concepts and techniques of biobanking strategies for *ex vivo* GB models were presented. Gliobank serves as a large collection of glioma samples together with clinical and research data, which is predominantly used in clinical and translational neuro-oncological research. During this PhD research, we collected over 170 GB samples from tumour edges and/or cores. From tumour tissues, we successfully established primary differentiated GB cells, GSCs, and GBOs with success rates of 49%, 34%, and 69%, respectively. These percentages slightly differ from those we hypothesised and depend on tissue quality and patient-specific tumour growth characteristics. We demonstrated that GB cells, GSCs, and GBOs remained viable in culture and after passaging. We confirmed the expression of stem cell markers in GSCs and differentiation markers in GB cells. Overall, the collection of specimens, GB models, and associated clinical data into one virtual location for ease of access by researchers will enable detailed studies of tumour evolution/progression and better identification of new therapeutic strategies. This could contribute to the design of new approaches for more efficient therapy in the future.

Second, we have successfully used patient-derived GB cell lines *in vitro* from our GlioBank as a platform for testing the efficacy of cannabinoids. Using GB cells and GSCs, we have demonstrated the potential use of CBD, THC, and CBG as anticancer drugs, particularly for overcoming the resistance of GSCs to the chemotherapeutic agent TMZ and for inhibiting the invasion of GB cells. More specifically, using GB cell models, we demonstrated that the combination of CBG and CBD (each at subcytotoxic concentrations) resulted in additive effects on decreased GB cell viability and induced apoptosis, which was sufficient to replace the application of psychoactive THC.

Third, we have successfully established novel *ex vivo* GBOs. We established GBOs from multiple patient tumours either from the invasive edge or core of tumours or from recurrent tumours. We confirmed our hypothesis that GBOs grow in culture and retain elements of the TME. Furthermore, we set up a transcriptomic profile for the GB subtypes, epithelial-to-mesenchymal transition markers, GSCs, immunosuppression markers, cytokine signalling, immune cells within the TME, and DNA damage response/cell cycle genes in GBOs, GB tissues, and GB cells. Comparing the transcriptional profiles of individual genes, we demonstrated similar clusters of correlated genes in GBOs and corresponding tumour tissues and thus confirmed our hypothesis that GBOs recapitulate the transcriptomic

fingerprint of the parental tumour. We applied standard clinical therapy to GBOs; however, no significant response regarding GBO viability or invasion was detected. Furthermore, we have shown that differentiated GB cells and GSCs respond differently to therapy than GBOs, which better represent the tumour *in vivo*. Thus, GBOs represent a more clinically relevant model than patient-derived 2D and 3D cell cultures. As such, they are an invaluable tool for exploring complex gene and cell composition and may better contribute to discovering new potential therapeutics.

Finally, we investigated the abundance and potential role of the biomarker cathepsin X in the GB TME, focusing on the regulation of its molecular target γ-enolase. We confirm our hypothesis that cathepsin X is upregulated in GB compared to nontumour brain tissue, both at the level of gene and protein expression as well as enzymatic activity. We confirm that it is mainly expressed in tumour-associated macrophages and microglia but also in GB cancer cells. Furthermore, we demonstrated that cathepsin X preferentially colocalises with its target γ-enolase in GB-associated macrophages and microglia. We observed that the γ-Eno peptide, which mimics the C-terminus of γ-enolase, increased the proliferation of GB cells, GSCs, and GB-associated immune cells *in vitro*. We demonstrated that there is a link between cathepsin X and C-terminal cleavage of γ-enolase in GB progression, although further studies on the molecular mechanisms of cathepsin X and its target γ-enolase are needed to explore their potential for antitumour therapies. We could not confirm our hypothesis that cathepsin X is a prognostic factor because high cathepsin X levels did not correlate with GB patient survival in this study. However, by selectively inhibiting cathepsin X, we showed that cathepsin X promotes the viability of GB cells and GB-associated macrophages and microglia as well as the proliferation and invasion of GB cells.

Appendix A

Supplementary Material

A.1 Characterization of GBOs From Patient Tumours and the Effect of Standard Therapy on Viability, Invasion and The Expression of Pre-specified Groups of Genes in GBOs

Table A.1 1: List of TaqMan gene expression assays (Thermo Fisher Scientific) used for RT-qPCR.

Gene name	Assay ID	Protein name
ACSBG1	Hs00209500_m1	Acyl-CoA Synthetase Bubblegum Family Member 1
AIF1	Hs00610419_g1	Allograft inflammatory factor 1
ATM	Hs00175892_m1	Ataxia telangiectasia mutated
ATR	Hs00992123_m1	Ataxia telangiectasia and Rad3 related
BAX	Hs99999001_m1	Bcl-2-like protein 4
BCL2	Hs00608023_m1	B-cell lymphoma 2
CCL2	Hs00234140_m1	Monocyte chemoattractant protein-1 (MCP-1)
CCL5	Hs00982282_m1	Chemokine (C-C motif) ligand 5
CD44	Hs00174139_m1	CD44 molecule
CD68	Hs00154355_m1	CD68 Molecule
CD9	Hs00233521_m1	CD9 antigen
CDH1	Hs01023895_m1	Cadherin 1
CDKN1A	Hs00355782_m1	Cyclin Dependent Kinase Inhibitor 1A
CDKN2A	Hs00923894_m1	Cyclin Dependent Kinase Inhibitor 2A
CHEK1	Hs00967506_m1	Checkpoint Kinase 1
CHI3L1	Hs01072228_m1	Chitinase-3-like protein 1; YKL-40

C-MYC	Hs00905030_m1	Myc proto-oncogene protein
COL1A1	Hs00164004_m1	Collagen Type I Alpha 1 Chain
COL1A2	Hs01028956_m1	Collagen Type I Alpha 2 Chain
CXCL12	Hs02829207_m1	C-X-C motif chemokine 12 (SDF-1)
CXCR4	Hs00607978_s1	C-X-C chemokine receptor type 4
DAB2	Hs01120074_m1	DAB Adaptor Protein 2
ERBB3	Hs00176538_m1	Erb-B2 Receptor Tyrosine Kinase 3
FCGR3A	Hs02388314_m1	Fc Gamma Receptor IIIa
FOXP3	Hs01085834_m1	Forkhead box P3
FUT4	Hs01106466_s1	Fucosyltransferase 4
GFAP	Hs00909233_m1	Glial Fibrillary Acidic Protein
ID1	Hs03676575_s1	Inhibitor Of DNA Binding 1
IDO1	Hs00984148_m1	Indoleamine 2,3-Dioxygenase 1
IL6	Hs00174131_m1	Interleukin 6
KCNF1	Hs00266908_s1	Potassium Voltage-Gated Channel Modifier Subfamilv F Member 1
MDM2	Hs01066930_m1	E3 ubiquitin-protein ligase
MTOR	Hs00234508_m1	Serine/threonine-protein kinase mTOR
NCAM1	Hs00941830_m1	Neural Cell Adhesion Molecule 1
NF-KB	Hs00765730_m1	Nuclear factor-kappa B
NOTCH1	Hs01062014_m1	Neurogenic locus notch homolog protein 1
OLIG2	Hs00377820_m1	Oligodendrocyte Transcription Factor 2
P2RX7	Hs00175721_m1	Purinergic Receptor P2X 7
PIK3CA	Hs00907957_m1	Phosphatidylinositol-4,5-Bisphosphate 3-Kinase Catalytic Subunit Alpha
POU5F1B	Hs01596605_s1	POU Class 5 Homeobox 1B; OCT4-PG1 (OCT4 pseudogene)
PROM1	Hs01009259_m1	prominin-1; CD133 antigen
S100A4	Hs00243202_m1	S100 Calcium Binding Protein A4
SNAI1	Hs00195591_m1	Snail Family Transcriptional Repressor 1
SOX10	Hs00366918_m1	SRY-Box Transcription Factor 10
SOX2	Hs01053049_m1	SRY-Box Transcription Factor 2

STAT3	Hs01047578_m1	Signal Transducer And Activator Of Transcription 3
STMN4	Hs00229288_m1	Stathmin 4
TGFB1	Hs00998133_m1	Transforming growth factor beta 1
THBS1	Hs00962908_m1	Thrombospondin 1
TUBB3	Hs00801390_s1	Tubulin Beta 3 Class III

Table A.1 2: Details of the 22 GB patients and their tumours operated at the Department Neurosurgery of the University Medical Centre Ljubljana, Slovenia, used for real-time quantitative PCR analysis, GBO cell viability and invasion.

Patient	Gender	Age (Years)	MGMT promoter methylation	Mutations				Chromosomal abnormalities
				IDH1	TP53	EGFR mutation/ amplification	Other	
NIB211	M	78	yes	wt	Variant of unknown significance in TP53 P190L	ampl EGFR	TERT C250T and TP53 splicing, PTEN C136R, ampl MET, MYCN in PDGFRA, del CDKN2A in CDKN2B	ampl 7, del 10q, part del 1p
NIB213	M	63	no	wt	mut C238Y	-	TERT C228T	ampl 7, del 10q
NIB214	F	74	no	wt	-	-	mut pTERT (c.-146C>T) and PTEN (c.254-2A>G); del CDKN2A in CDKN2B	ampl 7 and del 10q
NIB215	M	74	no	wt	-	ampl EGFR	TERT C228, mut ERBB3 (G337Q), del CDKN2A and CDKN2B	ampl 7, del 10q, 13q, 22q, part del 14q

NIB216	M	46	no	wt	-	EGFR R108K, ampl	pTERT C228T, ampl MET, PIK3CA, del CDKN2A and CDKN2B	del 10q

Table A.1.2. Continued

NIB218	F	67	yes	wt	mut p.(Cys242Tyr) (C242Y)	ampl EGFR, variant of unknown significance in EGFR p.(Pro589Ser) (P589S)	ampl MET and MDM2, variant of unknown significance in PTEN p.(Tyr88Cys) (Y88C)	ampl 7 and del 10q and 19q
NIB219	F	63	yes	wt	-	ampl EGFR	mut p TERT (C228T), del CDKN2A and CDKN2B	ampl 7 and del 10q
NIB220	M	56	no	wt	-	ampl EGFR	mut pTERT (C228T) mut PIK3CA p.(Gly118Asp) (G118D), ampl MET and PIK3CA; del CDKN2A and CDKN2B	ampl 7, del 10q, part del 1p and 19q
NIB225	N.A.	N.A.	N.A.	N.A.	N.A.	N.A.	N.A.	N.A.

NIB227	M	75	no	wt	-	mut p.(Ser229Cys) (S229C), ampl EGFR	mut p TERT (C228T) del CDKN2A and CDKN2B, variant of unknown significance PIK3CA p.(Phe355Ser) (F355S)	part del 7, del 10q and 19q
NIB228	F	44	no	wt	mut TP53	mut EGFR (A289V),	PTEN (P95L), del CDKN2A in CDKN2B	ampl 7, del 10q and 19q.

Table A.1.2. Continued

NIB231	M	76	yes	wt	mut TP53 p.(Tyr126His) (Y126H)	ampl EGFR	mut TERT (C228T) ampl MET and MYCN, del CDKN2A and CDKN2B	ampl 7 and del 10q.
NIB232	M	71	no	wt	mut TP53 p.(Arg196ProfsTer13) (R196Pfs*13)	mut EGFR p.(Ala289Val)(A289V)	mut ATRX p.(Thr932PhefsTer5) (T932Ffs*5), ampl MET and del CDKN2A and CDKN2B	part del 7 and part del 1p.
NIB235	F	64	no	wt	-	variant of unknown significance in EGFR p.(Lys609Asn) (K609N)	mut p TERT (C228T), del CDKN2A and CDKN2B	ampl 7 and del 10q

NIB237	M	65	no	wt	mut TP53 p.(Arg267Trp) (R267W) and p.(Arg342Ter) (R342*)	-	mut p TERT (C228T). mut PTEN p.(Gly36Val)(G36V). variant of unknown significance in FGFR1 p.(Arg455Cys) (R455C)	ampl 7, part del 1p and del 10q in 19q.
NIB239	M	68	no	wt	-	ampl EGFR	mut p TERT (C250T), ampl MYCN, FGFR1 and MDM2, del PDGFRA, CDKN2A and CDKN2B	ampl 7, del 10q and part del 19q.
NIB240	M	71	yes	wt	-	mut EGFR c.664C>T, p.(Arg222Cys) (R222C) and ampl EGFR	mut p TERT (C250T), ampl MDM4 and PIK3CA, del PDGFRA	LOH 7 and 10q in 19q
NIB246	M	56	no	wt	-	ampl EGFR, variant of unknown significance in EGFR 1964T>G, p.(Leu655Arg) (L655R).	mut p TERT (C228T) mut PTEN c.388C>T, p.(Arg130Ter) (R130*), ampl MDM4, PIK3CA in CIC and del CDKN2A, CDKN2B, PTEN and SETD2	part del 1p, ampl 7, del 10q and LOH 19q

Table A.1.2. Continued

NIB249 (NIB216 primary tumour)	M	47	no	wt	variant of unknown significance in TP53 p.(Pro190Leu) (P190L)	mut EGFR p.(Arg108Lys)(R108K), ampl EGFR	mut p TERT (C228T), ampl MET and PIK3CA, del CDKN2A and CDKN2B, variant of unknown significance in PTEN p.(Ile122Phe)(I122F)	del 10q
NIB253	F	58	yes	wt	del TP53	mut EGFR p.(Arg108Lys) (R108K) and p.(Gly598Val) (G598V). ampl EGFR	mut p TERT (C228T), ampl MET, MDM2, MDM4, PIK3CA, PIK3R1 and SETD2, del CDKN2A, CDKN2B, FGFR1 and CIC, variant of unknown significance in PTEN p.(Glu242Gly) (E242G)	ampl 7 and del 10q in 19q
NIB257 (astrocytoma WHO 2-3)	F	58	no	mut	mut TP53 p.(Arg273Cys) (R273C)	-	ıt IDH1 p.(Arg132His) (R132H) and ATRX p.(Arg1514Ter) (R1514*), ampl PIK3CA, CDKN2A and CDKN2B, del MDM2 and CIC.	part del 7 and del 19q.
NIB261	M	33	no	wt	-	ampl EGFR	mut p TERT (C228T) and PTEN (L182*), del CDKN2A and CDKN2B	ampl 7 and del 10q in 19q.

Table A.1.2. Continued

[1] Abbreviations: mut, mutated; del, deletion; part del, partial deletion; ampl, amplification; (-), No mutations identified, negative; wt, wild-type; LOH, loss of heterozygosity, N.A., Not performed

Table A.1 3: Pearson correlation coefficients p-values for GBOs correlation matrix.

	CDKN2A	PROM1	IDO1	AIF1	CXCR4	CD68	DAB2	S100A4	FCGR3A	CD9	CXCL12	COL1A1	IL6	CHI3L1	COL1A2
CDKN2A					*										
PROM1	0,14				*										
IDO1	-0,02	0,33		**	**	**	**	***	***	***	***				
AIF1	0,13	0,19	0,53		**	***	*	***	***	***	**				
CXCR4	0,47	0,41	0,52	0,6		**	**	***	***	***	***				*
CD68	0,03	0,1	0,58	0,63	0,56		***	***	***	***	***				
DAB2	0,11	0,23	0,59	0,49	0,58	0,9		***	***	***	***		*		
S100A4	0,07	0,3	0,8	0,74	0,77	0,75	0,74		***	***	***		*		**
FCGR3A	0,11	0,33	0,75	0,77	0,76	0,81	0,77	0,93		***	***				
CD9	0,01	0,25	0,83	0,65	0,69	0,82	0,81	0,95	0,91		***				*
CXCL12	0,04	0,39	0,75	0,6	0,68	0,84	0,88	0,9	0,9	0,93					*
COL1A1	0,25	0,01	-0,03	0,14	0,35	0,13	0,17	0,28	0,15	0,05	0,11		***	***	***
IL6	0,18	-0,02	0,17	0,16	0,2	0,28	0,42	0,4	0,25	0,29	0,28	0,7		*	***
CHI3L1	0,24	-0,2	-0,05	0,07	0,12	-0,01	-0,02	0,18	0	0,03	-0,03	0,62	0,48		***
COL1A2	-0,06	-0,03	0,32	0,31	0,4	0,33	0,34	0,61	0,39	0,46	0,44	0,67	0,66	0,74	
SNAI1	0,45	0,21	0,25	0,15	0,47	0,28	0,31	0,43	0,3	0,33	0,26	0,57	0,72	0,49	0,57
TGFB1	0,52	0,12	0,32	0,5	0,61	0,35	0,32	0,51	0,4	0,43	0,32	0,3	0,46	0,41	0,48
CCL2	0,16	0,27	0,08	0,25	0,51	0,38	0,42	0,37	0,28	0,26	0,3	0,59	0,49	0,41	0,43
THBS1	-0,09	0,04	0,3	0,32	0,27	0,49	0,54	0,43	0,31	0,44	0,47	0,1	0,24	0,12	0,28
FUT4	0,03	0,32	-0,06	-0,1	-0,08	-0,1	0,12	0,03	-0,06	-0,05	0,03	0,37	0,73	0,04	0,18
POU5F1B	-0,22	0,04	-0,09	-0,18	-0,22	-0,14	0,07	-0,07	-0,17	-0,1	-0,09	0,28	0,72	0,01	0,12
CD44	0,31	0,01	-0,34	-0,16	-0,23	-0,04	0,02	-0,22	-0,29	-0,19	-0,13	0,07	0,32	0,25	0,02
ID1	0,23	0,16	0,03	0,13	0,14	0,01	0,1	0,16	-0,04	0,09	0,04	0,31	0,59	0,39	0,39
CDKN1A	-0,09	-0,03	0,13	-0,08	-0,15	0,16	0,12	0,04	-0,01	0,11	0,04	-0,08	0,12	0,19	0,05
ACSBG1	0,11	-0,4	-0,16	-0,13	-0,12	-0,26	-0,2	-0,12	-0,28	-0,17	-0,21	0,09	0,03	0,22	0,23
KCNF1	-0,24	-0,28	-0,22	-0,18	-0,05	-0,25	-0,24	0,02	-0,23	-0,17	-0,2	0,68	0,53	0,69	0,73

ERBB3	-0,1	-0,07	0,2	-0,23	-0,17	-0,1	-0,09	-0,1	-0,19	-0,09	-0,13	-0,01	-0,01	-0,09	-0,02
P2RX7	-0,01	0,19	0,48	-0,15	0,05	-0,03	0,05	0,03	-0,02	0,04	0,03	-0,03	-0,05	-0,2	-0,08
SOX10	-0,07	0,08	0,4	-0,23	-0,19	0,04	0,05	-0,11	-0,13	-0,04	-0,05	-0,14	-0,06	-0,11	-0,11
SOX2	0,39	0,38	0,26	-0,1	0,12	-0,3	-0,23	-0,09	-0,15	-0,2	-0,19	0,16	-0,05	-0,04	-0,05
STMN4	0,37	0,14	0,23	-0,22	0,1	-0,05	0,06	-0,09	-0,08	-0,14	-0,06	0,27	0,05	-0,14	-0,12
NCAM1	0,36	0,22	-0,14	-0,14	0,11	-0,02	0,02	-0,19	-0,11	-0,25	-0,14	0,25	0,09	-0,2	-0,25
NF-KB	0,44	0,15	-0,01	0,28	0,26	0,07	0,23	0,09	0,07	-0,03	0,01	0,41	0,49	-0,04	-0,01
MDM2	0,17	-0,1	-0,09	0,08	0,03	-0,08	-0,03	-0,05	0,06	-0,1	-0,06	0,21	0,05	-0,18	-0,14
CHEK1	0,64	-0,05	-0,16	0,14	0,12	-0,23	-0,26	-0,13	-0,11	-0,17	-0,22	-0,16	-0,17	0,15	-0,19
ATR	0,04	0,15	-0,11	0,08	0,08	-0,23	-0,26	-0,06	-0,07	-0,15	-0,18	-0,01	-0,14	-0,2	-0,16
CDH1	0,1	-0,21	-0,09	-0,03	-0,12	-0,16	-0,23	-0,14	-0,11	-0,11	-0,2	-0,19	-0,17	-0,11	-0,19
FOXP3	0,03	0,52	-0,08	0	-0,13	-0,27	-0,17	-0,07	-0,17	-0,19	-0,05	0,24	0,15	0,24	0,21
PIK3CA	-0,18	-0,3	-0,23	-0,13	-0,26	-0,2	-0,11	-0,28	-0,29	-0,2	-0,25	-0,18	-0,23	-0,08	-0,3
NOTCH	-0,15	0,01	0,04	0	-0,19	-0,32	-0,33	-0,15	-0,24	-0,24	-0,28	0,01	-0,14	-0,02	0
OLIG2	-0,25	-0,04	0,18	-0,23	-0,22	-0,31	-0,31	-0,19	-0,22	-0,18	-0,25	-0,2	-0,25	-0,22	-0,19
STAT3	0,29	0,24	-0,06	0,32	0,18	-0,14	-0,12	-0,06	-0,07	-0,17	-0,19	0,13	-0,01	0	-0,15
ATM	-0,05	-0,01	-0,19	0,22	-0,14	-0,1	-0,07	-0,19	-0,13	-0,23	-0,21	0,01	-0,13	-0,01	-0,29
mTOR	-0,17	0,09	-0,2	0,19	-0,11	-0,17	-0,21	-0,17	-0,18	-0,26	-0,25	0,13	-0,19	-0,3	-0,25

	SNAI1	**TGFB1**	**CCL2**	**THBS1**	**FUT4**	**POU5F1B**	**CD44**	**ID1**	**CDKN1A**	**ACSBG1**	**KCNF1**	**ERBB3**	**P2RX7**	**SOX10**	**SOX2**
CDKN2A	*	*													
PROM1										*					
IDO1													*	*	
AIF1		*													
CXCR4	*	**	**												
CD68				*											
DAB2			*	**											

S100A4	*	**		*											
FCGR3A		*													
CD9		*		*											
CXCL12				*											
COL1A1	**		**								***				
IL6	***	*	*		***	***		**			**				
CHI3L1	*	*	*								***				
COL1A2	**	*	*								***				
SNAI1		***	**		*			**			*				
TGFB1	0,76		*					**							
CCL2	0,57	0,44		**				**							
THBS1	0,16	0,28	0,58					*							
FUT4	0,46	0,18	0,27	0,02		***	*	**							
POU5F1B	0,38	0,12	0,11	-0,01	0,93		*	**							
CD44	0,32	0,27	0,21	0,3	0,42	0,41		***							
ID1	0,57	0,55	0,56	0,5	0,57	0,54	0,63								
CDKN1A	0,01	-0,08	-0,08	-0,06	-0,11	-0,1	0,17	-0,08							
ACSBG1	-0,11	-0,02	-0,19	-0,15	0	0,18	-0,11	-0,04	0,01		*	**			
KCNF1	0,44	0,23	0,26	-0,06	0,26	0,25	0,09	0,28	-0,06	0,41					
ERBB3	-0,01	-0,18	-0,15	-0,19	0,07	0,25	-0,21	-0,08	0,17	0,55	0,04		***	***	**
P2RX7	0,02	-0,08	-0,09	-0,1	-0,01	0,06	-0,34	-0,12	-0,18	0,12	-0,13	0,74		***	***
SOX10	0,06	-0,08	-0,06	0	-0,06	0,01	-0,09	-0,02	0,21	-0,05	-0,15	0,62	0,85		***
SOX2	0,17	0,08	0,08	-0,25	0,1	0,04	-0,25	0,05	-0,14	0,06	0,07	0,55	0,8	0,67	
STMN4	0,05	-0,18	0,16	-0,1	0,05	0,06	-0,32	-0,13	-0,04	-0,01	-0,06	0,54	0,77	0,7	0,76
NCAM1	0,2	-0,03	0,31	-0,23	0,26	0,16	-0,03	-0,07	0,16	-0,09	-0,04	0,24	0,32	0,27	0,52
NF-KB	0,28	0,31	0,5	0,19	0,56	0,53	0,19	0,46	-0,15	0,03	0,02	0,08	0,15	0,03	0,33
MDM2	-0,14	-0,23	0,08	-0,25	0,15	0,11	-0,15	-0,26	-0,22	0,14	0,18	-0,1	-0,05	-0,09	0,21
CHEK1	0,19	0,47	-0,19	-0,47	0,09	0,13	0,19	0,06	0,04	0,33	0,15	-0,15	-0,23	-0,2	0,4
ATR	0,08	0,15	0,21	-0,24	0,52	0,6	-0,12	0,07	-0,08	0,1	0,44	-0,06	0,03	-0,14	0,56

CDH1	-0,13	-0,05	-0,16	-0,39	-0,13	-0,14	-0,06	-0,24	0,2	0,04	0,1	-0,11	-0,12	-0,03	0,05
FOXP3	0,04	-0,08	0,07	-0,21	0,44	0,27	0,26	0,25	0,32	0,18	0,25	0,2	0,08	0,05	0,36
PIK3CA	-0,43	-0,27	-0,37	-0,22	-0,37	-0,14	0,12	-0,21	0,14	0,21	-0,05	-0,07	0,31	-0,04	-0,04
NOTCH	-0,23	-0,22	-0,21	-0,42	-0,01	0,04	-0,38	-0,19	0,34	0,53	0,2	0,61	0,45	0,3	0,59
OLIG2	-0,27	-0,3	-0,34	-0,45	-0,13	-0,09	-0,53	-0,38	0,37	0,19	0,02	0,47	0,6	0,49	0,59
STAT3	0,06	0,27	0,28	-0,08	0,11	0	0,1	0,21	0,01	-0,02	0	-0,05	0,13	0,06	0,49
ATM	-0,33	-0,08	-0,12	-0,33	0,12	0,16	-0,1	-0,27	0,18	0,31	-0,04	0,07	0,21	0	0,36
mTOR	-0,35	-0,16	0,12	-0,17	0,33	0,31	-0,23	-0,05	0,28	0,14	0,17	0,04	0,11	-0,09	0,53

	STMN4	**NCAM1**	**NF-KB**	**MDM2**	**CHEK1**	**ATR**	**CDH1**	**FOXP3**	**PIK3CA**	**NOTCH**	**OLIG2**	**STAT3**	**ATM**	**mTOR**
CDKN2A					**									
PROM1								**						
IDO1														
AIF1														
CXCR4														
CD68														
DAB2														
S100A4														
FCGR3A														
CD9														
CXCL12														
COL1A1			*											
IL6			*											
CHI3L1														
COL1A2														
SNAI1														
TGFB1					*									
CCL2			*											
THBS1					*					*	*			

FUT4			**			*		*						
POU5F1B			**			**								
CD44											**			
ID1			*											
CDKN1A														
ACSBG1										**				
KCNF1														
ERBB3	**									**	*			
P2RX7	***									*	**			
SOX10	***										*			
SOX2	***	**				*				**	**	*		*
STMN4		***									*			
NCAM1	0,62		**			*					*	**		*
NF-KB	0,38	0,56				*						***	*	**
MDM2	0,31	0,31	0,4			*	**							
CHEK1	-0,05	0,32	0,31	0,24		*	**					*		
ATR	0,07	0,47	0,48	0,5	0,55		***			*	*	***		**
CDH1	-0,03	0,28	0,09	0,62	0,64	0,74					*	*		
FOXP3	0,05	0,16	0,17	0,25	0,39	0,35	0			*			***	***
PIK3CA	-0,14	-0,03	0,07	0,01	0,03	-0,02	0,15	0,21					**	
NOTCH	0,34	0,34	0,18	0,25	0,38	0,54	0,29	0,5	0,34		***	*	***	***
OLIG2	0,48	0,41	-0,01	0,07	0,3	0,55	0,42	0,1	0,28	0,73			*	***
STAT3	0,2	0,51	0,68	0,39	0,56	0,7	0,46	0,35	0,31	0,46	0,26		***	***
ATM	0,04	0,35	0,47	0,29	0,35	0,38	0,36	0,74	0,64	0,79	0,46	0,71		***
mTOR	0,21	0,53	0,56	0,24	0,28	0,61	0,43	0,72	0,35	0,91	0,68	0,75	0,76	

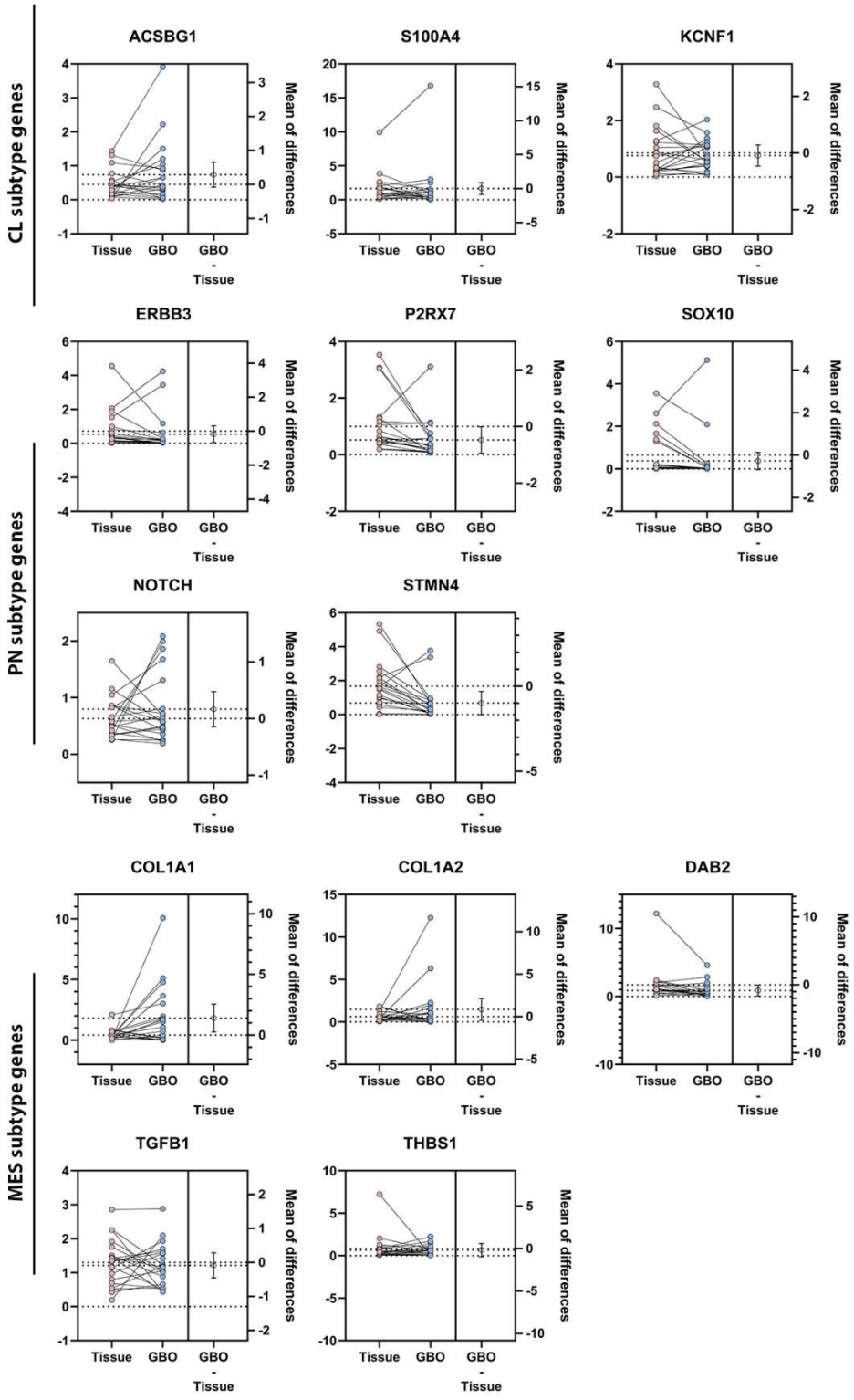

Figure A.1 1: Comparison of selective gene expressions between GBOs and corresponding tumour tissues. Differences in the expression of subtype related genes are presented. The paired mean difference between tissue and GBO is shown in the estimation plots. Both groups are plotted on the left axes as a scatter graph showing individual values: each paired set of the individual patient is connected by a line. The paired mean difference is plotted on the right axis and the 95 % confidence interval is indicated by the ends of the error bar.

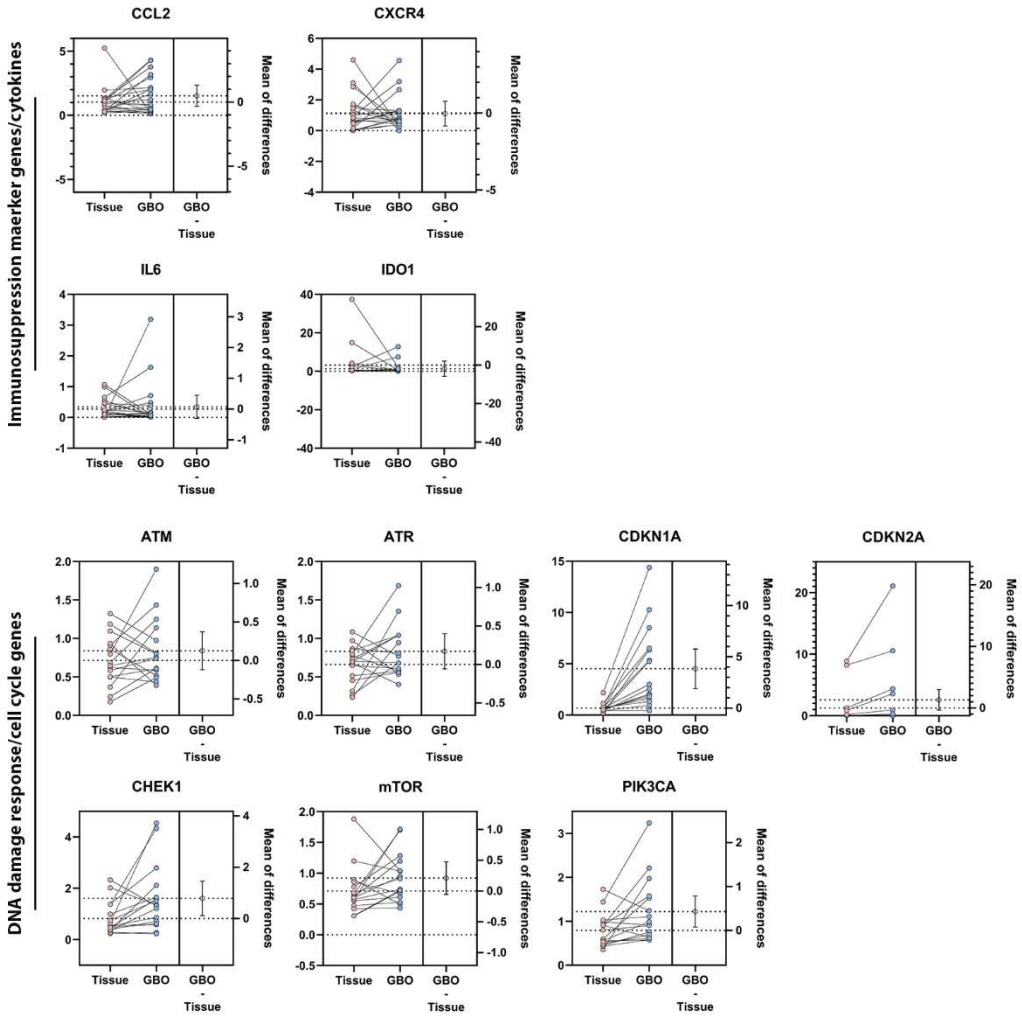

Figure A.1 2: Comparison of selective gene expressions between GBOs and corresponding tumour tissues. Differences in the expression of genes involved in immunosuppression and cytokine signalling, and genes involved in DNA damage response and cell cycle are presented. The paired mean difference between tissue and GBO is shown in the estimation plots. Both groups are plotted on the left axes as a scatter graph showing individual values: each paired set of the individual patient is connected by a line. The paired mean difference is plotted on the right axis and the 95 % confidence interval is indicated by the ends of the error bar.

A.2 Up-regulation of Cathepsin X in GB: Investigation of Selective Inhibitors and its Target γ-enolase

Table A.2 1: List of TaqMan gene expression assays (Thermo Fisher Scientific) used for RT-qPCR.

Gene name	Assay ID	Protein name
ACSBG1	Hs00209500_m1	Acyl-CoA Synthetase Bubblegum Family Member 1
CTSZ	Hs00938366_m1	Cathepsin X
CD15 (FUT4)	Hs01106466_s1	Fucosyltransferase 4
COL1A1	Hs00164004_m1	Collagen Type I Alpha 1 Chain
COL1A2	Hs01028956_m1	Collagen Type I Alpha 2 Chain
DAB2	Hs01120074_m1	DAB Adaptor Protein 2
ERBB3	Hs00176538_m1	Erb-B2 Receptor Tyrosine Kinase 3
GAPDH	Hs99999905_m1	Glyceraldehyde 3-phosphate dehydrogenase
GFAP	Hs00909233_m1	Glial Fibrillary Acidic Protein
HPRT1	Hs02800695_m1	Hypoxanthine Phosphoribosyltransferase 1
KCNF1	Hs00266908_s1	Potassium Voltage-Gated Channel Modifier Subfamily F Member 1
NFKB1	Hs00765730_m1	Nuclear factor-kappa B
NOTCH1	hs01062014_m1	Neurogenic locus notch homolog protein 1
OLIG2	Hs00377820_m1	Oligodendrocyte Transcription Factor 2
P2RX7	Hs00175721_m1	Purinergic Receptor P2X 7
POU5F1B	Hs01596605_s1	POU Class 5 Homeobox 1B; OCT4-PG1 (OCT4 pseudogene)
PROM1	Hs00195682_m1	Prominin-1; CD133 antigen
S100A4	Hs00243202_m1	S100 Calcium Binding Protein A4
SOX10	Hs00366918_m1	SRY-Box Transcription Factor 10
SOX2	Hs01053049_s1	SRY-Box Transcription Factor 2
STMN4	Hs00229288_m1	Stathmin 4
TGFBI	Hs00998133_m1	Transforming growth factor beta 1

THBS1	Hs00962908_m1	Thrombospondin 1
TUB33	Hs00801390_s1	Tubulin Beta 3 Class III

Table A.2 2: Details of the 43 GBM, 5 GBM rec, 14 LGG patients and their tumours operated at the Department Neurosurgery of the University Medical Centre Ljubljana, Slovenia, used for real-time quantitative PCR analysis.

Patient	Gender	Age (Years)	MGMT promoter methylation	Mutations				Chromosomal abnormalities	Survival (months)
				IDH1	TP53	EGFR mutation/ amplification	Other		
GB7	F	69	N.A.	N.A.	N.A.	N.A.	N.A.	N.A.	3
GB8	M	49	N.A.	-	-	N.A.	N.A.	N.A.	8
GB9	F	79	N.A.	-	-	N.A.	N.A.	1p del	4
GB10	F	64	N.A.	-	+	N.A.	N.A.	N.A.	4
GB11	M	70	N.A.	-	+	N.A.	N.A.	N.A.	9
GB12	F	81	N.A.	-	-	N.A.	N.A.	N.A.	6
GB13	F	58	N.A.	-	-	N.A.	N.A.	N.A.	50
GB14	F	66	N.A.	-	-	N.A.	N.A.	N.A.	3
GB15	M	81	N.A.	-	+	N.A.	N.A.	N.A.	6
GB16	F	67	N.A.	-	-	N.A.	ATRX mut	N.A.	2
GB17	M	71	N.A.	-	-	N.A.	N.A.	N.A.	12
GB18	M	58	N.A.	-	-	c.866C>T, p.Ala289Val (p.A289V)	N.A.	N.A.	0
GB19	M	53	N.A.	-	-	part of exons 2-7	N.A.	N.A.	33
GB20	F	59	N.A.	-	+	-	-	N.A.	6
GB21	M	61	N.A.	-	-	N.A.	N.A.	Aneuplodia (35% of cells)	2
GB22	M	62	N.A.	-	-	N.A.	N.A.	N.A.	22
GB23	M	51	N.A.	-	-	N.A.	N.A.	N.A.	0
GB24	M	65	N.A.	-	-	N.A.	N.A.	N.A.	6

GB25	F	84	N.A.	-	Dubious result	N.A.	-	N.A.	7
GB26	M	65	N.A.	-	+	N.A.	KRAS (p.Gly13Asp (G13D) and (kol 36) / NMYC ampl (kol 49)	N.A.	7
GB27	M	73	N.A.	-	-	wt	-	-	5
GB28	M	76	N.A.	-	-	wt	MET (c.3029C>T, p.Thr1010Ile) / PIK3CA (p.Glu542Lys (E542K))	N.A.	3
GB29	F	65	N.A.	-	-	EGFR ampl (kol. 76)	p.Ala289Val (A289V)	-	11
GB30	M	70	N.A.	-	-	EGFR ampl (kol. 85), del eks 2-7 (EGFRvIII)	-	N.A.	2
GB31	F	48	N.A.	-	-	N.A.	N.A.	N.A.	7
GB32	F	48	N.A.	N.A.	-	N.A.	-	N.A.	48
GB33	F	63	N.A.	-	-	-	-	N.A.	18
GB34	M	56	N.A.	-	+	EGFR ampl (kol. 54), part of exons. 2-7 EGFR	KIT ampl (kol.9) / PDGFRA ampl (kol.9)	N.A.	2
GB35	M	60	N.A.	-	-	EGFR ampl (kol. 45), del. eks. 2-7	-	N.A.	12

Table A.2.2. Continued

GB36	M	71	N.A.	-	-	EGFR ampl (kol. 41)	CDK4 ampl (kol. 49)	N.A.	2
GB37	M	77	yes	-	-	-	-	N.A.	9
GB38	M	56	N.A.	N.A.	N.A.	N.A.	-	N.A.	1
GB39	M	50	N.A.	-	-	EGFR ampl (kol. 106), del. eks. 2-7 EGFR	-	N.A.	22
GB40	M	80	yes	-	-	-	-	N.A.	22
GB41	M	34	N.A.	-	-	-	KRAS mut c.34G>C, p.(Gly12Arg) (G12R) in exn 2, KRAS amp (kol 14)	N.A.	28
GB42	F	69	yes	-	-	EGFR ampl (kol. 44), del. eks. 2-7 EGFR	-	N.A.	14
GB43	F	73	yes	-	-	EGFR ampl (kol. 34), del. eks. 2-7 EGFR	-	N.A.	4
GB rec	F	40	yes	-	-	part of exons 2-7 in EGFR (EGFRvIII) ATRX mut	ATRX mut	-	25
GB rec	F	58	N.A.	-	-	N.A.	N.A.	N.A.	22
GB rec	F	72	N.A.	-	-	part of exons 2-7 in EGFR (EGFRvIII) ATRX mut	N.A.	N.A.	20
GB rec	M	63	N.A.	-	+	ATRX mut	BRAF V600E	-	112
GB rec	M	65	N.A.	-	-	ATRX mut	N.A.	N.A.	16
LGG 1	M	33	N.A.	-	+	N.A.	N.A.	-	22

Table A.2.2. Continued

LGG 2	M	25	N.A.	+	-	N.A.	-	-	61
LGG 3	M	29	N.A.	+	-	N.A.	N.A.	-	102
LGG 4	M	36	N.A.	+	-	N.A.	-	-	41
LGG 5	F	57	N.A.	+	-	N.A.	-	Co-deletion 1p/19q	39
LGG 6	M	66	N.A.	+	-	N.A.	-	N.A.	162
LGG 7	M	73	N.A.	IDH1 R132 H	Dubious result	N.A.	ATRX mut	N.A.	51
LGG 8	F	61	N.A.	+	+	N.A.	ATRX mut	-	144
LGG 9	M	44	N.A.	+	-	N.A.	ATRX mut	-	73
LGG 10	M	32	N.A.	+	-	N.A.	ATRX mut	N.A.	23
LGG 11	M	28	N.A.	+	-	N.A.	ATRX mut	N.A.	72
LGG 12	F	59	N.A.	+	-	N.A.	N.A.	Co-deletion 1p/19q	43
LGG 13	M	51	N.A.	-	-	N.A.	-	-	21
LGG 14	M	44	N.A.	+	-	N.A.	N.A.	-	30

[1] Abbreviations: mut, mutated; del, deletion; part del, partial deletion; ampl, amplification; (-), No mutations identified, negative; (+), positive; N.A., Not performed

Table A.2 3: Details of the 6 GBM patients and their tumours operated at the Department Neurosurgery of the University Medical Centre Ljubljana, Slovenia, used for ELISA, cathepsin X activity assessment and immunofluorescence staining.

Patient	Gender	Age (Years)	MGMT promoter methylation	Mutations				Chromosomal abnormalities
				IDH1	TP53	EGFR mutation/ amplification	Other	
GB1	M	47	no	wt	mut (P190L)	mut (R108K) / ampl	CDKN2A and CDKN2B del / pTERT (C228T) / MET, PIK3CA ampl / PTEN (I122F)	10q del
GB2	M	63	yes	mut (R132H)	mut (V157G)	wt	CDKN2A and CDKN2B del / ATRX (Y2083N) / PIK3R1 (D464del)	chromosome 7 ampl
GB3	M	76	yes	wt	wt	ampl	CDKN2A and CDKN2B del / PTEN (G132S), MDM4 (K374G), PDGFRA (G79D)	chromosome 7 ampl / 10q, 19q del
GB4	M	79	yes	wt	Splice site mutation / mut (P190L)	ampl	CDKN2A and CDKN2B del / PTEN (C136R), TERT (C250T) / MET, MYCN, PDGFRA ampl	chromosome 7 ampl / 10q del / 1p part del
GB5	M	64	no	wt	mut (C238Y)	wt	TERT (C228T)	chromosome 7 ampl / 10q del
GB6	M	74	no	wt	mut (P190L)	ampl	CDKN2A and CDKN2B del / TERT (C228), ERBB3 (G337Q)	chromosome 7 ampl / 10q, 13q, 22q del / 14q part del

[1] Abbreviations: mut, mutated; del, deletion; part del, partial deletion; ampl, amplification; wt, wild type.

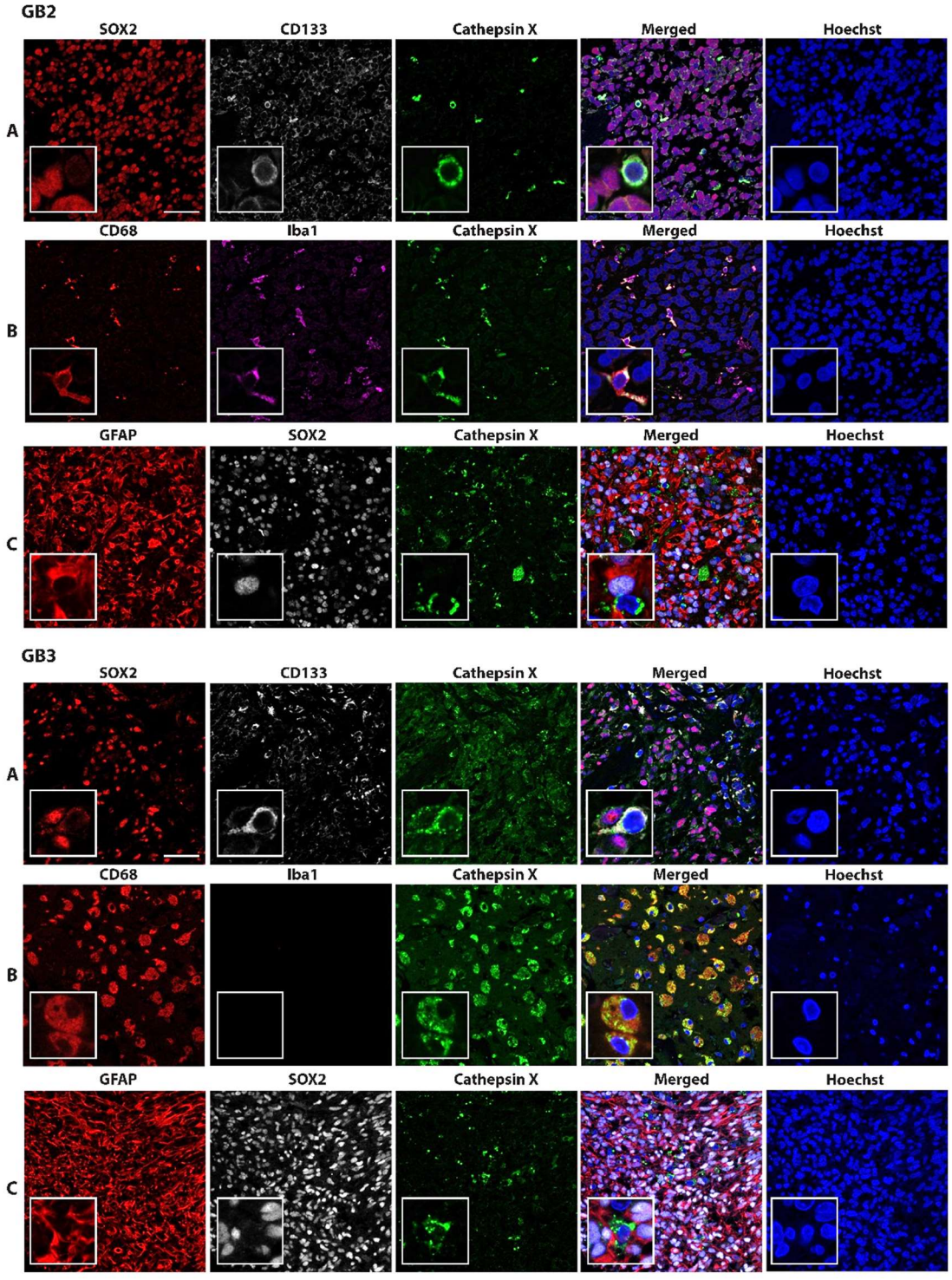
GB2
SOX2
CD133
Cathepsin X
Merged
Hoechst
A
CD68
Iba1
Cathepsin X
Merged
Hoechst
B
GFAP
SOX2
Cathepsin X
Merged
Hoechst
C
GB3
SOX2
CD133
Cathepsin X
Merged
Hoechst
A
CD68
Iba1
Cathepsin X
Merged
Hoechst
B
GFAP
SOX2
Cathepsin X
Merged
Hoechst
C

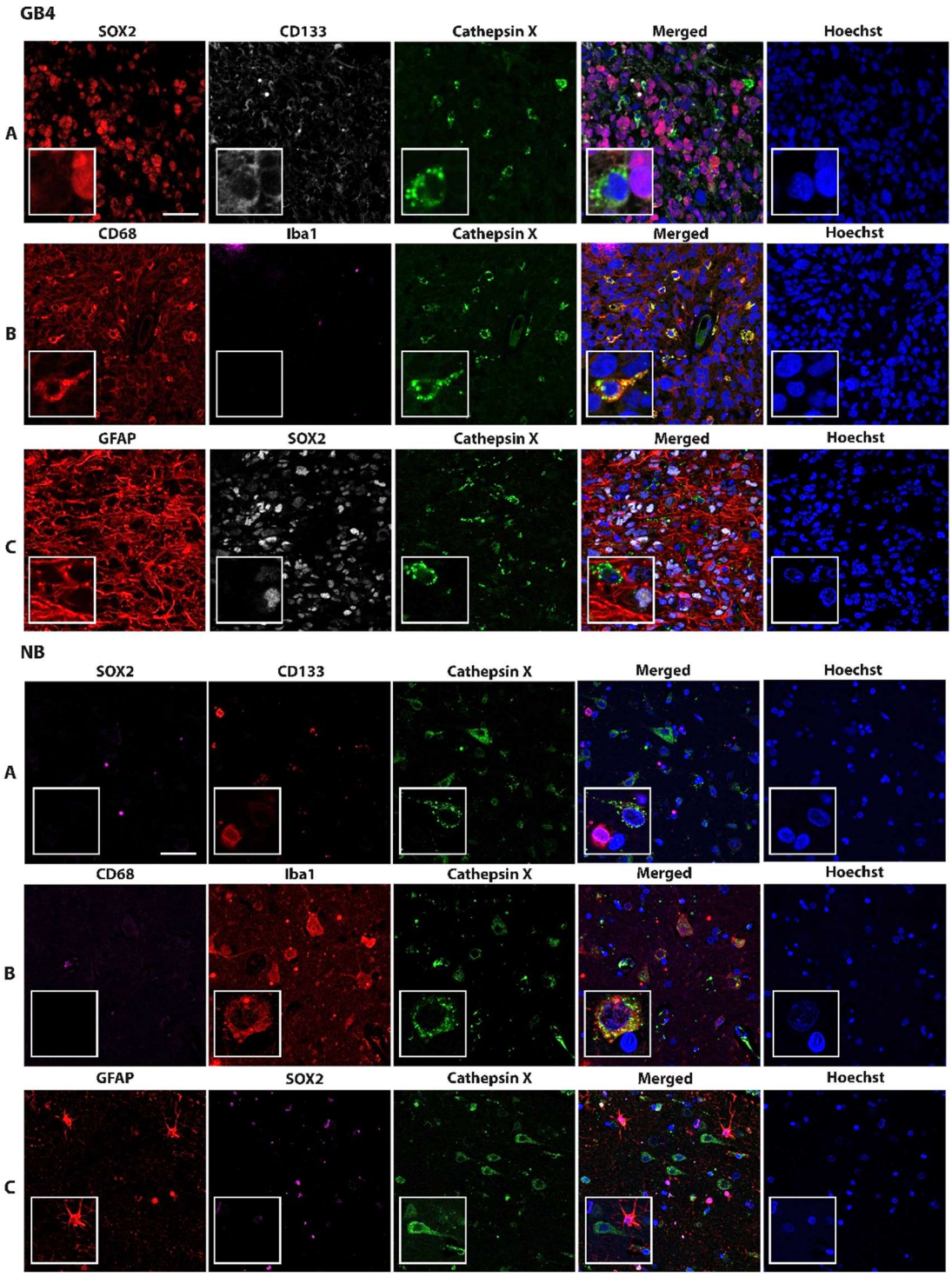

Figure A.2 1: Expression and cell-specific localisation of cathepsin X in GB tissues and non-tumour brain tissue. Representative images of triple immunofluorescence staining of cathepsin X (green) and markers of (A) GSCs (SOX2 (red in GB; purple in NB) and CD133 (grey in GB; Red in NB)), (B) macrophages (CD68 (red in GB; purple in NB)) and microglia (Iba1 (purple in GB; red in NB)), and (C) GB cells and astrocytes (GFAP (red)) and GSCs (SOX2 (grey in GB; purple in NB)) are shown. Cell nuclei were stained with Hoechst 33258 (blue). Scale bar: 50 µm.

References

Afrin, F., Chi, M., Eamens, A. L., Duchatel, R. J., Douglas, A. M., Schneider, J., … Dun, M. D. (2020). Can Hemp Help? Low-THC Cannabis and Non-THC Cannabinoids for the Treatment of Cancer. *Cancers*, *12*(4). https://doi.org/10.3390/CANCERS12041033

Ahmed, S. U., Carruthers, R., Gilmour, L., Yildirim, S., Watts, C., & Chalmers, A. J. (2015). Selective inhibition of parallel DNA damage response pathways optimizes radiosensitization of glioblastoma stem-like cells. *Cancer Research*, *75*(20), 4416–4428. https://doi.org/10.1158/0008-5472.CAN-14-3790/651855/AM/SELECTIVE-INHIBITION-OF-PARALLEL-DNA-DAMAGE

Aibaidula, A., Lu, J. feng, Wu, J. song, Zou, H. jian, Chen, H., Wang, Y. qian, … Zhou, L. fu. (2015). Establishment and maintenance of a standardized glioma tissue bank: Huashan experience. *Cell and Tissue Banking*, *16*(2), 271–281. https://doi.org/10.1007/S10561-014-9459-4

Akkari, L., Gocheva, V., Kester, J. C., Hunter, K. E., Quick, M. L., Sevenich, L., … Joyce, J. A. (2014). Distinct functions of macrophage-derived and cancer cell-derived cathepsin Z combine to promote tumor malignancy via interactions with the extracellular matrix. *Genes and Development*, *28*(19), 2134–2150. https://doi.org/10.1101/gad.249599.114

Antunes, A. R. P., Scheyltjens, I., Duerinck, J., Neyns, B., Movahedi, K., & Van Ginderachter, J. A. (2020). Understanding the glioblastoma immune microenvironment as basis for the development of new immunotherapeutic strategies. *ELife*, *9*. https://doi.org/10.7554/eLife.52176

Baebler, Š., Svalina, M., Petek, M., Stare, K., Rotter, A., Pompe-Novak, M., & Gruden, K. (2017). quantGenius: implementation of a decision support system for qPCR-based gene quantification. *BMC Bioinformatics*, *18*(1), 276. https://doi.org/10.1186/s12859-017-1688-7

Behnan, J., Stangeland, B., Hosainey, S. A. M., Joel, M., Olsen, T. K., Micci, F., … Brinchmann, J. E. (2016). *Differential propagation of stroma and cancer stem cells dictates tumorigenesis and multipotency.* (April), 1–15. https://doi.org/10.1038/onc.2016.230

Benavides, F., Perez, C., Blando, J., Contreras, O., Shen, J., Coussens, L. M., … Conti, C. J. (2012). Protective role of cathepsin L in mouse skin carcinogenesis. *Molecular Carcinogenesis*, *51*(4), 352–361. https://doi.org/10.1002/MC.20792

Bian, S., Repic, M., Guo, Z., Kavirayani, A., Burkard, T., Bagley, J. A., … Knoblich, J. A. (2018). Genetically engineered cerebral organoids model brain tumor formation.

Nature Methods, *15*, 631–639. https://doi.org/10.1038/s41592-018-0070-7

Blasi, F., & Carmeliet, P. (2002). uPAR: a versatile signalling orchestrator. *Nature Reviews. Molecular Cell Biology*, *3*(12), 932–943. https://doi.org/10.1038/NRM977

Borovski, T., De Sousa E Melo, F., Vermeulen, L., & Medema, J. P. (2011). Cancer stem cell niche: the place to be. *Cancer Research*, *71*(3), 634–639. https://doi.org/10.1158/0008-5472.CAN-10-3220

Bourdon, J. C., Fernandes, K., Murray-Zmijewski, F., Liu, G., Diot, A., Xirodimas, D. P., … Lane, D. P. (2005). p53 isoforms can regulate p53 transcriptional activity. *Genes and Development*, *19*(18), 2122–2137. https://doi.org/10.1101/gad.1339905

Bregy, A., Papadimitriou, K., Faber, D. A., Shah, A. H., Gomez, C. R., Komotar, R. J., & Egea, S. C. (2015). Banking Brain Tumor Specimens Using a University Core Facility. *Biopreservation and Biobanking*, *13*(4), 280–286. https://doi.org/10.1089/BIO.2014.0106

Breznik, B., Limbaeck Stokin, C., Kos, J., Khurshed, M., Hira, V. V. V., Bošnjak, R., … Van Noorden, C. J. F. (2018). Cysteine cathepsins B, X and K expression in peri-arteriolar glioblastoma stem cell niches. *Journal of Molecular Histology*, *49*(5), 481–497. https://doi.org/10.1007/s10735-018-9787-y

Breznik, B., Motaln, H., & Turnšek, T. L. (2017). Proteases and cytokines as mediators of interactions between cancer and stromal cells in tumours. *Biological Chemistry*, *398*(7), 709–719. https://doi.org/10.1515/hsz-2016-0283

Breznik, B., Motaln, H., Vittori, M., Rotter, A., & Turnšek, T. L. (2017). Mesenchymal stem cells differentially affect the invasion of distinct glioblastoma cell lines. *Oncotarget*, *8*(15), 25482–25499. https://doi.org/10.18632/oncotarget.16041

Brix, K., Dunkhorst, A., Mayer, K., & Jordans, S. (2008). Cysteine cathepsins: Cellular roadmap to different functions. *Biochimie*, *90*(2), 194–207. https://doi.org/10.1016/J.BIOCHI.2007.07.024

Cascio, M., Gauson, L., Stevenson, L., Ross, R., & Pertwee, R. (2010). Evidence that the plant cannabinoid cannabigerol is a highly potent α2-adrenoceptor agonist and moderately potent 5HT1A receptor antagonist. *British Journal of Pharmacology*, *159*(1), 129–141. https://doi.org/10.1111/j.1476-5381.2009.00515.x

Chai, G., Brewer, J. M., Lovelace, L. L., Aoki, T., Minor, W., & Lebioda, L. (2004). Expression, purification and the 1.8 angstroms resolution crystal structure of human neuron specific enolase. *Journal of Molecular Biology*, *341*(4), 1015–1021. https://doi.org/10.1016/J.JMB.2004.05.068

Clavreul, A., Soulard, G., Lemée, J. M., Rigot, M., Fabbro-Peray, P., Bauchet, L., … Zemmoura, I. (2019). The French glioblastoma biobank (FGB): a national clinicobiological database. *Journal of Translational Medicine*, *17*(1), 133. https://doi.org/10.1186/S12967-019-1859-6

Clevers, H. (2016). Modeling Development and Disease with Organoids. *Cell*, *165*(7), 1586–1597. https://doi.org/10.1016/j.cell.2016.05.082

Colin, C., Voutsinos-Porche, B., Nanni, I., Fina, F., Metellus, P., Intagliata, D., … Figarella-Branger, D. (2009). High expression of cathepsin B and plasminogen activator inhibitor type-1 are strong predictors of survival in glioblastomas. *Acta Neuropathologica*, *118*(6), 745–754. https://doi.org/10.1007/S00401-009-0592-2

Cuddapah, V. A., Robel, S., Watkins, S., & Sontheimer, H. (2014). A neurocentric perspective on glioma invasion. *Nature Reviews. Neuroscience*, *15*(7). https://doi.org/10.1038/NRN3765

De Petrocellis, L., Ligresti, A., Schiano Moriello, A., Iappelli, M., Verde, R., Stott, C. G., … Di Marzo, V. (2013). Non-THC cannabinoids inhibit prostate carcinoma growth in vitro and in vivo: Pro-apoptotic effects and underlying mechanisms. *British Journal of Pharmacology*, *168*(1), 79–102. https://doi.org/10.1111/j.1476-5381.2012.02027.x

De Petrocellis, L., Nabissi, M., Santoni, G., & Ligresti, A. (2017). Actions and Regulation of Ionotropic Cannabinoid Receptors. *Advances in Pharmacology (San Diego, Calif.)*, *80*, 249–289. https://doi.org/10.1016/bs.apha.2017.04.001

de Souza, N. (2018). Organoids. *Nature Methods*, *15*, 23. https://doi.org/10.1038/nmeth.4576

Deng, L., Ng, L., Ozawa, T., & Stella, N. (2017). Quantitative Analyses of Synergistic Responses between Cannabidiol and DNA-Damaging Agents on the Proliferation and Viability of Glioblastoma and Neural Progenitor Cells in Culture. *The Journal of Pharmacology and Experimental Therapeutics*, *360*(1), 215–224. https://doi.org/10.1124/jpet.116.236968

Dennemärker, J., Lohmüller, T., Mayerle, J., Tacke, M., Lerch, M. M., Coussens, L. M., … Reinheckel, T. (2009). Deficiency for the cysteine protease cathepsin L promotes tumor progression in mouse epidermis. *Oncogene*, *29*(11), 1611–1621. https://doi.org/10.1038/onc.2009.466

Deryugina, E. I., Ratnikov, B., Monosov, E., Postnova, T. I., DiScipio, R., Smith, J. W., & Strongin, A. Y. (2001). MT1-MMP initiates activation of pro-MMP-2 and integrin alphavbeta3 promotes maturation of MMP-2 in breast carcinoma cells. *Experimental Cell Research*, *263*(2), 209–223. https://doi.org/10.1006/EXCR.2000.5118

Deshaies, R. J. (2020). Multispecific drugs herald a new era of biopharmaceutical innovation. *Nature 2020 580:7803*, *580*(7803), 329–338. https://doi.org/10.1038/s41586-020-2168-1

Doherty, G. J., & de Paula, B. H. R. (2021). Cannabinoids in glioblastoma multiforme—hype or hope? *British Journal of Cancer 2021 124:8*, *124*(8), 1341–1343. https://doi.org/10.1038/s41416-021-01265-5

Dolenc, I., Štefe, I., Turk, D., Taler-Verčič, A., Turk, B., Turk, V., & Stoka, V. (2021). Human cathepsin X/Z is a biologically active homodimer. *Biochimica et Biophysica Acta - Proteins and Proteomics*, *1869*(2). https://doi.org/10.1016/j.bbapap.2020.140567

Dumitru, C. A., Sandalcioglu, I. E., & Karsak, M. (2018). Cannabinoids in glioblastoma therapy: New applications for old drugs. *Frontiers in Molecular Neuroscience*, *11*(May), 1–7. https://doi.org/10.3389/fnmol.2018.00159

Ehman, E. C., Johnson, G. B., Villanueva-meyer, J. E., Cha, S., Leynes, A. P., Eric, P., … Hope, T. A. (2017). *Molecular profiling reveals biologically discrete subsets and pathways of progression in diffuse glioma. 46*(5), 1247–1262. https://doi.org/10.1002/jmri.25711.PET/MRI

Eke, I., & Cordes, N. (2011, June 1). Radiobiology goes 3D: How ECM and cell morphology impact on cell survival after irradiation. *Radiotherapy and Oncology*, Vol. 99, pp. 271–

278. Elsevier. https://doi.org/10.1016/j.radonc.2011.06.007

Expression of ENO2 in cancer. The Human Protein Atlas. (n.d.). Retrieved January 5, 2022, from https://www.proteinatlas.org/ENSG00000111674-ENO2/pathology

Frosina, G., Marubbi, D., Marcello, D., Vecchio, D., & Daga, A. (2019). The efficacy and toxicity of ATM inhibition in glioblastoma initiating cells-driven tumor models. *Critical Reviews in Oncology/Hematology*, *138*, 214–222. https://doi.org/10.1016/J.CRITREVONC.2019.04.015

Galve-Roperh, I., Chiurchiù, V., Díaz-Alonso, J., Bari, M., Guzmán, M., & Maccarrone, M. (2013). Cannabinoid receptor signaling in progenitor/stem cell proliferation and differentiation. *Progress in Lipid Research*, *52*(4), 633–650. https://doi.org/10.1016/j.plipres.2013.05.004

Gimple, R. C., Yang, K., Halbert, M. E., Agnihotri, S., & Rich, J. N. (2022). Brain cancer stem cells: resilience through adaptive plasticity and hierarchical heterogeneity. *Nature Reviews Cancer*. Nature Research. https://doi.org/10.1038/s41568-022-00486-x

Glass, R., & Synowitz, M. (2014). CNS macrophages and peripheral myeloid cells in brain tumours. *Acta Neuropathologica*, *128*(3), 347–362. https://doi.org/10.1007/S00401-014-1274-2

Goldbrunner, R. H., Bernstein, J. J., & Tonn, J. C. (1999). Cell-extracellular matrix interaction in glioma invasion. *Acta Neurochirurgica*, *141*(3), 295–305. https://doi.org/10.1007/S007010050301

Gondi, C. S., Lakka, S. S., Yanamandra, N., Olivero, W. C., Dinh, D. H., Gujrati, M., … Rao, J. S. (2004). Adenovirus-mediated expression of antisense urokinase plasminogen activator receptor and antisense cathepsin B inhibits tumor growth, invasion, and angiogenesis in gliomas. *Cancer Research*. https://doi.org/10.1158/0008-5472.CAN-04-1243

Gousias, K., Theocharous, T., & Simon, M. (2022). Mechanisms of Cell Cycle Arrest and Apoptosis in Glioblastoma. *Biomedicines*, *10*(3). https://doi.org/10.3390/BIOMEDICINES10030564

Habič, A., Novak, M., Majc, B., Lah Turnšek, T., & Breznik, B. (2021). Proteases Regulate Cancer Stem Cell Properties and Remodel Their Microenvironment. *The Journal of Histochemistry and Cytochemistry : Official Journal of the Histochemistry Society*. https://doi.org/10.1369/00221554211035192

Hafner, A., Glavan, G., Obermajer, N., Živin, M., Schliebs, R., & Kos, J. (2013). Neuroprotective role of γ-enolase in microglia in a mouse model of Alzheimer's disease is regulated by cathepsin X. *Aging Cell*, *12*(4), 604–614. https://doi.org/10.1111/ACEL.12093

Hafner, A., Obermajer, N., & Kos, J. (2011). Gamma-1-syntrophin mediates trafficking of gamma-enolase towards the plasma membrane and enhances its neurotrophic activity. *NeuroSignals*, *18*(4), 246–258. https://doi.org/10.1159/000324292

Hafner, A., Obermajer, N., & Kos, J. (2012). γ-Enolase C-terminal peptide promotes cell survival and neurite outgrowth by activation of the PI3K/Akt and MAPK/ERK signalling pathways. *Biochemical Journal*, *443*(2), 439–450. https://doi.org/10.1042/BJ20111351

Hafner Pišlar, A., Zidar, N., Kikelj, D., & Kos, J. (2014). Cathepsin X promotes 6-hydroxydopamine-induced apoptosis of PC12 and SH-SY5Y cells. *Neuropharmacology*, *82*, 121–131. https://doi.org/10.1016/j.neuropharm.2013.07.040

Hanahan, D., & Coussens, L. M. (2012). Accessories to the Crime: Functions of Cells Recruited to the Tumor Microenvironment. *Cancer Cell*, *21*(3), 309–322. https://doi.org/10.1016/J.CCR.2012.02.022

Hara, T., Chanoch-Myers, R., Mathewson, N. D., Myskiw, C., Atta, L., Bussema, L., … Tirosh, I. (2021). Interactions between cancer cells and immune cells drive transitions to mesenchymal-like states in glioblastoma. *Cancer Cell*, *39*(6), 779-792.e11. https://doi.org/10.1016/J.CCELL.2021.05.002

Hatoum, A., Mohammed, R., & Zakieh, O. (2019). The unique invasiveness of glioblastoma and possible drug targets on extracellular matrix. *Cancer Management and Research*. https://doi.org/10.2147/CMAR.S186142

Hattori, T., Ohsawa, K., Mizuno, Y., Kato, K., & Kohsaka, S. (1994). Synthetic peptide corresponding to 30 amino acids of the C-terminal of neuron-specific enolase promotes survival of neocortical neurons in culture. *Biochemical and Biophysical Research Communications*, *202*(1), 25–30. https://doi.org/10.1006/BBRC.1994.1888

Hattori, Tatsuya, Takei, N., Mizuno, Y., Kato, K., & Kohsaka, S. (1995). Neurotrophic and neuroprotective effects of neuron-specific enolase on cultured neurons from embryonic rat brain. *Neuroscience Research*, *21*(3), 191–198. https://doi.org/10.1016/0168-0102(94)00849-B

Hira, V. V. V., Breznik, B., Vittori, M., Loncq de Jong, A., Mlakar, J., Oostra, R. J., … Van Noorden, C. J. F. (2019). Similarities Between Stem Cell Niches in Glioblastoma and Bone Marrow: Rays of Hope for Novel Treatment Strategies. *Journal of Histochemistry and Cytochemistry*, *68*(1). https://doi.org/10.1369/0022155419878416

Hou, H., Sun, D., & Zhang, X. (2019). The role of MDM2 amplification and overexpression in therapeutic resistance of malignant tumors. *Cancer Cell International*, *19*(1), 1–8. https://doi.org/10.1186/S12935-019-0937-4/TABLES/1

Hubert, C. G., Rivera, M., Spangler, L. C., Wu, Q., Mack, S. C., Prager, B. C., … Rich, J. N. (2016). A three-dimensional organoid culture system derived from human glioblastomas recapitulates the hypoxic gradients and cancer stem cell heterogeneity of tumors found in vivo. *Cancer Research*, *76*(8), 2465–2477. https://doi.org/10.1158/0008-5472.CAN-15-2402

Jacob, F., Ming, G. li, & Song, H. (2020). Generation and biobanking of patient-derived glioblastoma organoids and their application in CAR T cell testing. *Nature Protocols*, *15*(12), 4000–4033. https://doi.org/10.1038/s41596-020-0402-9

Jacob, F., Salinas, R. D., Zhang, D. Y., Nguyen, P. T. T., Schnoll, J. G., Wong, S. Z. H., … Song, H. (2020). A Patient-Derived Glioblastoma Organoid Model and Biobank Recapitulates Inter- and Intra-tumoral Heterogeneity. *Cell*, *180*(1), 188-204.e22. https://doi.org/10.1016/j.cell.2019.11.036

Kessenbrock, K., Plaks, V., & Werb, Z. (2010). Matrix Metalloproteinases: Regulators of the Tumor Microenvironment. *Cell*, *141*(1), 52–67. https://doi.org/10.1016/j.cell.2010.03.015

Khaddour, K., Johanns, T. M., & Ansstas, G. (2020). The landscape of novel therapeutics

and challenges in glioblastoma multiforme: Contemporary state and future directions. *Pharmaceuticals*, *13*(11), 1–26. https://doi.org/10.3390/ph13110389

Klein, E., Hau, A. C., Oudin, A., Golebiewska, A., & Niclou, S. P. (2020). Glioblastoma Organoids: Pre-Clinical Applications and Challenges in the Context of Immunotherapy. *Frontiers in Oncology*, *10*(December). https://doi.org/10.3389/fonc.2020.604121

Kong, F., Zhang, W., Qiao, L., Li, Q., Li, H., Cao, J., … Wang, Y. (2018). Establishment and quality evaluation of a glioma biobank in Beijing Tiantan Hospital. *PeerJ*, *6*(3). https://doi.org/10.7717/PEERJ.4450

Koom, W. S., Park, S. Y., Kim, W., Kim, M., Kim, J. S., Kim, H., … Seong, J. (2012). Combination of radiotherapy and adenovirus-mediated p53 gene therapy for MDM2-overexpressing hepatocellular carcinoma. *Journal of Radiation Research*, *53*(2), 202–210. https://doi.org/10.1269/JRR.11110

Kos, J., Sekirnik, A., Premzl, A., Bergant Zavašnik, V., Langerholc, T., Turk, B., … Turk, V. (2005). Carboxypeptidases cathepsins X and B display distinct protein profile in human cells and tissues. *Experimental Cell Research*, *306*(1), 103–113. https://doi.org/10.1016/j.yexcr.2004.12.006

Kos, J., Vižin, T., Fonović, U. P., & Pišlar, A. (2015, April 1). Intracellular signaling by cathepsin X: Molecular mechanisms and diagnostic and therapeutic opportunities in cancer. *Seminars in Cancer Biology*, Vol. 31, pp. 76–83. Academic Press. https://doi.org/10.1016/j.semcancer.2014.05.001

Krueger, S., Kalinski, T., Hundertmark, T., Wex, T., Küster, D., Peitz, U., … Roessner, A. (2005). Up-regulation of cathepsin X in Helicobacter pylori gastritis and gastric cancer. *Journal of Pathology*, *207*(1), 32–42. https://doi.org/10.1002/path.1820

Lah, T. T., Durán Alonso, M. B., & Van Noorden, C. J. F. (2006). Antiprotease therapy in cancer: Hot or not? *Expert Opinion on Biological Therapy*. https://doi.org/10.1517/14712598.6.3.257

Lah, T. T., Majc, B., Novak, M., Sušnik, A., Breznik, B., Porčnik, A., … Zomer, R. (2022). The Cytotoxic Effects of Cannabidiol and Cannabigerol on Glioblastoma Stem Cells May Mostly Involve GPR55 and TRPV1 Signalling. *Cancers 2022, Vol. 14, Page 5918*, *14*(23), 5918. https://doi.org/10.3390/CANCERS14235918

Lah, T. T., Novak, M., Pena Almidon, M. A., Marinelli, O., Žvar Baškovič, B., Majc, B., … Nabissi, M. (2021). Cannabigerol Is a Potential Therapeutic Agent in a Novel Combined Therapy for Glioblastoma. *Cells*, *10*(2), 340. https://doi.org/10.3390/cells10020340

Lathia, J. D., Mack, S. C., Mulkearns-hubert, E. E., Valentim, C. L. L., & Rich, J. N. (2015). *Cancer stem cells in glioblastoma*. 1203–1217. https://doi.org/10.1101/gad.261982.115.tumors

LeBlanc, V. G., Trinh, D. L., Aslanpour, S., Hughes, M., Livingstone, D., Jin, D., … Marra, M. A. (2022). Single-cell landscapes of primary glioblastomas and matched explants and cell lines show variable retention of inter- and intratumor heterogeneity. *Cancer Cell*, *40*(4), 379-392.e9. https://doi.org/10.1016/j.ccell.2022.02.016

Lee, J., Kotliarova, S., Kotliarov, Y., Li, A., Su, Q., Donin, N. M., … Fine, H. A. (2006). Tumor stem cells derived from glioblastomas cultured in bFGF and EGF more closely

mirror the phenotype and genotype of primary tumors than do serum-cultured cell lines. *Cancer Cell*. https://doi.org/10.1016/j.ccr.2006.03.030

Levicar, N., Strojnik, T., Kos, J., Dewey, R. A., Pilkington, G. J., & Lah T., T. (2002). Lysosomal enzymes, cathepsins in brain tumour invasion. *Journal of Neuro-Oncology*, *58*(1), 21–32. https://doi.org/10.1023/a:1015892911420

Li, Q., Chen, B., Cai, J., Sun, Y., Wang, G., Li, Y., … Jiang, C. (2016). Comparative analysis of matrix metalloproteinase family members reveals that MMP9 predicts survival and response to temozolomide in patients with primary glioblastoma. *PLoS ONE*. https://doi.org/10.1371/journal.pone.0151815

Li, X., Liu, R., Su, X., Pan, Y., Han, X., Shao, C., & Shi, Y. (2019). Harnessing tumor-associated macrophages as aids for cancer immunotherapy. *Molecular Cancer*, *18*(1). https://doi.org/10.1186/S12943-019-1102-3

Ligresti, A., De Petrocellis, L., & Di Marzo, V. (2016). From phytocannabinoids to cannabinoid receptors and endocannabinoids: Pleiotropic physiological and pathological roles through complex pharmacology. *Physiological Reviews*, *96*(4), 1593–1659. https://doi.org/10.1152/physrev.00002.2016

Ligresti, A., Moriello, A. S., Starowicz, K., Matias, I., Pisanti, S., De Petrocellis, L., … Di Marzo, V. (2006). Antitumor activity of plant cannabinoids with emphasis on the effect of cannabidiol on human breast carcinoma. *The Journal of Pharmacology and Experimental Therapeutics*, *318*(3), 1375–1387. https://doi.org/10.1124/jpet.106.105247

Linkous, A., Balamatsias, D., Snuderl, M., Edwards, L., Miyaguchi, K., Milner, T., … Fine, H. A. (2019). Modeling Patient-Derived Glioblastoma with Cerebral Organoids. *Cell Reports*, *26*(12), 3203-3211.e5. https://doi.org/10.1016/j.celrep.2019.02.063

López-Otín, C., & Matrisian, L. M. (2007). Emerging roles of proteases in tumour suppression. *Nature Reviews. Cancer*, *7*(10), 800–808. https://doi.org/10.1038/nrc2228

Louis, D. N. (2006). Molecular pathology of malignant gliomas. *Annual Reviews of Pathology: Mechanisms of Disease*, *1*, 97–117. https://doi.org/10.1146/ANNUREV.PATHOL.1.110304.100043

Lucey, B. P., Nelson-Rees, W. A., & Hutchins, G. M. (2009, September). Henrietta Lacks, HeLa cells, and cell culture contamination. *Archives of Pathology and Laboratory Medicine*, Vol. 133, pp. 1463–1467. Arch Pathol Lab Med. https://doi.org/10.1043/1543-2165-133.9.1463

Ma, J., Chen, C. C., & Li, M. (2021). Macrophages/Microglia in the Glioblastoma Tumor Microenvironment. *International Journal of Molecular Sciences*, *22*(11). https://doi.org/10.3390/IJMS22115775

Mackie, K. (2008). Cannabinoid receptors: where they are and what they do. *Journal of Neuroendocrinology*, *20 Suppl 1*(SUPPL. 1), 10–14. https://doi.org/10.1111/J.1365-2826.2008.01671.X

Majc, B., Habič, A., Novak, M., Rotter, A., Porčnik, A., Mlakar, J., … Breznik, B. (2022). Upregulation of Cathepsin X in Glioblastoma: Interplay with γ-Enolase and the Effects of Selective Cathepsin X Inhibitors. *International Journal of Molecular Sciences*, *23*(3), 1784. https://doi.org/10.3390/ijms23031784

Majc, B., Novak, M., Jerala, N. K., Jewett, A., & Breznik, B. (2021). Immunotherapy of Glioblastoma: Current Strategies and Challenges in Tumor Model Development. *Cells*, *10*(2), 1–22. https://doi.org/10.3390/cells10020265

Majc, B., Sever, T., Zarić, M., Breznik, B., Turk, B., & Lah, T. T. (2020). Epithelial-to-mesenchymal transition as the driver of changing carcinoma and glioblastoma microenvironment. *Biochimica et Biophysica Acta (BBA) - Molecular Cell Research*, *1867*(10), 118782. https://doi.org/10.1016/J.BBAMCR.2020.118782

Marusyk, A., & Polyak, K. (2010). Tumor heterogeneity: Causes and consequences. *Biochimica et Biophysica Acta - Reviews on Cancer*. https://doi.org/10.1016/j.bbcan.2009.11.002

Mason, S. D., & Joyce, J. a. (2011). Proteolytic networks in cancer. *Trends in Cell Biology*, *21*(4), 228–237. https://doi.org/10.1016/j.tcb.2010.12.002

Massi, P., Vaccani, A., Bianchessi, S., Costa, B., Macchi, P., & Parolaro, D. (2006). The non-psychoactive cannabidiol triggers caspase activation and oxidative stress in human glioma cells. *Cellular and Molecular Life Sciences*, *63*(17), 2057–2066. https://doi.org/10.1007/s00018-006-6156-x

McAllister, S. D., Christian, R. T., Horowitz, M. P., Garcia, A., & Desprez, P. Y. (2007). Cannabidiol as a novel inhibitor of Id-1 gene expression in aggressive breast cancer cells. *Molecular Cancer Therapeutics*, *6*(11), 2921–2927. https://doi.org/10.1158/1535-7163.MCT-07-0371

Mehta, G., Hsiao, A. Y., Ingram, M., Luker, G. D., & Takayama, S. (2012). Opportunities and challenges for use of tumor spheroids as models to test drug delivery and efficacy. *Journal of Controlled Release*. https://doi.org/10.1016/j.jconrel.2012.04.045

MEROPS - the Peptidase Database. (n.d.). Retrieved November 20, 2022, from https://www.ebi.ac.uk/merops/

Minata, M., Audia, A., Shi, J., Lu, S., Bernstock, J., Pavlyukov, M. S., … Bhat, K. P. (2019). Phenotypic Plasticity of Invasive Edge Glioma Stem-like Cells in Response to Ionizing Radiation. *Cell Reports*, *26*(7), 1893-1905.e7. https://doi.org/10.1016/j.celrep.2019.01.076

Mirabelli, P., Coppola, L., & Salvatore, M. (2019, August 1). Cancer cell lines are useful model systems for medical research. *Cancers*, Vol. 11. MDPI AG. https://doi.org/10.3390/cancers11081098

Moretto, E., Stuart, S., Surana, S., Vargas, J. N. S., & Schiavo, G. (2022). The Role of Extracellular Matrix Components in the Spreading of Pathological Protein Aggregates. *Frontiers in Cellular Neuroscience*, *16*. https://doi.org/10.3389/FNCEL.2022.844211/FULL

Nabissi, M., Morelli, M. B., Amantini, C., Liberati, S., Santoni, M., Ricci-Vitiani, L., … Santoni, G. (2015). Cannabidiol stimulates AML-1a-dependent glial differentiation and inhibits glioma stem-like cells proliferation by inducing autophagy in a TRPV2-dependent manner. *International Journal of Cancer*, *137*(8), 1855–1869. https://doi.org/10.1002/ijc.29573

Nabissi, M., Morelli, M. B., Santoni, M., & Santoni, G. (2013). Triggering of the TRPV2 channel by cannabidiol sensitizes glioblastoma cells to cytotoxic chemotherapeutic agents. *Carcinogenesis*, *34*(1), 48–57. https://doi.org/10.1093/carcin/bgs328

Nägler, D. K., Krüger, S., Kellner, A., Ziomek, E., Menard, R., Buhtz, P., … Kellner, U. (2004). Up-regulation of cathepsin X in prostate cancer and prostatic intraepithelial neoplasia. *Prostate*, *60*(2), 109–119. https://doi.org/10.1002/pros.20046

Neftel, C., Laffy, J., Filbin, M. G., Hara, T., Shore, M. E., Rahme, G. J., … Suvà, M. L. (2019). An Integrative Model of Cellular States, Plasticity, and Genetics for Glioblastoma. *Cell*, *178*(4), 835-849.e21. https://doi.org/10.1016/J.CELL.2019.06.024

Novak, M., Koprivnikar Krajnc, M., Hrastar, B., Breznik, B., Majc, B., Mlinar, M., … Lah Turnšek, T. (2020). CCR5-Mediated Signaling Is Involved in Invasion of Glioblastoma Cells in Its Microenvironment. *International Journal of Molecular Sciences*, *21*(12), 4199. https://doi.org/10.3390/ijms21124199

Obermajer, N., Jevnikar, Z., Doljak, B., Sadaghiani, A. M., Bogyo, M., & Kos, J. (2009). Cathepsin X-mediated β2 integrin activation results in nanotube outgrowth. *Cellular and Molecular Life Sciences*, *66*(6), 1126–1134. https://doi.org/10.1007/s00018-009-8829-8

Obermajer, Nataša, Doljak, B., Jamnik, P., Pečar Fonović, U., & Kos, J. (2009). Cathepsin X cleaves the C-terminal dipeptide of alpha- and gamma-enolase and impairs survival and neuritogenesis of neuronal cells. *International Journal of Biochemistry and Cell Biology*, *41*(8–9), 1685–1696. https://doi.org/10.1016/j.biocel.2009.02.019

Ogawa, J., Pao, G. M., Shokhirev, M. N., & Verma, I. M. (2018). Glioblastoma Model Using Human Cerebral Organoids. *Cell Reports*. https://doi.org/10.1016/j.celrep.2018.03.105

Olson, O. C., & Joyce, J. A. (2015). Cysteine cathepsin proteases : regulators of cancer progression and therapeutic response. *Nature Publishing Group*, *15*(12), 712–729. https://doi.org/10.1038/nrc4027

Pacheco, C., Martins, C., Monteiro, J., Baltazar, F., Costa, B. M., & Sarmento, B. (2022). Glioblastoma Vasculature: From its Critical Role in Tumor Survival to Relevant in Vitro Modelling. *Frontiers in Drug Delivery*, *0*, 1. https://doi.org/10.3389/FDDEV.2022.823412

Papapetrou, E. P. (2016). Patient-derived induced pluripotent stem cells in cancer research and precision oncology. *Nature Medicine*. https://doi.org/10.1038/nm.4238

Passier, R., Orlova, V., & Mummery, C. (2016). Complex Tissue and Disease Modeling using hiPSCs. *Cell Stem Cell*. https://doi.org/10.1016/j.stem.2016.02.011

Pečar Fonović, U., Jevnikar, Z., Rojnik, M., Doljak, B., Fonović, M., Jamnik, P., & Kos, J. (2013). Profilin 1 as a Target for Cathepsin X Activity in Tumor Cells. *PLoS ONE*, *8*(1), e53918. https://doi.org/10.1371/journal.pone.0053918

Pečar Fonović, U., Mitrović, A., Knez, D., Jakoš, T., Pišlar, A., Brus, B., … Kos, J. (2017). Identification and characterization of the novel reversible and selective cathepsin X inhibitors. *Scientific Reports*, *7*(1), 11459. https://doi.org/10.1038/s41598-017-11935-1

Pertwee, R. G., Howlett, A. C., Abood, M. E., Alexander, S. P. H., Marzo, V. Di, Elphick, M. R., … Kunos, G. (2010). Cannabinoid Receptors and Their Ligands : Beyond CB 1 and CB 2. *Pharmacological Reviews*, *62*(4), 588–631. https://doi.org/10.1124/pr.110.003004.588

Pisanti, S., Malfitano, A. M., Ciaglia, E., Lamberti, A., Ranieri, R., Cuomo, G., … Bifulco,

M. (2017). Cannabidiol: State of the art and new challenges for therapeutic applications. *Pharmacology and Therapeutics*, *175*, 133–150. https://doi.org/10.1016/j.pharmthera.2017.02.041

Pišlar, A., & Kos, J. (2014). Cysteine cathepsins in neurological disorders. *Molecular Neurobiology*, *49*(2), 1017–1030. https://doi.org/10.1007/S12035-013-8576-6/FIGURES/3

Pišlar, A., Tratnjek, L., Glavan, G., Zidar, N., Živin, M., & Kos, J. (2020). Neuroinflammation-Induced Upregulation of Glial Cathepsin X Expression and Activity in vivo. *Frontiers in Molecular Neuroscience*, *13*(November), 1–17. https://doi.org/10.3389/fnmol.2020.575453

Podergajs, N., Motaln, H., Rajčević, U., Verbovšek, U., Koršič, M., Obad, N., … Turnšek, T. L. (2015). Transmembrane protein CD9 is glioblastoma biomarker, relevant for maintenance of glioblastoma stem cells. *Oncotarget*, *7*(1), 593–609. https://doi.org/10.18632/oncotarget.5477

Prager, B. C., Xie, Q., Bao, S., & Rich, J. N. (2019). Cancer Stem Cells: The Architects of the Tumor Ecosystem. *Cell Stem Cell*, *24*(1), 41–53. https://doi.org/10.1016/j.stem.2018.12.009

Preamble WMA Declaration of Helsinki-Ethical Principles for Medical Research Involving Human Subjects. (n.d.).

Quail, D. F., & Joyce, J. A. (2017). The Microenvironmental Landscape of Brain Tumors. *Cancer Cell*, *31*(3), 326–341. https://doi.org/10.1016/J.CCELL.2017.02.009

Rak v Sloveniji Cancer in Slovenia. (n.d.).

Rama, A. R., Alvarez, P. J., Madeddu, R., & Aranega, A. (2014). ABC transporters as differentiation markers in glioblastoma cells. *Molecular Biology Reports*, *41*(8), 4847–4851. https://doi.org/10.1007/s11033-014-3423-z

Rawlings, N. D., Barrett, A. J., Thomas, P. D., Huang, X., Bateman, A., & Finn, R. D. (2018). The MEROPS database of proteolytic enzymes, their substrates and inhibitors in 2017 and a comparison with peptidases in the PANTHER database. *Nucleic Acids Research*, *46*(D1), D624–D632. https://doi.org/10.1093/nar/gkx1134

Recasens, A., & Munoz, L. (2019). Targeting Cancer Cell Dormancy. *Trends in Pharmacological Sciences*, *40*(2), 128–141. https://doi.org/10.1016/J.TIPS.2018.12.004

Rudzińska, M., Parodi, A., Soond, S. M., Vinarov, A. Z., Korolev, D. O., Morozov, A. O., … Zamyatnin, A. A. (2019). The role of cysteine cathepsins in cancer progression and drug resistance. *International Journal of Molecular Sciences*, *20*(14), 3602. https://doi.org/10.3390/ijms20143602

Ruiz-Moreno, C., Salas, S. M., Samuelsson, E., Brandner, S., Kranendonk, M. E. G., Nilsson, M., & Stunnenberg, H. G. (2022). Harmonized single-cell landscape, intercellular crosstalk and tumor architecture of glioblastoma. *BioRxiv*, 2022.08.27.505439. https://doi.org/10.1101/2022.08.27.505439

Sadaghiani, A. M., Verhelst, S. H. L., Gocheva, V., Hill, K., Majerova, E., Stinson, S., … Bogyo, M. (2007). Design, synthesis, and evaluation of in vivo potency and selectivity of epoxysuccinyl-based inhibitors of papain-family cysteine proteases. *Chemistry & Biology*, *14*(5), 499–511. https://doi.org/10.1016/J.CHEMBIOL.2007.03.010

Sato, A., Sunayama, J., Matsuda, K. I., Seino, S., Suzuki, K., Watanabe, E., … Kitanaka, C. (2011). MEK-ERK signaling dictates DNA-repair gene MGMT expression and temozolomide resistance of stem-like glioblastoma cells via the MDM2-p53 axis. *Stem Cells (Dayton, Ohio)*, *29*(12), 1942–1951. https://doi.org/10.1002/STEM.753

Sato, T., Stange, D. E., Ferrante, M., Vries, R. G. J., Van Es, J. H., Van Den Brink, S., … Clevers, H. (2011). Long-term Expansion of Epithelial Organoids From Human Colon, Adenoma, Adenocarcinoma, and Barrett's Epithelium. *Gastroenterology*, *141*(5), 1762–1772. https://doi.org/10.1053/J.GASTRO.2011.07.050

Saygin, C., Matei, D., Majeti, R., Reizes, O., & Lathia, J. D. (2019). Targeting Cancer Stemness in the Clinic: From Hype to Hope. *Cell Stem Cell*. https://doi.org/10.1016/j.stem.2018.11.017

Schmitt, M. J., Company, C., Dramaretska, Y., Barozzi, I., Göhrig, A., Kertalli, S., … Gargiulo, G. (2021). Phenotypic mapping of pathologic cross-talk between glioblastoma and innate immune cells by synthetic genetic tracing. *Cancer Discovery*, *11*(3), 754–777. https://doi.org/10.1158/2159-8290.CD-20-0219/333477/AM/PHENOTYPIC-MAPPING-OF-PATHOLOGICAL-CROSSTALK

Sehnal, D., Bittrich, S., Deshpande, M., Svobodová, R., Berka, K., Bazgier, V., … Rose, A. S. (2021). Mol* Viewer: modern web app for 3D visualization and analysis of large biomolecular structures. *Nucleic Acids Research*, *49*(W1), W431–W437. https://doi.org/10.1093/NAR/GKAB314

Solinas, M., Massi, P., Cinquina, V., Valenti, M., Bolognini, D., Gariboldi, M., … Parolaro, D. (2013). Cannabidiol, a Non-Psychoactive Cannabinoid Compound, Inhibits Proliferation and Invasion in U87-MG and T98G Glioma Cells through a Multitarget Effect. *PLoS ONE*, *8*(10). https://doi.org/10.1371/journal.pone.0076918

Soroceanu, L., Murase, R., Limbad, C., Singer, E., Allison, J., Adrados, I., … McAllister, S. D. (2013). Id-1 is a key transcriptional regulator of glioblastoma aggressiveness and a novel therapeutic target. *Cancer Research*, *73*(5), 1559–1569. https://doi.org/10.1158/0008-5472.CAN-12-1943

Stichel, C. C., & Luebbert, H. (2007). Inflammatory processes in the aging mouse brain: Participation of dendritic cells and T-cells. *Neurobiology of Aging*, *28*(10), 1507–1521. https://doi.org/10.1016/J.NEUROBIOLAGING.2006.07.022

Stupp, R., Mason, W. P., van den Bent, M. J., Weller, M., Fisher, B., Taphoorn, M. J. B., … Mirimanoff, R. O. (2005). Radiotherapy plus Concomitant and Adjuvant Temozolomide for Glioblastoma. *New England Journal of Medicine*, *352*(10), 987–996. https://doi.org/10.1056/NEJMoa043330

Takei, N., Kondo, J., Nagaike, K., Ohsawa, K., Kato, K., & Kohsaka, S. (1991). Neuronal survival factor from bovine brain is identical to neuron-specific enolase. *Journal of Neurochemistry*, *57*(4), 1178–1184. https://doi.org/10.1111/J.1471-4159.1991.TB08277.X

Talkenberger, K., Ada Cavalcanti-Adam, E., Voss-Böhme, A., & Deutsch, A. (2017). Amoeboid-mesenchymal migration plasticity promotes invasion only in complex heterogeneous microenvironments. *Scientific Reports 2017 7:1*, *7*(1), 1–12. https://doi.org/10.1038/s41598-017-09300-3

Tannock, I. F., Lee, C. M., Tunggal, J. K., Cowan, D. S. M., & Egorin, M. J. (2002). Limited penetration of anticancer drugs through tumor tissue: A potential cause of resistance of solid tumors to chemotherapy. *Clinical Cancer Research*.

Tapia, F. J., Barbosa, A. J. A., Marangos, P. J., Polak, J. M., Bloom, S. R., Dermody, C., & Pearse, A. G. E. (1981). Neuron-specific enolase is produced by neuroendocrine tumours. *Lancet (London, England)*, *1*(8224), 808–811. https://doi.org/10.1016/S0140-6736(81)92682-9

Thomas, R. P., Recht, L., & Nagpal, S. (2013). Advances in the management of glioblastoma: the role of temozolomide and MGMT testing. *Clinical Pharmacology : Advances and Applications*, *5*(1), 1. https://doi.org/10.2147/CPAA.S26586

Torras, N., García-Díaz, M., Fernández-Majada, V., & Martínez, E. (2018). Mimicking epithelial tissues in three-dimensional cell culture models. *Frontiers in Bioengineering and Biotechnology*. https://doi.org/10.3389/fbioe.2018.00197

Torres, S., Lorente, M., Rodriguez-Fornes, F., Hernandez-Tiedra, S., Salazar, M., Garcia-Taboada, E., … Velasco, G. (2011). A Combined Preclinical Therapy of Cannabinoids and Temozolomide against Glioma. *Molecular Cancer Therapeutics*, *10*(1), 90–103. https://doi.org/10.1158/1535-7163.MCT-10-0688

Turk, V., Stoka, V., Vasiljeva, O., Renko, M., Sun, T., Turk, B., & Turk, D. (2012). Cysteine cathepsins: from structure, function and regulation to new frontiers. *Biochimica et Biophysica Acta*, *1824*(1), 68–88. https://doi.org/10.1016/j.bbapap.2011.10.002

van Staveren, W. C. G., Solís, D. Y. W., Hébrant, A., Detours, V., Dumont, J. E., & Maenhaut, C. (2009). Human cancer cell lines: Experimental models for cancer cells in situ? For cancer stem cells? *Biochimica et Biophysica Acta - Reviews on Cancer*, *1795*(2), 92–103. https://doi.org/10.1016/j.bbcan.2008.12.004

Venkatesh, H. S., Morishita, W., Geraghty, A. C., Silverbush, D., Gillespie, S. M., Arzt, M., … Monje, M. (2019). Electrical and synaptic integration of glioma into neural circuits. *Nature 2019 573:7775*, *573*(7775), 539–545. https://doi.org/10.1038/s41586-019-1563-y

Verhaak, R. G. W., Hoadley, K. A., Purdom, E., Wang, V., Qi, Y., Wilkerson, M. D., … Hayes, D. N. (2010). Integrated genomic analysis identifies clinically relevant subtypes of glioblastoma characterized by abnormalities in PDGFRA, IDH1, EGFR, and NF1. *Cancer Cell*, *17*(1), 98–110. https://doi.org/10.1016/j.ccr.2009.12.020

Vizin, T., Christensen, I. J., Nielsen, H. J., & Kos, J. (2012). Cathepsin X in serum from patients with colorectal cancer: relation to prognosis. *Radiology and Oncology*, *46*(3), 207–212. https://doi.org/10.2478/v10019-012-0040-0

Vizin, T., & Kos, J. (2015). Gamma-enolase: a well-known tumour marker, with a less-known role in cancer. *Radiology and Oncology*, *49*(3), 217. https://doi.org/10.1515/RAON-2015-0035

Vizovisek, M., Ristanovic, D., Menghini, S., Christiansen, M. G., & Schuerle, S. (2021). The Tumor Proteolytic Landscape: A Challenging Frontier in Cancer Diagnosis and Therapy. *International Journal of Molecular Sciences*, *22*(5), 1–30. https://doi.org/10.3390/IJMS22052514

Wang, L. B., Karpova, A., Gritsenko, M. A., Kyle, J. E., Cao, S., Li, Y., … Zhu, J. (2021).

Proteogenomic and metabolomic characterization of human glioblastoma. *Cancer Cell*, *39*(4), 509-528.e20. https://doi.org/10.1016/J.CCELL.2021.01.006

Wang, M., Wang, T., Liu, S., Yoshida, D., & Teramoto, A. (2003). The expression of matrix metalloproteinase-2 and -9 in human gliomas of different pathological grades. *Brain Tumor Pathology*, *20*(2), 65–72. https://doi.org/10.1007/BF02483449

Weber, A. M., & Ryan, A. J. (2015). ATM and ATR as therapeutic targets in cancer. *Pharmacology & Therapeutics*, *149*, 124–138. https://doi.org/10.1016/J.PHARMTHERA.2014.12.001

Weller, M., van den Bent, M., Preusser, M., Le Rhun, E., Tonn, J. C., Minniti, G., … Wick, W. (2020). EANO guidelines on the diagnosis and treatment of diffuse gliomas of adulthood. *Nature Reviews Clinical Oncology*, *18*(3), 170–186. https://doi.org/10.1038/s41571-020-00447-z

Wen, P. Y., Weller, M., Lee, E. Q., Alexander, B. M., Barnholtz-Sloan, J. S., Barthel, F. P., … van den Bent, M. J. (2020). Glioblastoma in adults: a Society for Neuro-Oncology (SNO) and European Society of Neuro-Oncology (EANO) consensus review on current management and future directions. *Neuro-Oncology*, *22*(8), 1073–1113. https://doi.org/10.1093/neuonc/noaa106

Wick, W., Gorlia, T., Bendszus, M., Taphoorn, M., Sahm, F., Harting, I., … van den Bent, M. J. (2017). Lomustine and Bevacizumab in Progressive Glioblastoma. *The New England Journal of Medicine*, *377*(20), 1954–1963. https://doi.org/10.1056/NEJMOA1707358

Woroniecka, K., Chongsathidkiet, P., Rhodin, K., Kemeny, H., Dechant, C., Harrison Farber, S., … Fecci, P. E. (2018). T-cell exhaustion signatures vary with tumor type and are severe in glioblastoma. *Clinical Cancer Research*, *24*(17), 4175–4186. https://doi.org/10.1158/1078-0432.CCR-17-1846

Xu, H., Lyu, X., Yi, M., Zhao, W., Song, Y., & Wu, K. (2018). Organoid technology and applications in cancer research. *Journal of Hematology & Oncology*, *11*(1), 116. https://doi.org/10.1186/s13045-018-0662-9

Yan, T., Skaftnesmo, K. O., Leiss, L., Sleire, L., Wang, J., Li, X., & Enger, P. T. (2011). Neuronal markers are expressed in human gliomas and NSE knockdown sensitizes glioblastoma cells to radiotherapy and temozolomide. *BMC Cancer*, *11*, 524. https://doi.org/10.1186/1471-2407-11-524

Yeo, E. C. F., Brown, M. P., Gargett, T., & Ebert, L. M. (2021). The Role of Cytokines and Chemokines in Shaping the Immune Microenvironment of Glioblastoma: Implications for Immunotherapy. *Cells*, *10*(3), 1–25. https://doi.org/10.3390/CELLS10030607

Zalman, D., & Bar-Sela, G. (2017). Cannabis and Synthetic Cannabinoids for Cancer Patients : Multiple Palliative. In *Handbook of Cannabis and Related Pathologies*. Elsevier Inc.

Zamagni, A., Pasini, A., Pirini, F., Ravaioli, S., Giordano, E., Tesei, A., … Molinari, C. (2020). CDKN1A upregulation and cisplatin-pemetrexed resistance in non-small cell lung cancer cells. *International Journal of Oncology*, *56*(6), 1574–1584. https://doi.org/10.3892/IJO.2020.5024/DOWNLOAD

Zhou, W., Ke, S. Q., Huang, Z., Flavahan, W., Fang, X., Paul, J., … Bao, S. (2015).

Periostin secreted by glioblastoma stem cells recruits M2 tumour-associated macrophages and promotes malignant growth. *Nature Cell Biology*, *17*(2), 170–182. https://doi.org/10.1038/ncb3090

Zhu, L. X., Sharma, S., Stolina, M., Gardner, B., Roth, M. D., Tashkin, D. P., & Dubinett, S. M. (2000). Δ-9-Tetrahydrocannabinol Inhibits Antitumor Immunity by a CB2 Receptor-Mediated, Cytokine-Dependent Pathway. *The Journal of Immunology*, *165*(1), 373–380. https://doi.org/10.4049/jimmunol.165.1.373

Bibliography

Publications Related to the Thesis

Journal Articles

Lah, T. T., Novak, M., Pena Almidon, M. A., Marinelli, O., Žvar Baškovič, B., Majc, B., … Nabissi, M. (2021). Cannabigerol Is a Potential Therapeutic Agent in a Novel Combined Therapy for Glioblastoma. Cells, 10(2), 340. https://doi.org/10.3390/cells10020340

Majc, B., Habič, A., Novak, M., Rotter, A., Porčnik, A., Mlakar, J., … Breznik, B. (2022). Upregulation of Cathepsin X in Glioblastoma: Interplay with γ-Enolase and the Effects of Selective Cathepsin X Inhibitors. International Journal of Molecular Sciences, 23(3), 1784. https://doi.org/10.3390/ijms23031784

Lah, T. T., Majc, B., Novak, M., Sušnik, A., Breznik, B., Porčnik, A., … Zomer, R. (2022). The Cytotoxic Effects of Cannabidiol and Cannabigerol on Glioblastoma Stem Cells May Mostly Involve GPR55 and TRPV1 Signalling. Cancers 2022, Vol. 14, Page 5918, 14(23), 5918. https://doi.org/10.3390/CANCERS14235918

Majc, B., Novak, M., Jerala, N. K., Jewett, A., & Breznik, B. (2021). Immunotherapy of Glioblastoma: Current Strategies and Challenges in Tumor Model Development. Cells, 10(2), 1–22. https://doi.org/10.3390/cells10020265

Majc, B., Sever, T., Zarić, M., Breznik, B., Turk, B., & Lah, T. T. (2020). Epithelial-to-mesenchymal transition as the driver of changing carcinoma and glioblastoma microenvironment. Biochimica et Biophysica Acta (BBA) - Molecular Cell Research, 1867(10), 118782. https://doi.org/10.1016/J.BBAMCR.2020.118782

Habič, A., Novak, M., Majc, B., Lah Turnšek, T., & Breznik, B. (2021). Proteases Regulate Cancer Stem Cell Properties and Remodel Their Microenvironment. The Journal of Histochemistry and Cytochemistry : Official Journal of the Histochemistry Society. https://doi.org/10.1369/00221554211035192

Conference Paper

Habič, A., Majc, B., Porčnik, A., Lah Turnšek, T., Breznik, B., Novak, M. (2022). Exploring glioblastoma therapeutic resistance in a patient-derived organoid model. In: NOVAK, Rok (ed.), et al. 14. študentska konferenca Mednarodne podiplomske šole Jožefa Stefana = 14th Jožef Stefan International Postgraduate School Students' Conference : knjiga povzetkov = book of abstracts : 1. - 3. junij 2022, Kamnik,

Slovenia = 1st - 3rd June, 2022, Kamnik, Slovenia. 14. študentska konferenca Mednarodne podiplomske šole Jožefa Stefana, 1. - 3. junij 2022, Kamnik, Slovenia = 14th Jožef Stefan International Postgraduate School Students' Conference, 1st - 3rd June, 2022, Kamnik, Slovenia. Ljubljana: Jožef Stefan Institute: Jožef Stefan International Postgraduate School, 2022. Str.69. http://ipssc.mps.si/Book_of_Abstracts.pdf. [COBISS.SI-ID 114107139]

Majc, B., Habič, A., Novak, M., Porčnik, A., Mlakar, J., Kos, J., Lah Turnšek, T., Pišlar, A., Breznik, B.. Increased cathepsin X activity in glioblastoma : the effect of its inhibition and the interplay with γ-enolase. In: NOVAK, Rok (ed.), et al. 14. študentska konferenca Mednarodne podiplomske šole Jožefa Stefana = 14th Jožef Stefan International Postgraduate School Students' Conference : knjiga povzetkov = book of abstracts : 1. - 3. junij 2022, Kamnik, Slovenia = 1st - 3rd June, 2022, Kamnik, Slovenia. 14. študentska konferenca Mednarodne podiplomske šole Jožefa Stefana, 1. - 3. junij 2022, Kamnik, Slovenia = 14th Jožef Stefan International Postgraduate School Students' Conference, 1st - 3rd June, 2022, Kamnik, Slovenia. Ljubljana: Jožef Stefan Institute: Jožef Stefan International Postgraduate School, 2022. Str. 74. http://ipssc.mps.si/Book_of_Abstracts.pdf. [COBISS.SI-ID 114102275]

Habič, A., Majc, B., Porčnik, A., Bošnjak, R., Mlakar, J., Lah Turnšek, T., Breznik, B., Novak, M.. Patient-derived glioblastoma organoids : elucidating the mechanisms of glioblastoma therapeutic resistance in the context of tumor microenvironment. Neuro-oncology. Sept. 2022, vol. 24, iss. supplement_2, str. ii30–ii31. ISSN 1522-8517. https://doi.org/10.1093/neuonc/noac174.100, DOI: 10.1093/neuonc/noac174.100. [COBISS.SI-ID 124089603]

Breznik, B., Ko, M.W., Chen, P.C., Senjor, E., Majc, B., Novak, M., Habič, A., Jewett, A.. Natural killer cells lyse glioblastoma stem cells and increase their sensitivity to chemotherapy. Neuro-oncology. Sept. 2022, vol. 24, iss. supplement_2, str. ii39. ISSN 1522-8517. https://doi.org/10.1093/neuonc/noac174.131, DOI: 10.1093/neuonc/noac174.131. [COBISS.SI-ID 124077827]

Habič, A., Majc, B., Porčnik, A., Bošnjak, R., Markelc, B., Čemažar, M., Lah Turnšek, T., Breznik, B., Novak, M.. Organoidi glioblastoma kot model za preučevanje odpornosti na terapijo. In: MARINKO, Tanja (ed.), ČEMAŽAR, Maja (ed.), KRANJC BREZAR, Simona (ed.). Novosti na področju radioterapije in radiobiologije: od raziskav do klinike : zbornik prispevkov in povzetkov : znanstveni simpozij : 3. junij 2022, Onkološki inštitut Ljubljana. 1. izd. Ljubljana: Onkološki inštitut: Združenje za radioterapijo in onkologijo pri Slovenskem zdravniškem društvu, 2022. Str. 62. ISBN 978-961-7029-45-1. [COBISS.SI-ID 111106819]

Habič, A., Majc, B., Porčnik, A., Lah Turnšek, T., Breznik, B., Novak, M.. Dissecting glioblastoma therapeutic resistance with a patient-derived organoid model. In: Program and abstracts : (plenaries, orals and posters). 11th Brain Tumor Meeting, May 19 - 20, 2022, Berlin, Germany. [S. l.: s. n., 2022]. Str. 54. https://www.braintumor-berlin.de/sites/braintumor-berlin.de/files/Program_Brain_Tumor_Meeting2022.pdf. [COBISS.SI-ID 109507331]

Novak, M., Majc, B., Habič, A., Mlinar, M., Porčnik, A., Bošnjak, R., Mlakar, J., Sadikov, A., Malavolta, M., Skoblar Vidmar, M., Hren, M., Lah Turnšek, T., Breznik, B.. Gliobank connecting clinical and research data. In: Program and abstracts : (plenaries, orals and posters). 11th Brain Tumor Meeting, May 19 - 20, 2022, Berlin, Germany. [S. l.: s. n., 2022]. Str. 69. https://www.braintumor-berlin.de/sites/braintumor-berlin.de/files/Program_Brain_Tumor_Meeting2022.pdf. [COBISS.SI-ID 109507075]

Breznik, B., Ko, M.W., Chen, P.C., Senjor, E., Majc, B., Habič, A., Novak, M., Jewett, A. Super-charged natural killer cells lyse glioblastoma stem cells and increase their sensitivity to chemotherapy. In: Program and abstracts : (plenaries, orals and posters). 11th Brain Tumor Meeting, May 19 - 20, 2022, Berlin, Germany. [S. l.: s. n., 2022]. Str. 41-42. https://www.braintumor-berlin.de/sites/braintumor-berlin.de/files/Program_Brain_Tumor_Meeting2022.pdf. [COBISS.SI-ID 109506819]

Majc, B., Habič, A., Novak, M., Porčnik, A., Mlakar, J., Kos, J., Lah Turnšek, T., Pišlar, A., Breznik, B.. Up-regulation of cathepsin X in glioblastoma : investigation of selective inhibitors and its target gamma-enolase. In: Program and abstracts : (plenaries, orals and posters). 11th Brain Tumor Meeting, May 19 - 20, 2022, Berlin, Germany. [S. l.: s. n., 2022]. Str. 66. https://www.braintumor-berlin.de/sites/braintumor-berlin.de/files/Program_Brain_Tumor_Meeting2022.pdf. [COBISS.SI-ID 109506563]

Breznik, B., Majc, B., Ko, M.W., Tse, C., Chen, P.C., Senjor, E., Habič, A., Angelillis, N., Novak, M., Župunski, V., Mlakar, J., Nathanson, D., Jewett, A.. Super-charged NK cells in therapy of glioblastoma : preclinical evidences in 2D and 3D in vitro tumor models. In: Recent insights into immuno-oncology : 16-17 June, 2022, Leuven, BE. [Leuven: VIB, 2022]. Str. 80. VIB conference series. [COBISS.SI-ID 114842883]

Novak, M., Koprivnikar Krajnc, M., Hrastar, B., Breznik, B., Majc, B., Rotter, A., Porčnik, A., Mlakar, J., Pestell, R. G., Lah Turnšek, T. Chemokine CCL5 and its receptor CCR5 as potential therapeutic targets in glioblastoma. FEBS open bio. Jul. 2021, vol. 11, iss. s1, str. 417. ISSN 2211-5463. https://febs.onlinelibrary.wiley.com/doi/10.1002/2211-5463.13206. [COBISS.SI-ID 75950339]

Majc, B., Novak, M., Breznik, B., Habič, A., Bošnjak, R., Porčnik, A., Lah Turnšek, T. Setting up novel type of glioblastoma organoid model that recapitulates microenvironmental conditions in vivo. In: Molecules of life : towards new horizons : FEBS 2021 : the 45th FEBS Congress : 3-8 July 2021, Ljubljana, Slovenia : virtual : abstracts. [S. l.]: Federation of European Biochemical Societies. 2021, str. 315. https://febs.onlinelibrary.wiley.com/doi/epdf/10.1002/2211-5463.13205. [COBISS.SI-ID 76271363]

Lah Turnšek, T., Breznik, B., Majc, B., Novak, M., Porčnik, A., Habič, A., Mlinar, M., Bošnjak, R. The effect of microenvironment on glioblastoma stem cells therapeutic resistance. Neuro-oncology advances. 2021, vol. 3, iss. s2, str. ii9. ISSN 2632-2498.

https://academic.oup.com/noa/article/3/Supplement_2/ii9/6313927, DOI: 10.1093/noajnl/vdab070.035. [COBISS.SI-ID 73935107]

Breznik, B., Ko, M.W., Majc, B., Chen, P.C., Senjor, E., Lah Turnšek, T., Jewett, A.. Therapeutic potential of super-charged natural killer cells by lysis and increased chemotherapeutic sensitivity of glioblastoma stem-like cells. In: [3rd] CSC 2020, Cancer Stem Cells : impact on treatment : December 13-17, 2020, Seefeld, Tyrol, Austria. [S. l.: s. n.], 2020. Str. 24-25. ISBN 978-2-88963-598-6. https://www.csc-conference.at/conference-2020-materials-presentations-abstract-book/. [COBISS.SI-ID 61195011]

Majc, B., Novak, M., Breznik, B., Mlinar, M., Žvar Baškovič, B., Rotter, A., Porčnik, A., Mlakar, J., Skoblar Vidmar, M., Hren, M., Lah Turnšek, T.. GLIOBANK : connecting research and clinical data. In: NADIŽAR, Nejc (ed.). TranSYS training school : abstract book : virtual symposium : Slovenia, november 22nd - november 27th, 2020. Electronic version. Ljubljana: Faculty of Medicine, 2021. Str. 42. ISBN 978-961-267-199-0. [COBISS.SI-ID 96496899]

Novak, M., Koprivnikar Krajnc, M., Hrastar, B., Breznik, B., Majc, B., Hira, V. V. V., Mlinar, M., Rotter, Ana, Porčnik, A., Bošnjak, R., Mlakar, J., Lah Turnšek, T.. CCL5/CCR5 signaling is important for invasion of glioblastoma in its microenvironment. In: HRASTAR, Barbara (ed.), MLINAR, Mateja (ed.). Abstract book. International Conference Brain Tumors: from bench to clinic, 26. 11. 2019, Ljubljana. [S. l.: s. n., 2019]. Str. 28. [COBISS.SI-ID 34601945]

Žvar Baškovič, B., Majc, B., Novak, M., Breznik, B, Mlinar, M., Porčnik, A., Bošnjak, R., Mlakar, J., Lah Turnšek, T., Zomer, R.. Influence of cannabinoids THC and CBD on brain tumor glioblastoma with differentially expressed cannabinoid receptors CB1 and CB2. In: HRASTAR, Barbara (ed.), MLINAR, Mateja (ed.). Abstract book. International Conference Brain Tumors: from bench to clinic, 26. 11. 2019, Ljubljana. [S. l.: s. n., 2019]. Str. 33. [COBISS.SI-ID 5245263]

Lah Turnšek, T., Breznik, B., Novak, M., Majc, B., Hira, V. V. V., Mlinar, M. Research for a more efficient personalized therapy of glioblastoma. In: HRASTAR, Barbara (ed.), MLINAR, Mateja (ed.). Abstract book. International Conference Brain Tumors: from bench to clinic, 26. 11. 2019, Ljubljana. [S. l.: s. n., 2019]. Str. 17. [COBISS.SI-ID 5245519]

Majc, B., Novak, M., Žvar Baškovič, B., Breznik, B., Mlinar, M., Porčnik, A., Bošnjak, R., Mlakar, J., Lah Turnšek, T., Zommer, R.. Cannabidiol and [delta]9-tetrahydrocannabinol affect human glioblastoma cell proliferation and survival. In: KISOVEC, Matic (ed.). Book of abstracts = Knjiga povzetkov. 13th Meeting of the Slovenian Biochemical Society with International Participation = 13. srečanje Slovenskega biokemijskega društva z mednarodno udeležbo, Dobrna, 24 - 27 September 2019. Ljubljana: Slovenian Biochemical Society, 2019. Str. 128. ISBN 978-961-93879-8-6. [COBISS.SI-ID 5181007]

Majc, B., Novak, M., BREZNIK, Breznik, B., Mlinar, M Porčnik, A., Bošnjak, R., Mlakar, J., Vidic, A., Lah Turnšek, T. Vpliv kanabinoidnih substanc na glioblastom z različno izraženimi receptorji CB1 in CB2 = Influence of cannabinoids on glioblastoma with differentially expressed receptors CB1 and CB2. In: ČERNE, Katarina (ed.),

SOLLNER DOLENC, Marija (ed.). Kanabinoidi pod drobnogledom = Cannabinoids under scrutiny : njihova toksičnost in uporabnost = their toxicity and medical utility : 4. kongres Slovenskega toksikološkega društva : Ljubljana, 17. 1. 2019 : [zbornik povzetkov]. 4. kongres Slovenskega toksikološkega društva, Ljubljana, 17. 1. 2019. Ljubljana: Slovensko toksikološko društvo, 2019. Str. 38-39. ISBN 978-961-91445-3-4. [COBISS.SI-ID 4974671]

Noorden, C. J. F., Majc, B., Hira, V. V. V., Breznik, B.. Microscopic imaging of the activity of cathepsin B and K in human glioblastoma tumors with metabolic mapping (enzyme histochemistry). In: PIRKER, Luka (ed.), et al. Knjiga povzetkov. 3. slovensko posvetovanje mikroskopistov, 16. in 17. maj, Ankaran. 1. izd. Ljubljana: Slovensko društvo za mikroskopijo, 2019. Str. 82. ISBN 978-961-94264-1-8. [COBISS.SI-ID 5080143]

Novak, M., Koprivnikar Krajnc, M., Hrastar, B., Breznik, B., Majc, B., Hira, V. V. V., Mlinar, M., Rotter, Ana, P., Andrej, B., R., Mlakar, J., Lah Turnšek, T.. Localisation and the biological role of chemokine CCL5 and its receptor CCR5 in the glioblastoma microenvironment. In: Program and abstracts : (plenaries, orals and posters). 10th Brain Tumor Meeting, May 23 - 24, 2019, Berlin, Germany. [S. l.: s. n., 2019]. Str. 74. https://www.braintumor-berlin.de/sites/braintumor-berlin.de/files/images/Program%202019%20f%C3%BCr%20Druck.pdf. [COBISS.SI-ID 5084239]

Breznik, B., Hira, V. V. V., Novak, M., Porčnik, A., Mlakar, J., Majc, B., Noorden, C. J. F., Lah Turnšek, T. Glioblastoma stem cells are localized in peri-arteriolar niche regions and are retained there by SDF-1[alpha]/CXCR4 signaling. In: CSC 2018, 2nd International Conference "Cancer Stem Cells: Impact on Treatment" : December 11-15, 2018, Seefeld, Tyrol, Austria. [S. l.]: European School of Oncology, 2018. Str. 49-51. [COBISS.SI-ID 4932687]

Novak, M., Breznik, B., Majc, B., Podergajs, N., Nikšić Žakelj, M., Porčnik, Až., Mlakar, J., Lah Turnšek, T. Transmembrane protein CD9 as a biomarker in different subtypes of glioblastoma. European Journal of Cancer. [Print ed.]. 2018, vol. 103, suppl. 1, str. e103. ISSN 0959-8049. [COBISS.SI-ID 4902479]

Majc, B., Vittori, M., Breznik, B., Lah Turnšek, T. Silencing of RECQ1 helicase decreases the tumour growth of gliobrastoma cells in a zebrafish embryo xenotransplantation model. In: SZÜTS, Dávis (ed.), BUDAY, László (ed.). FEBS3+ Conference : [from molecules to living systems] : final programme & book of abstracts : 2-5 September 2018, Siófok, Hungary. Veszprém: OOK-Press, 2018. Str. 248. ISBN 978-615-5270-47-5. [COBISS.SI-ID 4808783]

Other Publications (optional)

Breznik, B., KO, M.W., TSE, C., Chen, P.C., Senjor, E., Majc, B., Habič, A., Angelillis, N., Novak, M., Župunski, V., Mlakar, J., Nathanson, D., Jewett, A. (2022). Infiltrating natural killer cells bind, lyse and increase chemotherapy efficacy in glioblastoma stem-like tumorospheres. Communications biology. https://doi.org/10.1038/s42003-022-03402-z, DOI: 10.1038/s42003-022-03402-z.

Porčnik, A., Novak, M., Breznik, B., Majc, B., Hrastar, B., Šamec, N., Zottel, A., Jovchevska, I., Vittori, M., Rotter, A., Komel, R., Lah Turnšek, T. (2021). TRIM28 selective nanobody reduces glioblastoma stem cell invasion. Molecules. https://doi.org/10.3390/molecules26175141.

Novak, M., Koprivnikar Krajnc, M., Hrastar, B., Breznik, B., Majc, B., Mlinar, M., Rotter, A., Porčnik, A., Mlakar, J., Stare, K., Pestell, R. G., Lah Turnšek, T. (2020). CCR5-mediated signaling is involved in invasion of glioblastoma cells in its microenvironment. International journal of molecular sciences. https://doi.org/10.3390/ijms21124199

Majc, B., Novak, M., Lah Turnšek, T., Križaj, I. (2022). Bioactive peptides from venoms against glioma progression. Frontiers in oncology. DOI: 10.3389/fonc.2022.965882.

Majc, B., Novak, M., Breznik, B. (2022). Z raziskavami iščemo nova zdravila za zdravljenje raka. Pisani list.

Breznik, B., Majc, B., Habič, A., Ušeničnik, U., Porčnik, A., Bošnjak, R., Mlakar, J., Skoblar Vidmar, M., Jesenko, T., Č., M., Lah Turnšek, T., Novak, M. (2022). Odpornost glioblastoma na radioterapijo: vpliv rakavih matičnih celic in mikrookolja tumorja. Novosti na področju radioterapije in radiobiologije: od raziskav do klinike: zbornik prispevkov in povzetkov.

Biography

The author of this thesis, Bernarda Majc, was born in Kranj on September 22, 1991. She graduated from elementary school Križe and high school Gimnazija Kranj. In 2010, she enrolled at the Faculty of Pharmacy at the University of Ljubljana to obtain a bachelor's degree in Biomedical Sciences: Laboratory Medicine. She graduated in 2013. In 2014, she enrolled in the master's study program Biochemistry at the Faculty of Chemistry and Chemical technology, University of Ljubljana. She defended her master's thesis, entitled Expression and characterization of C9ORF72 protein in June 2017. The master's thesis was performed and written under the supervision of Assis. Dr. Vera Župunski. As a student she worked at Lek d.d. company from April 2017 to September 2017, where she was involved in the development of new physiochemical and biochemical analyses to support smooth running of production or development processes in a timely and high quality analytical manner. From April 2018 to September 2018 she was European Solidarity Corps volunteer for Interreg TransGlioma project with the aim to increase cooperation among key research institutes, universities, and companies in the biomedical field, in order to promote the transfer of innovative biomedical techniques in the field of oncology, with specific regard to glioblastoma.

In October 2018, she enrolled in the PhD programme Nanosciences and Nanotechnologies at the Jožef Stefan International Postgraduate School and started her PhD research as a young researcher at the Department of Genetic Toxicology and Cancer Biology at the National Institute of Biology under the supervision of Prof. Dr. Tamara Lah Turnšek and co-mentor Dr. Metka Novak.

She presented her work at numerous national and international conferences "FEBS3 + [from molecules to living systems]" in Siófok (FEBS Youth travel grant), Biomolecular Science Day "BIOmolecularec 2018", scientific symposium on the 80th anniversary of Institute of Oncology in Ljubljana and the conference "Cancer stem cell: Impact on Treatment" in Seefeld (Austria), "Cannabinoids under scrutiny: their toxicity and usefulness" in Ljubljana, conferences "Controversies on Cannabis-Based Medicines" in Barcelona, "Summer School in Medical Oncology "at the Oncology Institute," Minisimposium on Tumor Microenvironment "in Ljubljana, conference" Meeting of the Slovenian Biochemical Society "in Dobrna, FEBS2021" The 45th FEBS Congress ", online Ljubljana, 14th Jožef Stefan International Postgraduate School Students' Conference in Kamnik, 11th Brain Tumor Meeting in Berlin, Recent insights into immuno-oncology in Leuven. At the TranSYS online Training school conference, she was selected to present the results in the form of a lecture. She also participated in expert workshops such as the "EORTC course" Clinical Trial Statistics for Non Statisticians "in Brussels", "R za neprogramerje- From Data to Science in Ljubljana. She was awarded two travel grants: FEBS3 + [from molecules to living systems]" in Siófok and a travel grant from the Slovenian Biochemical Society to attend the conference "Recent Insights into Immuno-Oncology" in Leuven.

She has also been involved in other scientific topics, such as scientific writing, communication, promotion of science, and in the organization of the conference "Brain tumors: from bench to clinic" as part of the Trans-Glioma Project. As an assistant in the Department of Biochemistry at the Faculty of Chemistry and Chemical Technology, she is actively involved in conducting laboratory practicals for 2nd year students in Biochemistry of Cancer at the Faculty of Chemistry and Chemical Technology.